STUDY OF BIOMEDICAL APPLICATIONS BASED ON IRON OXIDE NANOPARTICLE – NUCLEIC ACID CONJUGATES

By

Ms. RUTUJA P. GAMBHIR

Under the Supervision of

Dr. ARPITA P. TIWARI

Thesis Submitted to

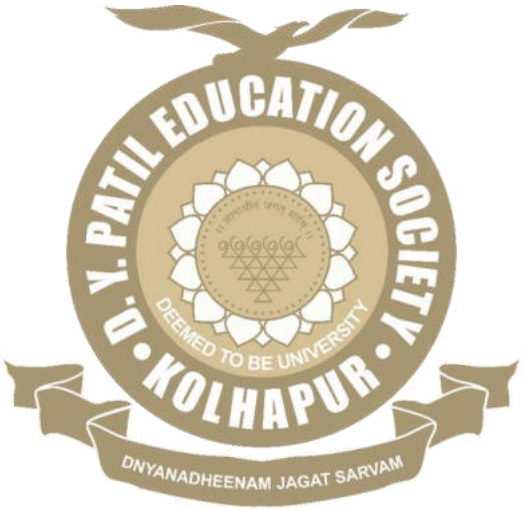

For the Degree of

Doctor of Philosophy

2024

STUDY OF BIOMEDICAL APPLICATIONS BASED ON IRON OXIDE NANOPARTICLE - NUCLEIC ACID CONJUGATES

A Thesis Submitted to

D. Y. PATIL EDUCATION SOCIETY
(DEEMED TO BE UNIVERSITY), KOLHAPUR

For the Degree of

DOCTOR OF PHILOSOPHY

In

Stem Cell Technology and Regenerative Biology

By

Ms. RUTUJA PRASHANT GAMBHIR

M.Sc.

Under the Supervision of

Dr. ARPITA PANDEY-TIWARI

M.Sc., Ph.D.

CENTRE FOR INTERDISCIPLINARY RESEARCH,

D. Y. PATIL EDUCATION SOCIETY

(DEEMED TO BE UNIVERSITY),

KOLHAPUR – 416006

2024

DECLARATION

I hereby declare that the thesis "**STUDY OF BIOMEDICAL APPLICATIONS BASED ON IRON OXIDE NANOPARTICLE - NUCLEIC ACID CONJUGATES**" submitted for the degree of **Doctor of Philosophy** in **Stem Cell Technology and Regenerative Biology** under the faculty of **Centre for Interdisciplinary Research** of the **D. Y. Patil Education Society (Deemed to be University), Kolhapur** is completed and written by me. This thesis has not been made before the basis for the award of any other higher education institute in India or any other country to the best of my knowledge. Further, I declare that, I have not violated any of the provisions under Copyright and Piracy/Cyber/IPR Act amended from time to time.

Research student

Place: Kolhapur
Ms. Rutuja Prashant Gambhir

Date:

CERTIFICATE

This is to certify that the thesis entitled "**STUDY OF BIOMEDICAL APPLICATIONS BASED ON IRON OXIDE NANOPARTICLE - NUCLEIC ACID CONJUGATES**" which is being submitted herewith for the award of **Doctor of Philosophy in Stem Cell Technology and Regenerative Biology** under the faculty of **Centre for Interdisciplinary Research** of **D. Y. Patil Education Society (Deemed to be University), Kolhapur** is the result of original research work completed by **Ms. Rutuja Prashant Gambhir** under my supervision and guidance and the best of my knowledge and belief, the work embodied in this thesis has not formed earlier the basis for the award of any degree or similar title of this or any other University or examining body.

Research guide

Place: Kolhapur
Date:

Dr. Arpita Pandey-Tiwari
Associate Professor

Forwarded through,

Prof. Dr. C. D. Lokhande
Dean and Research Director,
Centre for Interdisciplinary
Research

This Thesis is dedicated to my Parents and Brother – Nandan

For their endless love and support.

ACKNOWLEDGEMENT

Accomplishing PhD thesis is a successful milestone and I am grateful to ***myself*** for embarking on this. But I couldn't have achieved it without the help and support of many people.

Firstly, I would like to thank my guide ***Dr. Arpita Pandey-Tiwari*** for teaching, supporting, mentoring, and believing in me beyond academia. She has pushed me to step out of my comfort zone, challenge myself, and explore new horizons. She has cultivated in me a deep sense of curiosity, critical thinking, planning, execution of the plan, approaching challenges in resilience, and making a meaningful impact in my chosen field. I am profoundly grateful for the opportunities she has provided me to grow not only as a researcher but also as a strong independent woman.

I would like to express my gratitude to the honourable Vice-chancellor ***Prof. Dr. R. K. Mudgal*** and Registrar ***Dr. V. V. Bhosale*** for their inspiration and constant support. I would like to express sincere gratitude to ***Prof. Dr. C. D. Lokhande*** (Dean, CIR) for his time-to-time insightful feedback and valuable suggestions during these years. My special thanks to ***Dr. M. G. Joshi*** (HOD, SCRM & MBT), ***Dr. T. D. Dongale***, ***Dr. U. M. Patil***, ***Dr. J. L. Gunjakar***, ***Dr. S. M. Karuppayil***, and ***Dr. Arun kumar Parthasarathy*** for their guidance and empathy. I am thankful to my seniors ***Dr. Dhanaji Malavekar***, ***Dr. Shital Kale***, ***Dr. Somnath Kundale***, and ***Mr. Vikas Magdum*** for providing characterizations and related help. I am thankful to the wonderful teaching and non-teaching staff of CIR for their cooperation.

I extend my gratitude to ***Mr. Akash S. Patil*** for his every immeasurable assistance in my 'synopsis to thesis' journey. I am grateful to ***Ms. Shraddha B. Bhosale*** and ***Mr. Sambhaji S. Kumbhar*** for hanging in there in my sorrows and celebrations. I am thankful to my lab mates ***Tejaswini Patil***, ***Anuja Vibhute***, ***Sargun Basrani, Sayali Chougule, Tanjila Gavandi, Shivani Patil, Pranoti Kamble, Vishakha Parkhe, Mayuri Ghatage, Radhika Jadhav, Susmita Patil, Apurva Patil, Rushiraj Bhosale, Sohel Shaikh,*** and ***Shahabaj Mujawar*** for their support and wonderful help throughout the journey.

I want to thank my beloved father, ***Mr. Prashant Y. Gambhir*** for pushing me to surpass my expectations and strive for excellence. I am forever grateful to my incredible mother, ***Dr. Smita P. Gambhir*** for empowering me beyond the confines of traditional gender roles. I could not thank enough to my 'CA to be' younger brother, ***Mr. Nandan P. Gambhir*** for refining and making my thesis (also manuscripts) the best it can be. I am thankful to my younger brother, ***Mr. Tejas S. Alawani*** for every little help related to my thesis. I am thankful to ***Dr. Vidya Wagh*** for her constant support. Special thanks to my beautiful nieces ***Miraya*** and ***Radhya*** for becoming my all-time stress busters. And in the end, I am immensely grateful to my husband ***Mr. Ameya S. Joshi*** for bringing luck and bliss into my life!

Place: Kolhapur ~ Rutuja

LIST OF PATENTS, PUBLICATIONS, COPYRIGHTS, ATTENDED CONFERENCES, AND MAGAZINE ARTICLES

Patents granted/published (03):

1. A method for RNA isolation from viral/human serum samples using functionalized magnetic nanoparticle. Dr. Arpita Pandey-Tiwari, **Rutuja Prashant Gambhir**. Application no. 202221045186 (GRANTED).

2. Electrochemical biosensor apparatus for detecting stem cells. Dr. Arpita Pandey-Tiwari, **Rutuja Prashant Gambhir**, D. Y. Patil Education Society. Application no. 393145-001 (GRANTED).

3. Electrochemical method for detection of cancer. Dr. Arpita Pandey-Tiwari, Dr. Umakant M. Patil, **Rutuja Prashant Gambhir**, Shraddha B. Bhosale, Dr. C. D. Lokhande. Application no. 202321064185 (PUBLISHED).

Articles in International journals (07):

1. **Rutuja Prashant Gambhir**, Arun Kumar Parthasarathy, Shimpa Sharma, Shital Kale, Vikas Vijay Magdum, and Arpita Pandey-Tiwari. pH-responsive glycine functionalized magnetic iron oxide nanoparticles for SARS-CoV-2 RNA extraction from clinical sample. *Journal of materials science,* 57, 28 (2022): 13620 (I.F. 4.5).

2. **Rutuja Prashant Gambhir**, Sonali S. Rohiwal, Arpita Pandey-Tiwari. Multifunctional surface functionalized magnetic iron oxide nanoparticles for biomedical applications: a review. *Applied Surface Science Advances,* 11, 1 (2022): 100303 (I.F. 6.2).

3. **Rutuja Prashant Gambhir**, Shital Kale, T. D. Dongale, Snehal Patil, Dhanaji Malavekar, Arpita Pandey-Tiwari. Green synthesized magnetic nanoparticles for selective inhibition of osteosarcoma cancer. *Journal of Nanoparticle Research*. 25, 4 (2023): 83 (I.F. 2.5).

4. **Rutuja Prashant Gambhir**, Somnath Kundale, Sohel Shaikh, Arun kumar Parthasarathi, Rajanish K. Kamat, Tukaram D. Dongale, Yogendra Kumar Mishra, Arpita Pandey-Tiwari. DNA Biosensor for Hospital borne *Klebsiella pneumoniae* infections: Amplifying Electrochemical Sensing with Glycine-Modified Iron Oxide Nanoparticles. *Materials advances.* (Submitted to the Journal) (I.F. 6.6).

5. Anuja A. Vibhute, Tejaswini P. Patil, **Rutuja Prashant Gambhir**, Arpita Pandey-Tiwari. Fluorescent carbon quantum dots: Synthesis methods, functionalization and biomedical applications. *Applied Surface Science Advances*. 11, 1 (2022):100311 (I.F. 6.2).

6. Tejaswini P. Patil, **Rutuja Prashant Gambhir**, Anuja A. Vibhute, Arpita Pandey-Tiwari. Gold nanoparticles: Synthesis methods, functionalization and biological applications. *Journal of Cluster Science*. 34, 2 (2023): 705 (I.F. 2.8).

7. Mayuri M. Ghatage, Pranoti A. Mane, **Rutuja Prashant Gambhir**, Vishakha S. Parkhe, Pranoti A. Kamble, Chandrakant D. Lokhande, Arpita Pandey-Tiwari. Green synthesis of silver nanoparticles via *Aloe barbadensis miller* leaves: Anticancer, antioxidative, antimicrobial and photocatalytic properties. *Applied Surface Science Advances*. 16, 1 (2023): 100426 (I.F. 6.2).

Book chapters (01):

1. **Rutuja Prashant Gambhir,** Anuja A. Vibhute, Tejaswini P. Patil, Arpita Pandey-Tiwari, Surface-functionalized iron oxide (Fe_3O_4) nanoparticles for biomedical applications.

Book: Chemically deposited metal chalcogenide-based carbon composites for versatile applications. Springer, Cham, (2023), F. I. Ezema, C. D. Lokhande, A. C. Lokhande (Editors).

Granted copyrights (02):

1. Detection of bacterial DNA by surface functionalized magnetic nanoparticles. Dr. Arpita Pandey-Tiwari, **Rutuja Prashant Gambhir**, D. Y. Patil Education Society, Kolhapur. Application no. L-133651/2023 (GRANTED).

2. Multifunctional nanoparticles for biomedical applications. Dr. Arpita Pandey-Tiwari, **Rutuja Prashant Gambhir**, D. Y. Patil Education Society, Kolhapur. Application no. L-133610/2023 (GRANTED).

Conference/seminar/workshop participation & presentations (09):

1. **Rutuja Prashant Gambhir.** Completed one month hands-on training on '*Insilico drug designing certification*' conducted by Readmy Course Bioinformatics. (10 July 2021).

2. **Rutuja Prashant Gambhir**, Arpita Pandey-Tiwari. Presented a poster on Magnetic nanoparticle based combat against COVID-19 Virus. Dyanshodh-2022 (Search for Knowledge), conducted by Centre for Interdisciplinary Research, D. Y. Patil Education Society, Kolhapur. (28 February 2022).

3. **Rutuja Prashant Gambhir**, Arpita Pandey-Tiwari. Magnetic Nanoparticle-based combat against COVID-19 virus. International conference on emerging and re-emerging infections, conducted by D. Y. Patil medical College and Hospital, Kolhapur. (8 April 2022).

4. **Rutuja Prashant Gambhir.** Attended Industry-academia interaction and workshop on Protein purification techniques in polyclonal antibody development, conducted jointly by Centre for Interdisciplinary Research, D. Y. Patil Education Society, Kolhapur and iSERA Biological Pvt. Ltd. Shirala. (21-22 April 2022).

5. **Rutuja Prashant Gambhir.** Attended hands on training on - Synergistic training program utilizing the scientific and technological infrastructure (STUTI) sponsored by – DST, Govt. of India at Banasthali Vidyapith, Rajasthan, India. (17-23 December 2022).

6. **Rutuja Prashant Gambhir**, Arpita Pandey-Tiwari. Presented a poster and (received second prize) on Electrochemical DNA biosensing for *Klebsiella pneumoniae* infections. Dyanshodh-2023 (Search for Knowledge), conducted by Centre for interdisciplinary research, D. Y. Patil Education Society, Kolhapur. (9 March 2023).

7. **Rutuja Prashant Gambhir.** Attended webinar on Tackling dengue: a short overview of the integrated vector control strategies. Conducted jointly by Global biomedical research foundation, Chennai, and Kairos Kinetic (OPC) Pvt. Ltd., Chennai on behalf of Dr. Sree Academy. (12 October 2023).

8. **Rutuja Prashant Gambhir.** Attended seminar on 'Transforming ICUs into smart ICUs. Global biomedical research foundation, Chennai, and Kairos kinetic (OPC) Pvt. Ltd., Chennai on behalf of Dr. Sree Academy. (21 October 2023).

9. **Rutuja Prashant Gambhir**, Arpita Pandey-Tiwari. Magnetic nanoparticles: warriors against Osteosarcoma. National conference on physics of materials and materials based device fabrication 2023, conducted by Shivaji University, Kolhapur. (25-26 November 2023).

Articles for Newsletter/magazines (02):

1. **Rutuja Prashant Gambhir**, Insights into the stem cell therapy and regenerative medicine. Article published in the RuBisCo newsletter, MIT, Pune (September 2022).

2. **Rutuja Prashant Gambhir**, Stem cells – Punarnirmana che rahasya. Article published in Aadhunik Sarathi (Aarogyam) magazine (September 2021).

CONTENT

LIST OF FIGURES

LIST OF TABLES

LIST OF ABBREVIATIONS

No.	Abbreviation	Full form
1	AgNPs	Silver nanoparticles
2	APTES	3-aminopropyltriethyloxysilane
3	ASEA	Accelerated denaturation bubbles mediated strand exchange amplification
4	CBNs	Carbon-based nanoparticles
5	CNC	Carbon nanochips
6	CNTs	Carbon nanotubes
7	COVID19	Corona virus disease 2019
8	CsCl	Cesium chloride
9	CT	Computed Tomography
10	CV	Cyclic voltammetry
11	DDW	Double distilled water
12	DEAE	Diethylaminoethyl cellulose
13	DLS	Dynamic light scattering
14	DMEM	Dulbecco's modified eagle medium
15	DMSO	Dimethyl sulfoxide
16	DNA	Deoxyribo nucleic acid
17	dNTPs	Deoxynucleoside triphosphates
18	dsDNA	Double stranded deoxyribonucleic acid
19	E. coli	Escherichia coli
20	EDTA	Ethylenediamine tetraacetic acid
21	E gene	Envelope gene
22	EIA	Enzyme immunoassays
23	EIS	Electrochemical impedance spectroscopy
24	ELISA	Enzyme-linked immunosorbent assay
25	ESI	Electrospray ionization
26	EtBr	Ethidium bromide
27	FA-TEG-PGA	Folate-tetra(ethylene glycol)-poly(glycerol monoacrylate)
28	FBS	Fetal bovine serum
29	FITC	Fluorescein Isothiocyanate
30	GCE	Glassy carbon electrode
31	Glycine@Fe_3O_4	Glycine-modifying iron oxide magnetic nanoparticles
32	GO	Graphene oxide
33	GQDs	Graphene quantum dots
34	HIV	Human Immunodeficiency virus
35	IEC	Ion-exchange chromatography
36	IFA	Immunofluorescence assays
37	IONPs	Iron oxide nanoparticles
38	JCPDS	Joint committee on powder diffraction standard
39	LAMP	Loop-mediated isothermal amplification
40	LFA	Lateral flow assays
41	MALDI	Matrix-assisted laser desorption/ionization
42	MMT	Mineral montmorillonite
43	MNPs	Magnetic nanoparticles
44	MOF	Metal-organic framework
45	MPTES	Mercaptopropyltriethoxysilane
46	MRI	Magnetic resonance imaging
47	MS	Mass spectrometry
48	MTT	3-(4,5-Dimethylthiazol-2-yl)-2,5-diphenyltetrazolium bromide
49	NA	Nucleic acid
50	NAAT	Nucleic acid amplification testing
51	Nanotech	Nanotechnology
52	NCCS	National centre for cell science
53	N gene	Nucleocapsid gene

54	NGS	Next-generation sequencing
55	NPs	Nanoparticles
56	NSs	Nanosheets
57	OD	Optical density
58	PBS	Phosphate-buffered saline
59	PCR	Polymerase chain reaction
60	PDMAEMA	Poly[2-(dimethylamino)ethyl methacrylate
61	PEG	Poly-ethylene glycol
62	PEI	Polyethylenimine
63	PEO	Poly ethylene oxide
64	PLA	Poly (D, L-lactide)
65	PLL	Poly-l-lysine
66	PLT	Platelet
67	PPE	Personal protective equipment
68	PPY	Polypyrrole
69	PSA	Prostate-specific antigen
70	PVA	Poly vinyl alcohol
71	PVP	Poly vinyl pyrrolidone
72	qPCR	Real time PCR
73	RDRP	RNA dependent RNA polymerase (RDRP) genes
74	RNA	Ribonucleic acid
75	RTPCR	Reverse transcription PCR
76	SARS-CoV-2	Severe acute respiratory syndrome corona virus 2
77	SAS	Sulfasalazine
78	SEC	Size exclusion chromatography
79	SEM	Scanning electron microscopy
80	SERS	Surface–enhanced Raman scattering
81	SiRNA	Small interfering RNA
82	SPIONs	Superparamagnetic iron oxide nanoparticles
83	SQUID	Superconducting quantum interference device
84	TE	Tris acetate
85	TEM	Transmission electron microscopy
86	TGA	Therno gravimetric analysis
87	XPS	X-ray photoelectron spectroscopy
88	XRD	X-ray diffraction

Chapter 1

Introduction: Iron oxide nanoparticle-nucleic acid (DNA and RNA) conjugates

1.1. INTRODUCTION

The study of biomedical applications involving iron oxide nanoparticle-nucleic acid (IONP-NA) conjugates merges nanotechnology with biological systems. IONPs, with their unique magnetic properties, and NAs (the building blocks of genetic material) and their conjugates offer a promising avenue in various biomedical fields, including targeted drug delivery, imaging, and therapeutic interventions. Magnetic properties enable precise navigation within the body, allowing for targeted delivery of therapeutic agents to specific sites.

Research in this area aims to optimize the synthesis, and application of these conjugates, considering their biocompatibility, stability, and targeting efficiency. By exploring the conjugation of IONPs and NAs, researchers endeavor to unlock new frontiers in biomedical science, diagnostics, therapies and ultimately improving patient care.

Research based on IONPs is accelerating the development of nanotechnology. 'Nano' form of particles possesses novel optical, magnetic, and electrical properties due to quantum size effect. For example, superparamagnetic behavior will be increased and ferromagnetic behavior will deteriorate as nanoparticle size decreases [1]. **Figure 1.1** illustrates the wide range of important uses for IONPs in various fields.

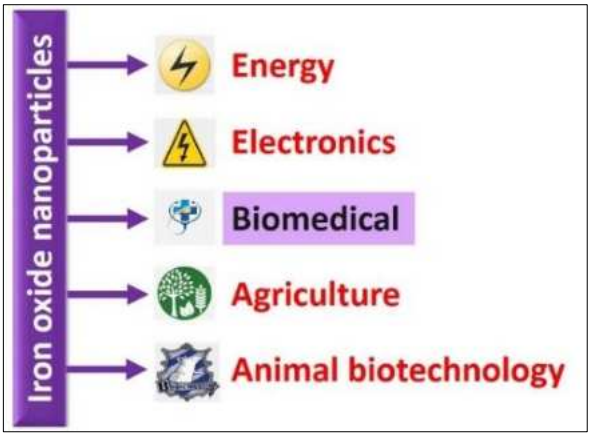

Figure 1.1. Applications of iron oxide nanoparticles (IONPs).

Uniform synthesis of IONPs can be performed by regulating parameters like temperature, concentration, pH, stirring rate, particle distribution, size control, control over shape, and nanoparticle composition

and structure, including crystallinity, and purity. Among various IONP synthesis methods (like microwave, spray pyrolysis, laser pyrolysis, pulse wire discharge, chemical vapor condensation, thermal decomposition, micro-emulsion, polyol, sol-gel, sonochemical, biological, and co-precipitation), the commonly used one is chemical co-precipitation due to its easy and rapid synthesis, cost-effectiveness, and control over size. IONPs need to follow certain criteria for their biomedical applications; (a) size should be less than 20 nm, (b) cost-effective preparation, and (c) surface should be free from any entities so that desired surface modification would be possible on it [2].

Various polymers and surfactants are used, including polyvinyl alcohol (PVA), polyvinyl pyrrolidone (PVP), polyethylene glycol (PEG), oleic acid, and polyacrylic acid (PAA) for the surface modification of IONPs. Although modification improves shape and prevents aggregation, it may change the characteristics of nanoparticles. Surfactants and polymers are very expensive and their natural degradation is difficult. As a result, their utilization limits the uses of IONPs in medicinal science and may possibly have negative environmental effects [1, 2]. To limit such drawbacks, surface modifications can be performed using biomolecules. This helps in mimicking biological system and skipping immune reactions. Biomolecules like, nucleic acids, protein can be conjugated with IONPs to carry out desired biomedical applications [3].

Nucleic acids; deoxyribonucleic acid (DNA), and ribonucleic acid (RNA) carry genetic information, which is read by cells to produce the RNA and proteins that allow living organisms to function. This genetic information is duplicated and passed on to the next generation. Adenine, guanine, cytosine, and thymine are the four bases which make up DNA. Likewise, RNA is made up of Adenine, guanine, cytosine, and uracil [4].

Both DNA and RNA are chains of related monomers and they are chemically similar. The building blocks of DNA and RNA are nucleotides that contain the nitrogenous base, phosphate, and 5-carbon ribose sugar.

Compared to DNA, RNA is more labile and does not typically form stable secondary structures [3-5].

The structural differences between DNA and RNA have been shown in **Figure 1.2**. Both RNA and DNA can be conjugated with IONPs due to their chemical resemblance [6, 7]. As mentioned earlier, DNA and RNA have some structural differences. DNA possesses deoxyribose sugar and RNA contains ribose sugar. DNA generally occurs in double stranded form and RNA often has single strand.

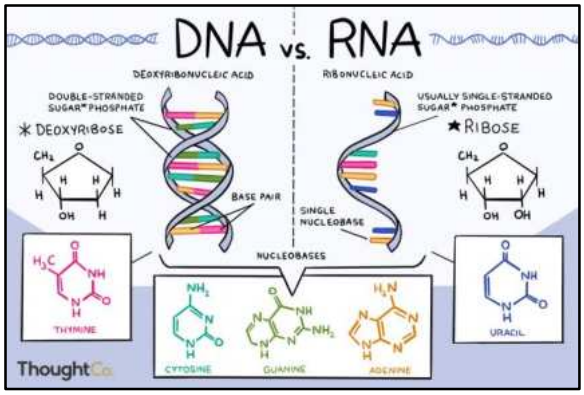

Figure 1.2. Major types of nucleic acids – DNA and RNA [4].

Irrespective of their structural differences, both DNA and RNA molecules make similar interactions with IONPs. These interactions result into IONP-NA conjugate formation.

Figure 1.3 provides visual representation of different interactions between IONPs and NA. **Figure 1.3 a** provides electrochemical interactions between temporarily-charged IONPs and negatively charged NA. These interactions are comparatively less stable due to unstable positive charge on pristine IONPs. Hence, surface modification with positively-charged entities is strongly recommended on pristine IONPs.

Figure 1.3 b provides interactions between surface-modified IONPs and NA. Surface modifications can be carried out with specific ligands or molecules to pertain positive surface charge on IONPs. Such positively-charged IONPs tend to attract negatively charged NA as shown in figure.

Further, **Figure 1.3 c** shows co-precipitation interactions. Co-precipitation involves the formation of a precipitate containing both IONPs and NA. In this process, the nanoparticles and NA are mixed in a solution containing a precipitating agent, leading to their simultaneous precipitation and co-localization. These interactions are often used to immobilize NA onto the surfaces of IONPs for various applications in biomedicine.

Figure 1.3 d gives overview of hydrogen bonding interactions between IONPs and NA. These IONPs form hydrogen bonds with NA, particularly through phosphate backbone and nitrogenous bases of NA. This interaction is specific and depends on the NA sequence. Complementary hydrogen bond formation can be utilized for the NA hybridization assays and targeted drug delivery systems.

Figure 1.3 e shows targeted non-covalent interactions which involve the formation of covalent bonds between functional groups on the surface of IONPs and specific chemical entities present in the NA. These interactions can be engineered to be highly selective and stable, allowing for the precise conjugation of NA to IONP. Targeted non-covalent interactions are essential for the design of NA-based therapeutics, gene delivery systems, and molecular imaging probes.

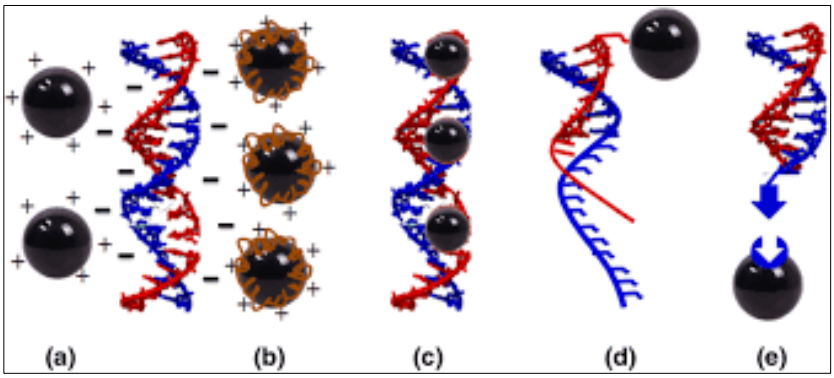

Figure 1.3. Interactions of IONP-NA conjugates; (a) pristine IONP-NA electrochemical interactions, (b) surface functionalized IONP-NA electrochemical interactions, (c) co-precipitation, (d) complementary hydrogen bonding, and (e) targeted nano-covalent interactions [8].

These conjugation interactions between IONPs and NA enhance properties like nucleic acid stability and cell permeability as well as the

biocompatibility of nanoparticles. In fact, the IONP-NA conjugate system can be used for gene analysis in diagnostics and therapeutics by utilizing the superparamagnetic properties of nanoparticles, which have a well-established role in biomedicine, in addition to the ability of NA to target DNA and RNA sequences in a very specific manner. Despite of their biomedical importance, insufficient literature is available on IONP-NA conjugates [6-9].

Hence, present thesis focuses on the study of biomedical applications that are based on IONP-NA conjugation. The study makes clear that the mechanism involved in the IONP-NA conjugation is covered with related biomedical applications like bacterial pathogen detection, magnetofection, and virus detection. The detailed description of above mentioned topics has been given below.

1.2. NANOTECHNOLOGY BASED BIOMEDICAL APPLICATIONS

Biomedical research deals with the study of science that focuses on human health and healthcare. Biomedical nanotechnology, a recent subfield of biomedicine that uses different nanomaterials (metallic, polymeric, etc.) for human well-being and health management in terms of precautions as well as therapy as shown in **Figure 1.4**. The figure shows different types of nanomaterials which are being used for biomedical applications [13-18].

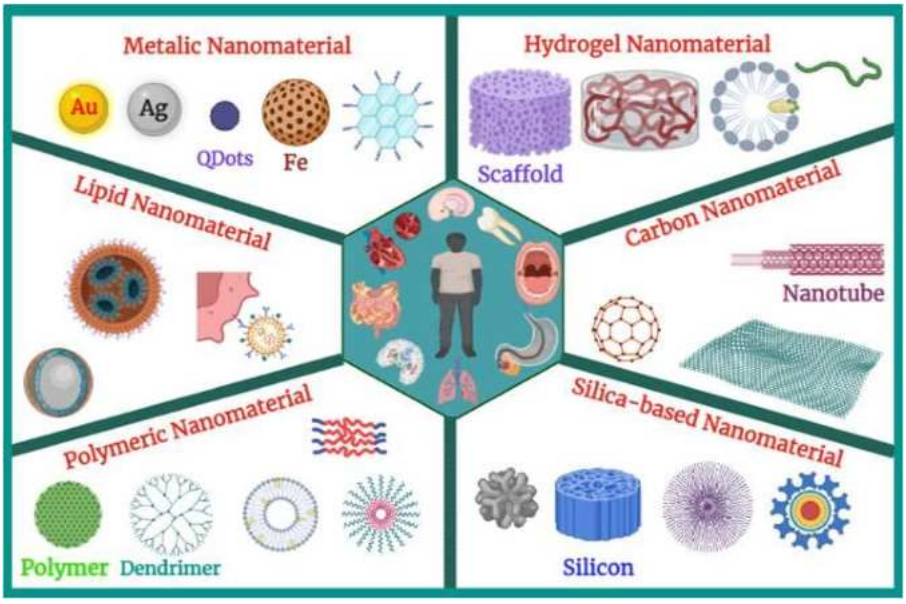

Figure 1.4. Types of nanomaterials used in biomedical applications.

The intersection of nanotechnology and the biomedical field makes cost-effective, easily available, and accessible diagnostics and therapies. Recently, nanotechnology-based personalized health care management is designed for the diagnosis and therapeutics [10]. Additionally, artificial intelligence, bioinformatics, and bio-statistical analyses can be possible by converging nanotechnology with biomedicine [11].

Nano-materials exhibit tunable surface modification, molecular, physical, optical, as well as electrochemical properties, etc. However, the choice of nanomaterial depends on the targeted application. For example, magnetic nanomaterials are being widely used as contrasting agents in magnetic resonance imaging (MRI). Likewise, gold nanoparticles are used in optical biosensors as they exhibit optical (color change) properties. They tend to detect targeted biomolecules at low concentrations. Hence, early-disease diagnosis becomes achievable. Metal nanoparticles (gold, iron oxide, and quantum dots) with a diameter one-thousandth the width of a strand of hair exhibit details about the prevalence of the diseases, and therapeutic interventions, and assess pathogen or infectious agents. The Food and Drug Administration (FDA) has approved nanoparticle-based thermal therapy, imaging, therapeutic monitoring, and iron supplements for chronic kidney disease as a result of significant investment in the research and development of nanotechnology [12].

Table 1.1 describes exosome, mxene molecule, carbon nanochips, metal nanosheets, aptamers, drugs like vancomycine, probes, polymers, grapheme-based nanocomposites, which have been tested for cancer therapy, antibacterial potential, bacteria like *Staphylococcus aureus* detection, virus like SARS-CoV-2 detection, and fungal detection, extraction of nucleic acids, etc. Nanoparticles like iron oxide, gold, silver, zinc are used for different types of biomedical studies.

Table 1.1. Nanotechnology-based biomedical applications.

No	Biomedical application	Nanomaterial involved	Interactions/mechanisms involved	Ref.
1	Targeted cancer therapy	M1-exosome nanoconjugates	Exosome-mediated CD47 antibody and CD47 surface antigen on tumor cell interactions	[5]
2	Site-specific cancer therapy	Carbon nanochips (CNC) combined with mineral montmorillonite (MMT)	CNC-MMT-mediated reactive oxygen species (ROS) generation for the destruction of site-specific tumor cells	[19]
3	Hyperthermia	Fe_3O_4 nanoparticles combined with Mxene	Fe_3O_4-Mxene-mediated photo-thermal breast tumor eradication	[20]
4	Cancer imaging and therapy	Lanthanide-based porphyrin metal-organic framework (MOF) nanosheets (NSs)	Doxorubicin-loaded MOF-NSs for cancer Imaging (by fluorescence) and targeted therapy	[21]
5	Cancer therapy	Isolongifolene-loaded chitosan nanoparticles	Nanoparticles acted as adjuvants for combating multi-drug resistant solid tumors	[22]
6	Cancer immunotherapy	sulfasalazine (SAS) and platelet (PLT) membrane-loaded mesoporous magnetic nanoparticles (Fe_3O_4)	Fe_3O_4-mediated apoptosis of cancer cells via inhibition of the glutamate-cystine antiporter system X_c^- pathway	[23]
7	Antibacterial property	ZnO-NiO nanoparticles	Against gram-positive and gram-negative microbes	[24]
8	Detection of *Staphylococcus aureus*	Fe_3O_4 conjugated with aptamer and vancomycin and gold nanoparticles	Magnet-responsive calorimetric detection of Gram negative bacteria – *S. aureus*	[25]

9	Detection of *Salmonella enterica*	Tryptamine-functionalized MNPs (Indole@MNPs)	pH-responsive electrostatic interactions between *Salmonella enterica* and indole@MNPs	[26]
10	Extraction of nucleic acids	Magnetic nanoparticles	Accelerated denaturation bubbles mediated strand exchange amplification (ASEA) using a Pasteur pipette for nucleic acid amplification testing (NAAT)	[27]
11	Detection of SARS-CoV-2	Red probe-conjugated gold nanoparticles	Calorimetric detection and absorption spectrum analysis using an achromatic nanosensor producing a green color	[28]
12	Detection of *Staphylococcus aureus*	Yellow probe-conjugated silver nanoparticles	Calorimetric detection and absorption spectrum analysis using an achromatic nanosensor producing a purple color	[28]
13	Detection of *Staphylococcus typhimurium*	Blue probe-conjugated triangle silver nanoparticles	Calorimetric detection and absorption spectrum analysis using an achromatic nanosensor producing an orange color	[28]
14	Detection of *Escherichia coli*	Polymer nanoparticles	Polymers promote ionic and electronic transport properties via antifouling	[29]
15	Detection of *Candida albicans*	Fe_3O_4 @polyethyleneimine conjugated with positively charged silver nanoparticles	Surface–enhanced Raman scattering (SERS)-mediated interactions between *Candida albicans* and positively-charged nanoparticles	[30]
16	Detection of *Staphylococcus aureus*	*S. aureus* protein A conjugated Fe_3O_4 and gold (Au) nanoparticles	Surface–enhanced Raman scattering (SERS)-label immunodetection via protein A and antibody interactions	[31]
17	Detection of *Escherichia coli*	3D graphene nanohybrids conjugated with AuNPs	Laser induction-mediated impedimetric immunosensing	[32]

18	DNA sensing	Metal-doped polydopamine nanoparticles	DNA adsorption onto polydopamine	[33]
19	DNA sensing	Acrydite-modified DNA-functionalized hydrogel	Poly-adenyl chain mediated DNA hybridization on Acrydite-modified DNA-functionalized hydrogel	[34]
20	DNA sensing	Gallium plasmonic nanoparticles	Immobilization of thiolated capture probe from Helicobacter pylori onto gallium plasmonic nanoparticles	[35]
21	MicroRNA sensing	Multipedal polydopamine nanoparticles coupled with DNA	Ca^{2+} mediated interactions between probe sequence and microRNA	[36]
22	Adenosine sensing	Hydrogel-capped magnetic mesoporous silica nanoparticles	Synthesized nanomaterial-mediated interactions between DNA-coated hydrogel and adenosine-free unit through Chemiluminescence	[37]
23	Lead ion (Pb^{+}) sensing	Copper nanomaterial based on DNA scaffold	Interactions between sticky ends on DNA and lead metal	[38]
24	DNA sensing of E. coli sequence	Neutral red molecule-conjugated quantum dots	Fluorescence and hybridization between synthesized quantum dots and single-stranded and double-stranded DNA	[39]
25	DNA sensing	Citrate-reduced gold nanoparticles	Optical response i.e. color change when interactions between particles and DNA happen	[40]

1.3. MAGNETIC NANOPARTICLES (MNPS)

MNPs are made up of the magnetic elements iron (Fe), cobalt (Co), manganese (Mn), and nickel (Ni). Due to their large spin magnetic moments and low toxicity, magnetic iron oxide nanoparticles (IONPs) are often used in biological activities.

The modification of MNPs with various substances, such as organic polymers, inorganic materials, drugs, fluorescent dyes, or antibodies, allow for their use in a broad range of biomedical domains. Recent developments using multifunctional MNPs have been made in many sectors, including biosensing and pathogen detection, magnetic resonance imaging (MRI) and biomarker tracking, magnetofection and gene therapy, hyperthermia and chemotherapy, drug delivery and targeted cell killing, bio-imaging and therapeutics, stem cell detection and therapy, tissue engineering and organ transplant, nano-vaccines and immune system activation, microbe targeting and destruction, and COVID19 prevention and treatment. MNPs are becoming increasingly popular in the fields of nanotechnology, nanomedicine, nanochemistry, nanoelectronics, and nanotherapy [42-52].

MNPs possess three layers in terms of structure: the surface layer, which shows functionalized small molecules, doped metals or polymers, antibodies, proteins, etc.; the shell layer which shows chemical components other than the prominent component; and the core layer which contains the main chemical entity, which is typically a nanoparticle [52].

Figure 1.5 suggests the synthesis of MNPs using co-precipitation method followed by their surface modification with modifying entities like carbohydrates, proteins, etc. Further, the modified MNPs are dried in the powder form and used for according biomedical applications. They are frequently being used in biomedical applications due to their intrinsic tunable physical and chemical characteristics, size, crystalline or amorphous structure, biocompatibility, cost-effectiveness, low-cost synthesis, easy availability of precursors, quick synthesis, *in-vitro* and *in-vivo* transport, magnetic switchability, versatility in surface functionalization, manipulation

in the magnetic nature of nanoparticles with an external magnetic field, etc. [53]. The figure also shows the common surface modifications of MNPs that allow them to be used in several biomedical applications.

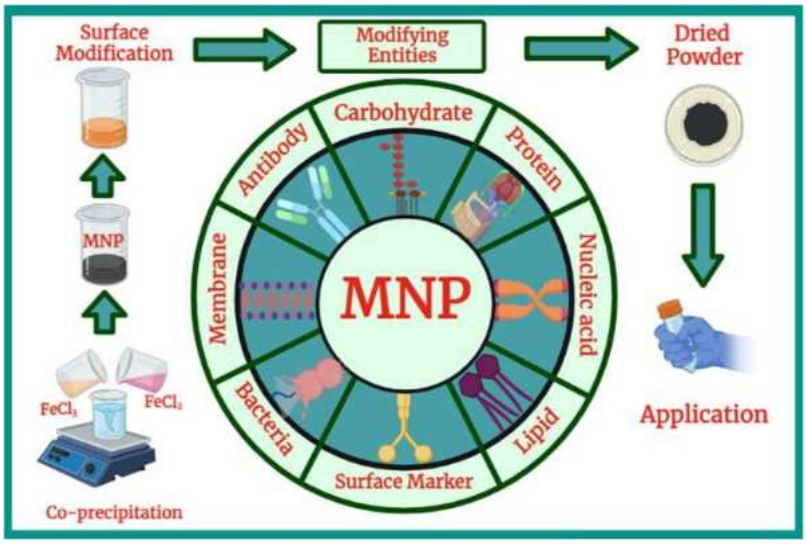

Figure 1.5. Synthesis and Surface Modification of MNPs.

1.4. IRON OXIDE NANOPARTICLES (IONPs)

Iron is the foundation of earth's chemical composition in the crust. It contributes in many biological and geological processes. Iron (Fe) and oxygen (O) combine to form IONP in its natural condition. Among many, three most prevalent types of IONPs are magnetite (Fe_3O_4), maghemite (γFe_2O_3), and hematite (αFe_2O_3) as shown in **Figure 1.6**.

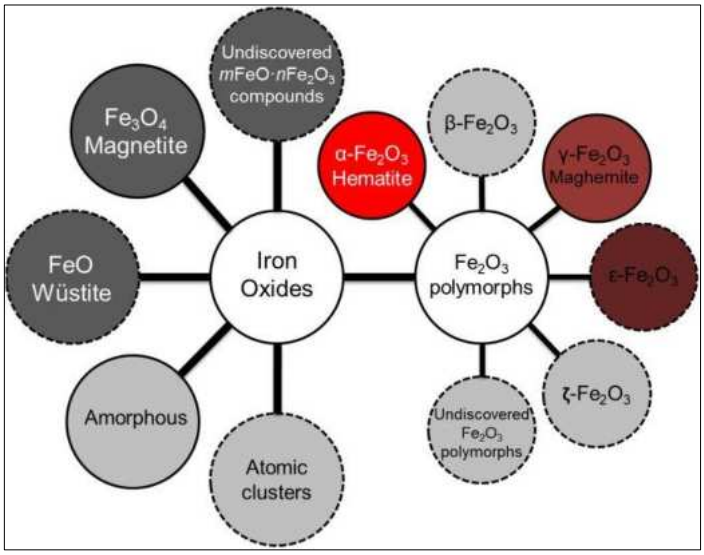

Figure 1.6. Diversity of types of magnetic iron oxide nanoparticles [54].

Hematite is produced when magnetite undergoes further oxidation. Compared to other types of IONPs, magnetite has recently attracted significant study focus. They have notable advantages including super-paramagnetism, a greater surface area, a high surface-to-volume ratio, and a quick and simple technique of separating the target molecule from the solution due to change with respect to an external magnetic field. As a result, Fe_3O_4 (magnetite) IONPs have undergone outstanding research and are being used in the disciplines of biomedicine [55].

1.5. BIOMEDICAL IMPORTANCE OF MAGNETITE (Fe_3O_4)

IONPs (particularly Fe_3O_4) have been extensively incorporated in biomedicine as discussed earlier. These Fe_3O_4 nanoparticles are surface-modified to achieve desired applications. Additionally, it is suggested that surface modification with biocompatible molecules provides overall biocompatibility to Fe_3O_4 nanoparticles [56, 57].

The surface of Fe_3O_4 can be modified with different chemical (organic or inorganic) and biological moieties depending on the area of application. Fe_3O_4 coated with organic materials have several potential uses.

Despite numerous noteworthy advancements in the synthesis of organic material-functionalized Fe_3O_4, it is still difficult to regulate the structure, stability, biocompatibility, and magnetic characteristics of these materials at the same time. Additionally, the use of Fe_3O_4 in catalysis, bio-labeling, and bio-separation is particularly promising. Silica, metal, non-metal, metal oxides, and sulfides are some of the inorganic materials used as the coating [58].

Toxicity of Fe_3O_4 can be reduced by surface functionalization with biocompatible entities (such as polymers, antibodies, aptamers, antibodies, fluorophores, etc.) that cover the entire surface of Fe_3O_4 and thereby provide biocompatibility and easy entry inside the cell and immune escape [49].

1.6. SURFACE MODIFICATION OF MAGNETITE (Fe_3O_4)

According to the data from **Table 1.2**, surface modification of Fe_3O_4 nanoparticles is occurred through three types of modifying agents viz. organic, inorganic, and biological. The selection of modifying agent is completely dependent on the availability of resources as well as targeted biomedical application.

Both natural, as well as synthetic polymers, are extensively used in cancer therapy and imaging applications as surface modifying agents. Silica, dextran, Poly D, L-lactide, PLA, PEG, PEI, and starch are commonly used as surface modifying entities. Chitosan and silica functionalized Fe_3O_4 are reported for possessing around 80 % DNA adsorption and 98 % DNA elution efficiency from human saliva samples [59]. Surface functionalization with reactive groups like –COOH, $–NH_2$, -OH, and –SH act as a surface modifiers. Mercaptopropyltriethoxysilane (MPTES)-modified Fe_3O_4 along with APTES acts against inflammation and osteoclast activity [60]. Polyethylenimine (PEI) is another molecule that provides better functionalization on the surface of Fe_3O_4 and is hence used for various applications. [61]. Another approach to exert therapeutic application for the treatment of cancer was reported by oleic acid functionalized magnetic Fe_3O_4-based hyperthermia. It was observed that the material possessed efficient tumor destruction [62].

Surface functionalization or modification by using biomolecules has been used in applications like biosensing [63]. Nucleic acids, biotin-avidin, proteins, enzymes, antibodies, and serum albumin are used in recent research [64]. Surface functionalization with inorganic materials like manganese or cobalt provides better magnetic moment whereas functionalization with gold or silver gives robust visual adsorption and higher electron density [65]. Graphite-activated carbon functionalized Fe_3O_4 are used to develop screen-printed electrode sensors which show rutin (Vitamin P) detection [66]. It was also reported that surface functionalization of Fe_3O_4 prevents their oxidation due to air and makes them efficient for related applications [67].

Table 1.2. Surface modifications of IONPs (Fe_3O_4) used for biomedical applications.

No.	Material	Modification	Multifunctional Applications	Ref.
1	Fe_3O_4	PVA	To reduce the toxicity of NPs and gas vacuole formation	[68]
2	Fe_3O_4	PEO	For intracellular targeting and cytotoxicity	[69]
3	Fe_3O_4	PDMAEMA	For targeted drug delivery and controllable release	[70]
4	Fe_3O_4	FA-TEG- PGA	MRI applications and multi-modal bioimaging.	[71]
5	Fe_3O_4	Sophorolipids	Biocompatibility and biomedical application	[72]
6	Fe_3O_4	polypyrrole (PPY)	For intracellular cancer cell targeting and hyperthermia treatment of cancer tumors.	[73]
7	Fe_3O_4	PVP	For MRI and biosensors.	[74]
8	Fe_3O_4	Chitosan	Cell targeting and hyperthermia cancer therapy	[75]
9	Fe_3O_4	Chitosan	Cancer cell targeting and hyperthermia application	[76]
10	Fe_3O_4	Dextran	Hyperthermia and chemotherapy	[77]
11	Fe_3O_4	PEG	Hyperthermia and chemotherapy	[78]
12	Fe_3O_4	PEG	For drug delivery and magnetic resonance imaging application	[79]
13	Fe_3O_4	Fluorescent polystyrene	For *in-vivo* imaging and hyperthermia application	[80]
14	Fe_3O_4	Casein	For *in-vivo* hyperthermia and chemotherapy	[81]
15	Fe_3O_4	Arginine	*Chlorella sp* harvesting and biodiesel production	[82]

16	Fe_3O_4	Natural rubber latex	Higher magnetization and stabilization for biomedical applications	[83]
17	Fe_3O_4	Arginine	Drug delivery and anti-cancer activity against breast cancer	[84]
18	Fe_3O_4	Glycan	Biosensing and pulmonary tuberculosis detection	[85]
19	Fe_2O_3	Alumina	Cathepsin B detection for drug delivery and biosensing applications	[86]
20	Fe_3O_4	Quantum dots	Optical biosensing and detection of *Streptococcus agalactiae*	[87]
21	Fe_3O_4	PSA antibody	Immunosensing and detection of prostate-specific antigen (PSA)	[88]
22	Fe_3O_4	Stem cell membrane	Targeting cancer cells and destruction of carcinoma cells	[89]
23	Fe_3O_4	Stem cell membrane	Targeted gene delivery of siRNA for photothermal therapy and gene therapy	[90]
24	Fe_3O_4	Calcium phosphate	Scaffold preparation and biocompatibility for bone tissue engineering	[91]
25	Fe_3O_4	Bacterial cellulose	Scaffold preparation and biocompatibility for bone tissue engineering	[92]

1.7. IRON OXIDE NANOPARTICLE -NUCLEIC ACID (Fe_3O_4-NA) CONJUGATES

The interaction between NA (DNA and RNA) surfaces with Fe_3O_4 leads to diagnosis and therapy of diseases. Magnetic properties of Fe_3O_4 aid in the development of risk-free and efficient gene delivery vectors for the treatment of diseases like cancer. The Fe_3O_4-NA interactions also allow diagnosis of diseases by separating and detecting NA of related pathogens. However, both of these applications face significant challenges in the advancement of their respective applications [7].

The conjugation between Fe_3O_4 and nucleic acid fragments (DNA and RNA) is a robust example of combinations of magnetic properties and target-specific selectivity that aims to enhance the capability of disease diagnosis and therapy. Fe_3O_4–NA conjugates have emerged as a novel area of research, combining the unique properties of IONPs with the functionality of NAs.

The formation of iron Fe_3O_4-NA conjugates involves a series of steps that aim to establish a stable and efficient linkage between the two components. Various strategies have been explored, such as covalent bonding, electrostatic interactions, and physical adsorption to achieve the desired conjugation. Covalent bonding methods often involve surface modifications of Fe_3O_4, allowing for the attachment of functional groups that can react with nucleic acids. Electrostatic interactions, on the other hand, rely on the charge interactions between the negatively charged nucleic acids and the positively charged iron oxide surface. Physical adsorption methods exploit the affinity of nucleic acids towards iron oxide surfaces, facilitating their non-covalent attachment [93-100].

The resulting Fe_3O_4-NA conjugates exhibit unique properties and functionalities that can be tailored based on the choice of nucleic acids and the conjugation methods employed as described in **Table 1.3**.

Table 1.3. Biomedical applications based on Fe_3O_4–NA (DNA and RNA) interactions.

No	MNP	Surface modifier	Binding entity	Biomedical activity	Ref.
1	Fe_3O_4	Silica	DNA	Binding and elution of bacterial DNA	[93]
2	Fe_3O_4	Polyacrylic acid	Pyrrolidinyl peptide	Adsorption of DNA	[94]
3	Fe_3O_4	Arabinogalactan	Aptamers	Anticancer activity – Carcinoma cells	[95]
4	Fe_3O_4	Bovine serum albumin	dsDNA	Anticancer activity - osteosarcoma cell line	[96]
5	Fe_3O_4-silica	-	DNA oligonucleotide	Pathogen (*S. aureus*) detection	[97]
6	Fe_3O_4	Hyaluron	Aptamer	Drug delivery for colorectal cancer	[98]
7	Fe_3O_4	Polyethylene glycol – polyethylenimine	siRNA	Prostate cancer gene therapy	[99]
8	Fe_3O_4	Bovine serum albumin	Genomic DNA	Adsorption and elution of calf thymus DNA	[100]
9	Fe_3O_4	Silica, Chitosan	Genomic DNA	Adsorption and purification of genomic DNA	[59]

As research in this field progresses, novel synthesis strategies and innovative applications are expected to emerge, further expanding the potential of Fe_3O_4-NA conjugates in diverse areas of science and technology.

1.8. ADSORPTION AND DESORPTION STUDIES OF IRON OXIDE NANOPARTICLES (Fe_3O_4) WITH NUCLEIC ACIDS (NA)

1.8.1 ADSORPTION STUDIES

Fe_3O_4-NA interactions possess adsorption of NA on Fe_3O_4 and desorption of NA from Fe_3O_4 in controlled manner. The on-and-off magnetic switchable properties of Fe_3O_4 pave the way into regulation of several biomedical applications.

Understanding the nature of these interactions is crucial for designing Fe_3O_4-NA conjugates and harnessing their unique properties. The interactions between IONPs and NAs can occur through different mechanisms, including electrostatic interactions, hydrophobic interactions, and specific binding [8].

Electrostatic interactions are primarily driven by the charge characteristics of both Fe_3O_4 and nucleic acids. Fe_3O_4 modified with positively charged modifier typically carry a net positive charge on their surface, whereas nucleic acids, such as DNA and RNA, possess negatively charged phosphate backbones. This charge complementarity allows for strong electrostatic interactions, facilitating the binding of nucleic acids onto the iron oxide surface [8].

Hydrophobic interactions, on the other hand, arise from the nonpolar regions of nucleic acids and the hydrophobic patches present on the surface of iron oxide nanoparticles. These interactions play a role in the adsorption and stabilization of nucleic acids onto the nanoparticle surface. Furthermore, specific binding interactions can occur between functional groups present on nucleic acids and specific ligands or surface moieties on the Fe_3O_4. These specific interactions can enhance the stability and selectivity of the conjugates, allowing for precise control over their properties. The strength

and nature of Fe_3O_4-NA interactions can be influenced by several factors, including pH and surface modifications of the nanoparticles. Understanding these factors and their impact on the interactions is crucial for optimizing the conjugation process and tailoring the properties of the resulting conjugates [8].

Overall, the study of Fe_3O_4-NA interactions provides valuable insights into the design and development of advanced functional materials. By unraveling the intricacies of these interactions, researchers can pave the way for innovative approaches in drug delivery, imaging, biosensing, and other fields, where the combination of Fe_3O_4 and nucleic acids can lead to significant advancements [7-8]. By incorporating nucleic acids, such as DNA or RNA, into Fe_3O_4, the resulting conjugates can selectively target specific cells or tissues, improving the efficacy and reducing off-target effects of therapeutic interventions. Additionally, the magnetic properties of Fe_3O_4 allow for precise imaging and tracking of the conjugates *in-vivo*, aiding in diagnosis and monitoring of diseases. Overall, Fe_3O_4-NA conjugation provides distinct biomedical applications with improved specificity, sensitivity, and therapeutic outcomes [101-103].

1.8.2. DESORPTION STUDIES

Desorption of NAs from Fe_3O_4 is an essential process to consider in applications such as controlled release or recycling of the conjugates. Several factors influence desorption of nucleic acids, including the strength of the binding interactions and the surrounding environmental conditions.

One method for elution is the use of competitive agents. By introducing molecules with a higher affinity for the nanoparticle surface, the nucleic acids can be displaced and released. For example, introducing an excess of negatively charged molecules, such as citrate ions, can compete with the negatively charged nucleic acids, leading to their detachment from the nanoparticle surface. pH can also be utilized to control elution. Altering the pH can disrupt electrostatic interactions between the positively charged Fe_3O_4 and negatively charged nucleic acids. Increasing the pH to a basic

range can weaken the binding, resulting in the release of nucleic acids. Temperature can impact elution as well. Higher temperatures can increase the mobility and energy of the nucleic acid molecules, weakening their interactions with the nanoparticle surface and promoting release. However, the temperature should be optimized to prevent the denaturation or degradation of nucleic acids.

Furthermore, enzymatic degradation can be employed for desorption. Enzymes that specifically target nucleic acids, such as nucleases, can be used to degrade the bound nucleic acids, allowing their release from the Fe_3O_4. The choice of desorption method depends on the specific application and the desired release profile. By understanding and manipulating these desorption factors, researchers can achieve controlled release of nucleic acids from Fe_3O_4, enabling precise temporal and spatial control in applications such as drug delivery, gene therapy, or recycling of the conjugates for repeated use [104].

1.9. IRON OXIDE NANOPARTICLES-NUCLEIC ACID (Fe_3O_4-NA) CONJUGATES IN BIOMEDICAL APPLICATIONS

Fe_3O_4-NA conjugates have following biomedical applications.

1.9.1. BIOMOLECULE SEPARATION

Fe_3O_4-NA conjugates can be utilized for biomolecule separation. In this approach, the conjugates are functionalized with specific affinity ligands, such as antibodies or aptamers, which can selectively bind to target biomolecules of interest. The magnetic properties of the Fe_3O_4 allow for the efficient capture and isolation of the conjugates, along with the bound biomolecules, by applying a magnetic field. Subsequently, the conjugates can be separated from the biomolecules by altering the environmental conditions, such as pH or temperature, to disrupt the conjugation. This strategy enables the rapid and specific separation of biomolecules, offering a valuable tool for various applications, including protein purification, diagnostics, and biosensing [102].

1.9.2. MAGNETO-SEPARATION OF NUCLEIC ACIDS

Magneto-separation of nucleic acids using Fe_3O_4-NA conjugates is an effective technique for their rapid and selective separation. When a magnetic field is applied, the conjugates are attracted and aggregated, facilitating the efficient capture and isolation of NAs. Subsequently, the magnetic field is removed, and the separated NAs can be collected for downstream applications. This approach eliminates the need for traditional separation methods like centrifugation or filtration, providing a simple and efficient alternative. Magneto-separation of nucleic acids using IONP-NA conjugates holds promise for various applications in biotechnology, diagnostics, and genomics research [105, 106].

1.9.3. BIOSENSING AND PATHOGEN DETECTION

Fe_3O_4-NA conjugates have emerged as promising tools for biosensing and pathogen detection due to their unique properties. These conjugates combine the high surface area and magnetic properties of Fe_3O_4 with the specific binding capabilities of NA. The nucleic acid component can be designed to target specific pathogen sequences, enabling highly sensitive and selective detection. The magnetic properties of the nanoparticles facilitate the separation and concentration of the target pathogens from complex samples. Furthermore, the conjugates can be easily functionalized with various labels or signaling molecules to achieve signal amplification or visualization. This innovative approach holds great potential for rapid and reliable pathogen detection in diverse applications, ranging from clinical diagnostics to environmental monitoring [107].

1.9.4. GENE THERAPY

Fe_3O_4-NA conjugates offer a promising platform for gene therapy applications. These conjugates leverage the unique properties of Fe_3O_4 and the specific targeting capabilities of nucleic acids. The nanoparticles can serve as efficient carriers for delivering therapeutic nucleic acids, such as plasmid DNA or small interfering RNA (siRNA), to target cells or tissues. The conjugates can be engineered to possess surface modifications that enhance

cellular uptake, protect the nucleic acids from degradation, and facilitate endosomal escape. Additionally, the magnetic properties of the nanoparticles allow for spatial and temporal control over gene delivery through the application of external magnetic fields. This innovative approach holds potential for precise and effective gene therapy treatments, addressing various genetic diseases and disorders [8].

1.9.5. STEM CELL THERAPY AND REGENERATIVE MEDICINE

Fe_3O_4-NA conjugates have emerged as a valuable tool in stem cell technology and regenerative medicine. These conjugates combine the unique properties of iron oxide nanoparticles with the therapeutic potential of nucleic acids. The nanoparticles can serve as efficient carriers for delivering nucleic acids, such as plasmid DNA or microRNAs, to stem cells. This enables targeted modulation of stem cell behavior, including differentiation, proliferation, and migration. The conjugates can also be used for tracking and imaging stem cells *in-vivo* due to their magnetic properties. Furthermore, the nanoparticles can be functionalized with specific ligands to enhance stem cell targeting and retention at the site of injury or tissue regeneration. This innovative approach holds promise for advancing stem cell-based therapies and accelerating the development of regenerative medicine strategies [108].

Biomedical applications viz. bacteria nucleic acid separation, virus pathogen detection, magnetofection in breast cancer cells were performed in subsequent chapters by maintaining the principle of magnetic iron oxide nanoparticle-nucleic acid conjugate formation.

1.10. STATEMENT OF THE PROBLEM

The optimization of iron oxide nanoparticle-nucleic acid conjugates for biomedical applications necessitates an understanding of their properties and interactions to enhance their efficacy in pathogen detection and nucleic acid delivery.

1.11. REFERENCES

[1] M. Kalita, M. M. Payne, S. H. Bossmann. **Glyco-nanotechnology: a biomedical perspective**. Nanomedicine: NBM. 2022; 42: 102542.

[2] P. Sharma, N. Holliger, P. H. Pfromm, B. Liu, V. Chikan. **Size-controlled synthesis of iron and iron oxide nanoparticles by the rapid inductive heating method**. ACS omega. 2020; 5 (31): 19853.

[3] U. Singh, V. Morya, A. Rajwar, A. R. Chandrasekaran, B. Datta, C. Ghoroi, D. Bhatia. **DNA-functionalized nanoparticles for targeted biosensing and biological applications**. ACS omega. 2020; 5 (48): 30767.

[4] A. M. Helmenstine, "**Difference between DNA and RNA**", ThoughtCo, *https://www.thoughtco.com/dna-versus-rna-608191*.

[5] W. Nie, G. Wu, J. Zhang, L. L. Huang, J. Ding, A. Jiang, Y. Zhang, Y. Liu, J. Li, K. Pu, H. Y. Xie. **Responsive exosome nano-bioconjugates for synergistic cancer therapy**. Angew. Chemie Int. Ed. 2020; 59(5): 2018.

[6] A. P. Tiwari, S. J. Ghosh, S. H. Pawar. **Biomedical applications based on magnetic nanoparticles: DNA interactions**. Anal. Methods. 2015; 7(24): 10109.

[7] Z. Zhao, H. Cui, W. Song, X. Ru, W. Zhou, X. Yu. **A simple magnetic nanoparticles-based viral RNA extraction method for efficient detection of SARS-CoV-2.** BioRxiv, 2020.

[8] J. R. Sosa-Acosta, C. Iriarte-Mesa, G. A. Ortega, A. M. Díaz-García. **DNA-iron oxide nanoparticles conjugates: functional magnetic nanoplatforms in biomedical applications.** Surface-modified Nanobiomaterials for Electrochemical and Biomedicine Applications. 2020; 378 (13): 19.

[9] M. Galli, A. Guerrini, S. Cauteruccio, P. Thakare, D. Dova, F. Orsini, P. Arosio, C. Carrara, C. Sangregorio, A. Lascialfari, D. Maggioni. **Superparamagnetic iron oxide nanoparticles functionalized by peptide nucleic acids**. Rsc Advances. 2017; 7(25): 15500.

[10] M. A. Alghamdi, A. N. Fallica, N. Virzì, P. Kesharwani, V. Pittalà, K. Greish. **The promise of nanotechnology in personalized medicine**. J. Pers. Med. 2022; 12(5): 673.

[11] K. P. Das. **Nanoparticles and convergence of artificial intelligence for targeted drug delivery for cancer therapy: Current progress and challenges**. Front. Med. Technol. 2023; 4:1067144.

[12] R. M. Williams, E. A. Jaimes, D. A. Heller. **Nanomedicines for kidney diseases**.KI. 2016; 90(4): 740.

[13] Z. Cheng, M. Li, R. Dey, Y. Chen. **Nanomaterials for cancer therapy: current progress and perspectives.** Journal of hematology & oncology. 2021; 14: 1.

[14] E. M. Steele, Z. L. Carr, E. Dosmar. **Bioprinting of Hydrogel-Based Drug Delivery Systems for Nerve Tissue Regeneration**. Biophysica. 2024; 4 (1): 58.

[15] S. Zheng, Y. Tian, J. Ouyang, Y. Shen, X. Wang, J. Luan. **Carbon nanomaterials for drug delivery and tissue engineering**. Frontiers in Chemistry. 2022; 10: 990362.

[16] A. A. Nayl, A. I. Abd-Elhamid, A. A. Aly, S. Bräse. **Recent progress in the applications of silica-based nanoparticles**. RSC advances. 2022; 12 (22): 13706.

[17] B. Begines, T. Ortiz, M. Pérez-Aranda, G. Martínez, M. Merinero, F. Argüelles-Arias, A. Alcudia. **Polymeric nanoparticles for drug delivery: Recent developments and future prospects**. Nanomaterials. 2020; 10 (7): 1403.

[18] L. Rethi, C. Mutalik, D. Anurogo, L. S. Lu, H. Y. Chu, S. Yougbaré, T. R. Kuo, T. M. Cheng, F. L. Chen. **Lipid-based nanomaterials for drug delivery systems in breast cancer therapy**. Nanomaterials. 2022; 12 (17): 2948.

[19] M. Yin, J. Tong, F. Meng, C. Liu, X. Liu, F. Fang, Z. He, X. Qin, C. Liu, D. Ni, Y. Gao, H. Liang, X. Zhang, L. Luo. **Near-infrared-II activatable symbiotic 2D carbon–clay nanohybrids for dual imaging-guided combinational cancer therapy**. ACS Appl. Mater. Interfaces. 2022; 14(44): 49471.

[20] Z. Liu, M. Zhao, L. Yu, W. Peng, Y. Chen, S. Zhang. **Redox chemistry-enabled stepwise surface dual nanoparticle engineering of 2D MXenes for tumor-sensitive T1 and T2 MRI-guided photonic breast-cancer hyperthermia in the NIR-II biowindow**. Biomater. Sci. 2020; 10(6): 1562.

[21] J. Xia, Y. Xue, B. Lei, L. Xu, M. Sun, N. Li, H. Zhao, M. Wang, M. Luo, C. Zhang, B. Huang, Y. Du. **Multimodal channel cancer chemotherapy by 2D functional gadolinium metal–organic framework**. Natl. Sci. Rev. 2021; 8(7): 221.

[22] D. Manimaran, N. Elangovan, P. Mani, K. Subramanian, D. Ali, S. Alarifi, C. P. Palanisamy, H. Zhang, K. Rangasamy, V. Palanisamy, R. Mani, K. Govarthanan, W. Aruni, R. Shanmugam, G. P. Srinivasan, A. Kalirajan. **Isolongifolene-loaded chitosan nanoparticles synthesis and characterization for cancer treatment**. Sci. Rep. 2022; 12(1): 19250.

[23] Q. Jiang, K. Wang, X. Zhang, B. Ouyang, H. Liu, Z. Pang, W. Yang. **Platelet membrane-camouflaged magnetic nanoparticles for ferroptosis-enhanced cancer immunotherapy**. Small. 2020; 16(22): 2001704.

[24] H. J. Imran, K. A. Hubeatir, K. A. Aadim. **A novel method for ZnO@NiO core-shell nanoparticle synthesis using pulse laser ablation in liquid and plasma jet techniques**. Sci Rep. 2023; 13(1): 5441.

[25] R. Sun, H. Zou, Y. Zhang, X. Zhang, L. Chen, R. Lv, R. Sheng, T. Du, Y. Li, H. Wang, Q. Yanfei. **Vancomycin recognition and induced-aggregation of**

the Au nanoparticles through freeze-thaw for foodborne pathogen Staphylococcus aureus detection. Anal. Chim. Acta. 2022; 1190(1), 339253.

[26] S. Y. Lee, F. Chen, T. Y. Lee. **Tryptamine-functionalized magnetic nanoparticles for highly sensitive detection of Salmonella typhimurium**. Analyst. 2021; 146(8): 2559.

[27] J. Kang, Y. Li, Y. Zhao, Y. Wang, C. Ma, C. Shi. **Nucleic acid extraction without electrical equipment via magnetic nanoparticles in pasteur pipettes for pathogen detection**. Anal. Biochem. 2021; 635(1): 114445.

[28] C. Y. Wen, X. Liang, J. Liu, T. Y. Zhao, X. Li, Y. Zhang, G. Guo, Z. Zhang, J. Zeng. **An achromatic colorimetric nanosensor for sensitive multiple pathogen detection by coupling plasmonic nanoparticles with magnetic separation**. Talanta; 1(1): 124271.

[29] N. Elgiddawy, S. Ren, A. Yassar, A. Louis-Joseph, H. Sauriat-Dorizon, M. A. El-Rouby, A. O. El-Gendy, A. A. Farghali, H. Korri-Youssoufi. **Dispersible conjugated polymer nanoparticles as biointerface materials for label-free bacteria detection**. ACS Appl. Mater. Interfaces; 12(36): 39979.

[30] S. Hu, H. Kang, F. Gu, C. Wang, S. Cheng, W. Gong, L. Wang, B. Gu, Y. Yang. **Rapid detection method for pathogenic Candida captured by magnetic nanoparticles and identified using SERS via AgNPs+**. Int. J. Nanomedicine. 2021; 16(1): 941.

[31] Z. Zhou, R. Xiao, S. Cheng, S. Wang, L. Shi, C. Wang, K. Qi, S. Wang. **A universal SERS-label immunoassay for pathogen bacteria detection based on Fe_3O_4@Au-aptamer separation and antibody-protein A orientation recognition**. Anal. Chim. Acta. 2021; 1160(1): 338421.

[32] Z. You, Q. Qiu, H. Chen, Y. Feng, X. Wang, Y. Wang, Y. Ying. **Laser-induced noble metal nanoparticle-graphene composites enabled flexible biosensor for pathogen detection**. Biosens. Bioelectron. 2020; 150(1): 2020.

[33]M. Zandieh, J. Liu. **Metal-doped polydopamine nanoparticles for highly robust and efficient DNA adsorption and sensing**. Langmuir. 2020; 37(30): 8953.

[34] Y. Li, H. Gao, Z. Qi, Z. Huang, L. Ma, J. Liu. **Freezing-assisted conjugation of unmodified diblock DNA to hydrogel nanoparticles and monoliths for DNA and Hg2+ sensing**. Angew. Chemie Int. Ed. 2021; 60(23): 12985.

[35] A. G. Marín, T. García-Mendiola, C. N. Bernabeu, M. J. Hernández, J. Piqueras, J. L. Pau, F. Pariente, E. Lorenzo. **Gallium plasmonic nanoparticles for label-free DNA and single nucleotide polymorphism sensing**. Nanoscale. 2016; 8(18): 9842.

[36] T. Bao, R. Fu, Y. Jiang, W. Wen, X. Zhang, S. Wang. **Metal-mediated polydopamine nanoparticles–DNA nanomachine coupling**

electrochemical conversion of metal–organic frameworks for ultrasensitive MicroRNA sensing. Anal. Chem. 2021; 93(40): 13475.

[37] Y. Hou, R. Han, Y. Sun, C. Luo, X. Wang. **Chemiluminescence sensing of adenosine using DNA cross-linked hydrogel-capped magnetic mesoporous silica nanoparticles**. Anal. Chim. Acta. 2022; 1195(1): 39386.

[38] M. Li, Y. N. Cai, C. F. Peng, X. L. Wei, Z. P. Wang. **DNA dendrimer–templated copper nanoparticles: self-assembly, aggregation-induced emission enhancement and sensing of lead ions**. Microchimica. 2021; 188(1): 1.

[39] E. Martínez-Periñán, A. Martínez-Sobrino, I. Bravo, T. García-Mendiola, E. Mateo-Martí, F. Pariente, E. Lorenzo. **Neutral red-carbon nanodots for selective fluorescent DNA sensing**. Anal. Bioanal. Chem. 2022; 414(18): 5537.

[40]S. Khurana, S. Kukreti, M. Kaushik. **Designing a two-stage colorimetric sensing strategy based on citrate reduced gold nanoparticles: sequential detection of Sanguinarine (anticancer drug) and visual sensing of DNA**. Spectrochim. Acta Part A Mol. Biomol. Spectrosc. 2021; 246(1): 119039.

[41] K. Wu, R. Saha, D. Su, V. D. Krishna, J. Liu, M. C. Cheeran, J. P. Wang. **Magnetic-nanosensor-based virus and pathogen detection strategies before and during COVID-19**. ACS Applied Nano Materials. 2020; 3(10): 9560.

[42] A. Avasthi, C. Caro, E. Pozo-Torres, M. P. Leal, M. L. García-Martín. **Magnetic nanoparticles as MRI contrast agents**. Surface-modified Nanobiomaterials for Electrochemical and Biomedicine Applications. 2020; 378(3): 49.

[43] A. A. Sizikov, M. V. Kharlamova, M. P. Nikitin, P. I. Nikitin, E. L. Kolychev. **Nonviral locally injected magnetic vectors for in vivo gene delivery: A review of studies on magnetofection**. Nanomaterials. 2021; 11(5): 1078.

[44] R. Montes-Robles, H. Montanaro, M. Capstick, J. Ibáñez-Civera, R. Masot-Peris, E. García-Breijo, N. Laguarda-Miró, R. Martínez-Máñez. **Tailored cancer therapy by magnetic nanoparticle hyperthermia: A virtual scenario simulation method**. Comput. Methods Programs Biomed. Update. 2020; 226:107185.

[45] J. F. Liu, B. Jang, D. Issadore, A. Tsourkas. **Use of magnetic fields and nanoparticles to trigger drug release and improve tumor targeting**. Wiley Interdiscip. Rev. Nanomed. Nanobiotechnol. 2019; 11(6): 1571.

[46] A. Mohsin, M. H. Hussain, M. Z. Mohsin, W. Q. Zaman, M. S. Aslam, A. Shan, Y. Dai, I. M. Khan, S. Niazi, Y. Zhuang, M. Guo. **Recent advances of magnetic nanomaterials for bioimaging, drug delivery, and cell therapy**. ACS Appl. Nano Mater. 2022; 5(8): 10118.

[47] Y. Chen, S. Hou. **Application of magnetic nanoparticles in cell therapy**. Stem Cell Res. Ther. 2022; 13(1): 1.

[48] A. Dasari, J. Xue, S. Deb. **Magnetic nanoparticles in bone tissue engineering**. Nanomaterials. 2022; 12(5): 757.

[49] L. Huang, Z. Liu, C. Wu, J. Lin, N. Liu. **Magnetic nanoparticles enhance the cellular immune response of dendritic cell tumor vaccines by realizing the cytoplasmic delivery of tumor antigens**. Bioeng. Transl. Med. 2023; 8(2): 10400.

[50] C. Xu, O. U. Akakuru, J. Zheng, A. Wu. **Applications of iron oxide-based magnetic nanoparticles in the diagnosis and treatment of bacterial infections**. Front. Bioeng. Biotechnol. 2019; 7(141): 1.

[51] R. P. Gambhir, S. S. Rohiwal, A. P. Tiwari. **Multifunctional surface functionalized magnetic iron oxide nanoparticles for biomedical applications: a review**. Appl. Surf. Sci. Adv. 2022; 11: 100303.

[52] I. Khan, K. Saeed, I. Khan. **Nanoparticles: Properties, applications and toxicities**. Arab. J. Chem. 2019; 12(7): 908.

[53] K. Wu, D. Su, J. Liu, R. Saha, J. P. Wang. **Magnetic nanoparticles in nanomedicine: a review of recent advances**. Nanotechnology. 2019; 30(50): 502003.

[54] K. G. Gareev. **Diversity of iron oxides: mechanisms of formation, physical properties and applications**. Magnetochemistry. 2023; 9(5): 119.

[55] V. Manescu, G. Paltanea, I. Antoniac, M. Vasilescu. **Magnetic nanoparticles used in oncology**. Materials (Basel). 2021; 14(20): 5948.

[56] G. Cotin, S. Piant, D. Mertz, D. Felder-Flesch, S. Begin-Colin. **Iron oxide nanoparticles for biomedical applications: Synthesis, functionalization, and application**. InIron Oxide Nanoparticles Biomed. Appl. 2018; 1(1): 43.

[57] N. Zhu, H. Ji, P. Yu, J. Niu, M. U. Farooq, M.W. Akram, I. O. Udego, H. Li, X. Ni. **Surface modification of magnetic iron oxide nanoparticles**. Nanomaterials. 2018; 8(10): 810.

[58] W. Wu, Q. He, C. Jiang. **Magnetic iron oxide nanoparticles: synthesis and surface functionalization strategies.** Nanoscale Res. Lett. 2008; 1(1): 397.

[59] A. P. Tiwari, R. K. Satvekar, S. S. Rohiwal, V. A. Karande, A. V. Raut, P. G. Patil, P. B. Shete, S. J. Ghosh. **Magneto-separation of genomic deoxyribose nucleic acid using pH responsive Fe_3O_4@silica@chitosan nanoparticles in biological samples**. Rsc Adv. 2015; 5(11): 8463.

[60] K. Marycz, K. Kornicka-Garbowska, A. Patej, P. Sobierajska, A. Kotela, E. Turlej, M. Kepska, A. Bienko, R. Wiglusz. **Aminopropyltriethoxysilane**

(APTES)-modified nanohydroxyapatite (nHAp) incorporated with iron oxide (IO) nanoparticles promotes early Osteogenesis, reduces inflammation and inhibits osteoclast activity. Materials (Basel). 2022; 15(6): 2095.

[61] C. A. Albornoz, M. A. Paulin, A. A. Cristóbal, D. R. Vega, A. G. Leyva, C. P. Ramos. **Microwave-assisted hydrothermal nanoarchitectonics of polyethyleneimine-coated iron oxide nanoparticles**. Appl. Phys. A. 2022; 128(1): 1.

[62] O. A. Kulikov, M. N. Zharkov, V. P. Ageev, D. E. Yakobson, V. I. Shlyapkina, A. V. Zaborovskiy, V. I. Inchina, L. A. Balykova, A.M. Tishin, G. B. Sukhorukov, N. A. Pyataev. **Magnetic hyperthermia nanoarchitectonics via iron oxide nanoparticles stabilised by oleic acid: anti-tumour efficiency and safety evaluation in animals with transplanted carcinoma**. Int. J. Mol. Sci. 2022; 23(8): 4234.

[63] J. M. George, A. Antony, B. Mathew. **Metal oxide nanoparticles in electrochemical sensing and biosensing: a review**. Microchim. Acta. 2018; 185(7): 1.

[64] M. Magro, D. Baratella, G. Miotto, J. Frömmel, M. Šebela, M. Kopečná, E. Agostinelli, F. Vianello. **Enzyme self-assembly on naked iron oxide nanoparticles for aminoaldehyde biosensing**. Amino Acids. 2019; 51(4): 679.

[65] C. Chen, J. Ge, Y. Gao, L. Chen, J. Cui, J. Zeng, M. Gao. **Ultrasmall superparamagnetic iron oxide nanoparticles: a next generation contrast agent for magnetic resonance imaging**. Nanomed. Nanobiotechnol. 2022; 14(1): 1740.

[66] M. Elancheziyan, S. Ganesan, K. Theyagarajan, M. Duraisamy, K. Thenmozhi, C. Weng, Y. Lin, V. K. Ponnusamy. **Novel biomass-derived porous-graphitic carbon coated iron oxide nanocomposite as an efficient electrocatalyst for the sensitive detection of rutin (vitamin P) in food and environmental samples**. Environ. Res. 2022; 211(1): 113012.

[67] J. Darson, M. Mohan. **Iron oxide nanoparticles and nano-composites: an efficient tool for cancer theranostics**. In Iron Oxide Nanoparticles Intechopen. 2022; 1(1): 1.

[68] M. Mahmoudi, A. Simchi, M. Imani, M. A. Shokrgozar, A. S. Milani, U. O. Häfeli, P. Stroeve. **A new approach for the in vitro identification of the cytotoxicity of superparamagnetic iron oxide nanoparticles**. Colloids Surf. B. 2010; 75(1): 300.

[69] U. O. Häfeli, J. S. Riffle, L. H. Shekhawat, A. C. Baranauskas, F. Mark, J. P. Dailey, D. Bardenstein. **Cell uptake and in vitro toxicity of magnetic nanoparticles suitable for drug delivery**. Mol. Pharm. 2009; 6(5): 1417.

[70] L. Zhou, J. Yuan, W. Yuan, X. Sui, S. Wu, Z. Li, D. Shen. **Synthesis, characterization, and controllable drug release of pH-sensitive hybrid magnetic nanoparticles**. J. Magn. Magn. Mater. 2009; 321(18): 2799.

[71] Q. Zhang, C. Wang, L. Qiao, H. Yan, K. Liu. **Superparamagnetic iron oxide nanoparticles coated with a folate-conjugated polymer**. J. Mater. Chem. 2009; 19(44): 8393.

[72] N. Baccile, R. Noiville, L. Stievano, I. V. Bogaert. **Sophorolipids-functionalized iron oxide nanoparticles**. Phys. Chem. Chem. Phys. 2013; 15(5): 1606.

[73] S. C. Wuang, K. G. Neoh, E. T. Kang, D. W. Pack, D. E. Leckband. **Synthesis and functionalization of polypyrrole-Fe_3O_4 nanoparticles for applications in biomedicine**. J. Mater. Chem. 2007; 17(31): 3354.

[74] H. L. Liu, S. P. Ko, J. H. Wu, M. H. Jung, J. H. Min, J. H. Lee, B. H. An, Y. K. Kim. **One-pot polyol synthesis of monosize PVP-coated sub-5 nm Fe_3O_4 nanoparticles for biomedical applications**. J. Magn. Magn. Mater. 2007; 310(2): e815.

[75] J. Qu, G. Liu, Y. Wang, R. Hong. **Preparation of Fe_3O_4–chitosan nanoparticles used for hyperthermia**. Adv. Powder Technol. 2010; 21(4): 461.

[76] K. H. Bae, M. Park, M. J. Do, N. Lee, J. H. Ryu, G. W. Kim, C. G. Kim, T. G. Park, T. Hyeon. **Chitosan oligosaccharide-stabilized ferrimagnetic iron oxide nanocubes for magnetically modulated cancer hyperthermia**. ACS Nano. 2012; 6(6): 5266.

[77] C. L. Dennis, A. J. jackson, J. A. Borchers, R. Inkov, A. R. Foreman, P. J. Hoopes, R. Strawbridge, Z. Pierce, E. Goerntiz, J. W. Lau. **The influence of magnetic and physiological behaviour on the effectiveness of iron oxide nanoparticles for hyperthermia**. J. Phys. D. Appl. Phys. 2008; 41(13): 134020.

[78] R. Ghosh, L. Pradhan, Y. P. Devi, S. S. Meena, R. Tewari, A. Kumar, S. Sharma, N. S. Gajbhiye, R. K. Vatsa, B. N. Pandey, R. S. Ningthoujam. **Induction heating studies of Fe_3O_4 magnetic nanoparticles capped with oleic acid and polyethylene glycol for hyperthermia**. J. Mater. Chem. 2011; 21(35):13388.

[79] M. M. Yallapu, S. P. Foy, T. K. Jain, V. Labhasetwar. **PEG-functionalized magnetic nanoparticles for drug delivery and magnetic resonance imaging applications**. Pharm. Res. 2010; 27(11): 2283.

[80] X. Zhang, W. Lin, S. Chen, H. Xu, H. Gu. **Development of a stable dual functional coating with low non-specific protein adsorption and high sensitivity for new superparamagnetic nanospheres**. Langmuir. 2011; 27(22): 13669.

[81] M. S. Bani, S. Hatamie, M. Haghpanahi. **Biocompatibility and hyperthermia cancer therapy of casein-coated iron oxide nanoparticles in mice**. Polym. Adv. Technol. 2020; 31(7): 1544.

[82] P. Liu, T. Wang, Z. Yang, Y. Hong, X. Xie, Y. Hou. **Effects of Fe_3O_4 nanoparticle fabrication and surface modification on Chlorella sp. harvesting efficiency**. Sci. Total Environ. 2020; 704: 135286.

[83] S. Arsalani, E. J. Guidelli, J. F. D. F. Araujo, A. C. Bruno, O. Baffa. **Green synthesis and surface modification of iron oxide nanoparticles with enhanced magnetization using natural rubber latex**. ACS Sustain. Chem. Eng. 2018; 6(11): 13756.

[84] E. Attari, H. Nosrati, H. Danafar, and H. Kheiri Manjili. **Methotrexate anticancer drug delivery to breast cancer cell lines by iron oxide magnetic based nanocarrier**. J. Biomed. Mater. Res. Part A. 2019; 107(11): 2492.

[85] C. Gordillo-Marroquín, A. G. Velasco, H. J. Sanchez-Perez, K. Pryg, J. Shinners, N. Murray, S. G. Munoz-Jimenez, A. Bencomo-Alerm, A. Gomez-Bustamante, L. Jonapa-Gomez, N. Enriquez-Rios, M. Martin, N. Romero-Sandoval, E. C. Alocilja. **Magnetic nanoparticle-based biosensing assay quantitatively enhances acid-fast Bacilli Count in paucibacillary pulmonary tuberculosis**. Biosensors. 2018; 8(4): 128.

[86] J. T. Domagalski, E. Xifre-Perez, M. A. Tabrizi, J. Ferre-Borrull, L. F. Marsal. **Magnetic nanoparticle decorated anodic alumina nanotubes for fluorescent detection of cathepsin B**. J. Colloid Interface Sci. 2021; 584: 236.

[87] R. Ghasemi, S. Z. Mirahmadi-zare, M. H. Nasr-Esfahani, A. Allafchian, M. Behmanesh. **Optical biosensing of Streptococcus agalactiae based on core/shell magnetic nanoparticle-quantum dot**. Anal. Bioanal. Chem. 2019; 411(25): 6733.

[88] A. Farshchi, F., Hasanzadeh, M., Mokhtarzadeh. **A novel electroconductive interface based on Fe_3O_4 magnetic nanoparticle and cysteamine functionalized AuNPs: Preparation and application as signal amplification element to minoring of antigen-antibody immunocomplex and biosensing of prostate cancer**. J. Mol. Recognit. 2020; 33(4): 2825.

[89] L. Bu, L. Rao, G. T. Yu, L. Chen, W. W. Deng, J. F. Liu, H. Wu, Q. F. Meng, S. S. Guo, X. Z. Zhao, W. F. Zhang, G. Chen, Z. Gu, W. Liu, Z. J. Sun. **Cancer stem cell-platelet hybrid membrane-coated magnetic nanoparticles for enhanced photothermal therapy of head and neck squamous cell carcinoma**. Adv. Funct. Mater. 2019; 29(10): 1807733.

[90] X. Mu, J. Li, S. Yan, H. Zhang, W. Zhang, F. Zhang, J. Jiang. **siRNA delivery with stem cell membrane-coated magnetic nanoparticles for imaging-**

guided photothermal therapy and gene therapy. ACS Biomater. Sci. Eng. 2018; 4(11): 3895.

[91] F. D. Cojocaru, V. Balan, M. I. Popa, A. Lubiuc, A. antoniac, I. V. Antoniac, L. Verestiuc. **Biopolymers – calcium phosphates composites with inclusions of magnetic nanoparticles for bone tissue engineering**. Int. J. Biol. Macromol. 2019; 125: 612.

[92] S. Torgbo, P. Sukyai. **Fabrication of microporous bacterial cellulose embedded with magnetite and hydroxyapatite nanocomposite scaffold for bone tissue engineering**. Mater. Chem. Phys. 2019; 237: 121868.

[93] I. J. Bruce, T. Sen. **Surface modification of magnetic nanoparticles with alkoxysilanes and their application in magnetic bioseparations**. Langmuir. 2005; 21(15): 7029.

[94] S. Khadsai, N. Seeja, N. Deepuppha, M. Rutnakornpituk, T. Vilaivan, M. Nakkuntod, B. Rutnakornpituk. **Poly (acrylic acid)-grafted magnetite nanoparticle conjugated with pyrrolidinyl peptide nucleic acid for specific adsorption with real DNA**. Colloids Surf. B. 2018; 165(1): 243.

[95] O. S. Kolovskaya, T. N. Zamay, G. S. Zamay, V. A. Babkin, E. N. Medvedeva, N. A. Neverova, A. K. Kirichenko, S. S. Zamay, I. N. Lapin, E. V. Morozov, A. E. Sokolov, A. A. Narodov, D. G. Fedorov, F. N. Tomilin, V. N. Zabluda, Y. Alekhina, K. A. Lukyanenko, Y. E. Glazyrin, V. A. Svetlichnyi, M. V. Berezovski, A. S. Kichkailo. **Aptamer-conjugated superparamagnetic ferroarabinogalactan nanoparticles for targeted magnetodynamic therapy of cancer**. Cancers (Basel). 2020; 12(1): 216.

[96] P. M. Jurek, K. Zabłocki, U. Waśko, M. P. Mazurek, J. Otlewski, F. Jelen. **Anti-FGFR1 aptamer-tagged superparamagnetic conjugates for anticancer hyperthermia therapy**. Int. J. Nanomedicine. 2017; 12(1): 2941.

[97] B. A. Borsa, B. G. Tuna, F. J. Hernandez, L. I. Hernandez, G. Bayramoglu, M. Y. Arica, V. C. Ozalp. **Staphylococcus aureus detection in blood samples by silica nanoparticle-oligonucleotides conjugates**. Biosens. Bioelectron. 2016; 86(1): 27.

[98] C. Chen, S. Zhou, Y. Cai, F. Tang. **Nucleic acid aptamer application in diagnosis and therapy of colorectal cancer based on cell-SELEX technology**. NPJ Precis. Oncol. 2017; 1(1): 37.

[99] R. Panday, A. M. Abdalla, M. Yu, X. Li, C. Ouyang, G. Yang. **Functionally modified magnetic nanoparticles for effective siRNA delivery to prostate cancer cells in vitro**. J. Biomater. Appl. 2020; 34(7): 952.

[100] A. P. Tiwari, S. S. Rohiwal, M. V. Suryavanshi, S. J. Ghosh, S. H. Pawar. **Detection of the genomic DNA of pathogenic α-proteobacterium Ochrobactrum anthropi via magnetic DNA enrichment using pH responsive BSA@Fe_3O_4 nanoparticles prior to in-situ PCR and electrophoretic separation**. Microchim. Acta. 2016; 183: 675.

[101] L. Abarca-cabrera, P. Fraga-garcia, Berensmeier. **Bio-nano interactions: binding protens, polysaccharides, lipids, and nucleic acids onto magnetic nanoparticles**. Biomater. Res. 2021; 25(1): 1.

[102] A. G. Pershina, A. E. Sazonov, V. D. Filimonov. **Magnetic nanoparticles-DNA interactions: design and applications of nanohybrid systems**. Russ. Chem. Rev. 2014; 83(4): 299.

[103] H. H. P. Yu, L. Bouffier, P. Boldrin, J. Long, J. B. Claridge, M. J. Rosseinsky. **Comprehensive study of DNA binding on iron (II, III) oxide nanoparticles with a positively charged polyamine three-dimentional coating**. Langmuir. 2013; 29(36): 11354.

[104] A. V. Tyumentseva, R. N. Yaroslavtsev, S. V. Stolyar, A. T. Saitova, E. S. Tyutrina, A. S. Gorbenko, M. A. Stolyar, I. A. Olkhovskiy. **Silica-coated iron oxide nanoparticles for DNA isolation for molecular genetic studies in hematology**. Genet. Test. Mol. Biomark. 2021; 25(9): 611.

[105] L. T. Nguyen, N. H. Thi Le, H. K. Thi Ta, K. D. Nguyen. **Isolation of DNA from Arthrospira platensis and whole blood using magnetic nanoparticles (Fe_3O_4@OA and Fe_3O_4@OA@SiO_2)**. J. Anal. Sci. Technol. 2022; 13(1): 1.

[106] T. B. Gerzsenyi, A. M. Llosvai, G. Szilagyi, M. Szori, C. Varadi, B. Viskolcz, L. Vanyorek, E. S. Doroghazi. **Simplified and efficient method for production of manganese ferrite magnetic nanoparticles and their application in DNA isolation**. Int. J. Mol. Sci. 2023; 24(3): 2156.

[107] J. M. George, A. Antony, B. Mathew. **Metal oxide nanoparticles in electrochemical sensing and biosensing: a review**. Microchim. Acta. 2018; 185(7): 1.

[108] B. Cao, P. Qui, C. Mao. **Mesoporous iron oxide nanoparticles prepared by polyacrylic acid etching and their application in gene delivery to mesenchymal stem cells**. Microsc. Res. Tech. 2013; 76(9): 936.

Chapter 2

Synthesis, characterization, and analysis of biological properties of glycine-modified iron oxide nanoparticles

2.1. INTRODUCTION

The synthesis of Fe_3O_4 nanoparticles for biomedical applications involves the fabrication of nano-scale (1-100 nm) materials with specific characteristics and functionalities. Various synthesis methods such as co-precipitation, thermal decomposition, and sol-gel processes have been employed to produce Fe_3O_4 with precise control over their size and composition [1, 2] as shown in **Figure 2.1**.

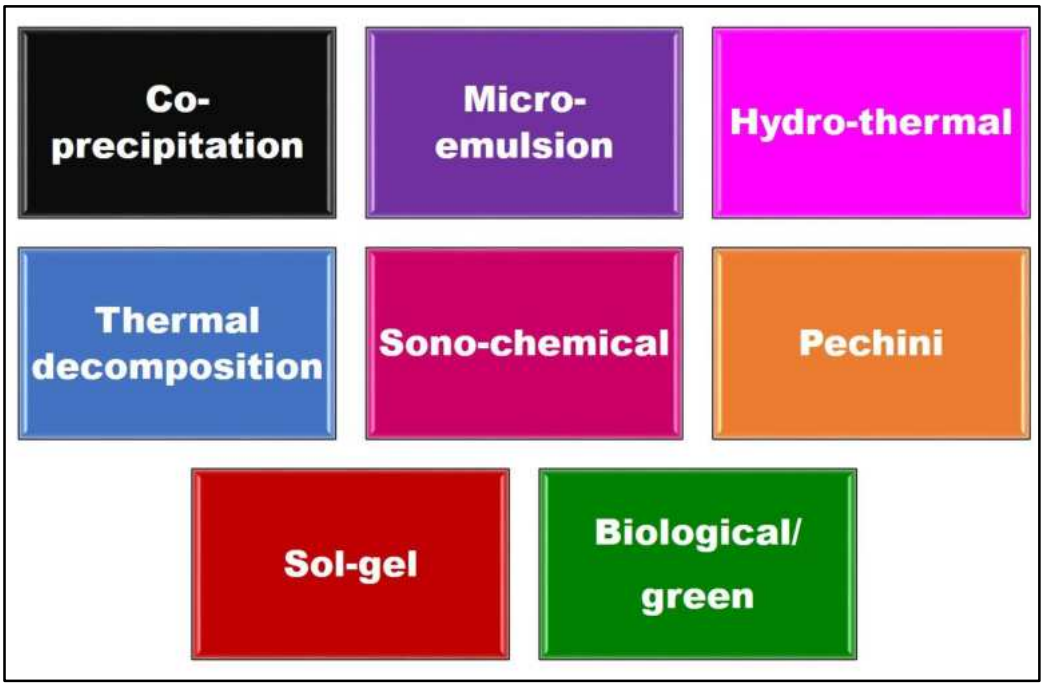

Figure 2.1. Synthesis methods of iron oxide nanoparticles (Fe_3O_4).

However, it's important to note that the choice of synthesis method should be based on the specific needs of the application. Other methods, such as sol-gel, thermal decomposition, hydrothermal, and microemulsion, have their own advantages and disadvantages as described in **Table 2.1**. The selection of the most suitable method considers the desired properties of the Fe_3O_4, specific requirements of applications, and the expertise and resources available to the researcher. It's important to choose the method that aligns "best" with the research goals.

Table 2.1. Synthesis methods for Fe_3O_4, their advantages and disadvantages [3-10].

No.	Method	Advantages	Disadvantages
1	Microemulsion	Precise control, high stability, scalable, versatile, and environment friendly.	Complex formulation, limited applicability, time consuming, cost, complex purification, and energy intensive.
2	Hydrothermal	Control over size and shape, high purity, crystalline structure, improved magnetic properties, and uniformity.	High temperature and pressure, energy intensive, complex equipment, limited scalability, reaction time, and environmental loss.
3	Thermal decomposition	Control over particle properties, versatility, high purity, cost-effective, and scalability.	Precursor's sensitivity, complex precursor synthesis, special equipment, and reaction time.
4	Sonochemical	Rapid reaction, precise control, and versatile precursors.	Complex equipment, safety concern, and potential agglomeration.
5	Pechini	Broad applicability, simplicity, chelating agents, and uniformity.	Limited scalability, specialized equipment, safety concern, long reaction time.
6	Sol-gel	Homogeneity, tailored composition, uniform dispersion, and chemical purity.	Energy consumption, limited scalability, safety concern, and specialized equipment.
7	Green synthesis	Environment friendly, sustainable, low energy consumption, and biocompatible.	Variable product quality, complex optimization, limited control, biological contamination, and scale-up challenges.
8	**Co-precipitation**	**Simple, cost-effective, high yield, magnetic properties, control over size, easily available precursors, and less equipment.**	**Agglomeration, requirement of high temperature, and surface modification required.**

2.2. CHEMICAL CO-PRECIPITATION: THE TOP CHOICE

The choice of the "best" method for synthesizing Fe_3O_4 depends on the specific requirements of the application and the desired properties of the nanoparticles. The chemical co-precipitation method has several advantages that make it a preferred choice. Following are some reasons in favor of chemical co-precipitation as synthesis method [11]. Chemical co-precipitation is a relatively simple and cost-effective method. It doesn't require specialized equipment or complex procedures. This method typically results in a high yield of nanoparticles, making it suitable for large-scale production. By adjusting reaction conditions, such as temperature, pH, and reactant concentrations, researchers can control the size of the nanoparticles, offering a degree of customization. Fe_3O_4 synthesized using this method often exhibit strong magnetic properties, which are essential for applications like magnetic targeting, drug delivery, and magnetic resonance imaging (MRI). It can be used to synthesize various iron oxide phases, such as magnetite (Fe_3O_4) and maghemite (γ-Fe_2O_3), depending on the reaction conditions.

2.3. ADDRESSING CO-PRECIPITATION DISADVANTAGES

Overcoming the disadvantages associated with the chemical co-precipitation synthesis of Fe_3O_4 requires careful consideration and often involves various strategies. To reduce polydispersity, the reaction conditions are optimized such as temperature, pH, and reactant concentrations. Tighter control of these parameters can lead to a narrower size distribution.

Surface modification methods like ligand exchange or coating with stabilizing agent are employed to prevent agglomeration of Fe_3O_4. These methods are performed during synthesis or post-synthesis of Fe_3O_4. Application of ultrasonication can be used to disperse and break up agglomerates, promoting better dispersion of the Fe_3O_4. Purification techniques such as dialysis, centrifugation, or size exclusion chromatography can be employed to remove contaminants or impurities

introduced during the synthesis process. By implementing these strategies, researchers can significantly improve the outcomes of chemical co-precipitation synthesis of Fe_3O_4 and reduce the impact of its inherent disadvantages [12].

2.4. MODIFYING IRON OXIDE NANOPARTICLES (Fe_3O_4) WITH AMINO ACIDS

Surface modification of Fe_3O_4 with amino acids holds significant importance in various fields of research and applications due to its unique properties and advantages.

Surface modification with amino acids enhances the biocompatibility of Fe_3O_4. Amino acids are natural compounds found in living organisms, and their presence on the nanoparticle surface can reduce potential toxicity and immunogenicity. This makes them suitable for various biomedical applications, such as drug delivery, diagnostics, and therapeutics. Amino acids act as capping agents, forming a stable and protective layer around the nanoparticles. Amino acids have functional groups (e.g., amine and carboxyl groups) that can serve as anchor points for further bioconjugation. This allows for the attachment of various molecules, including NAs, drugs, and antibodies, targeting ligands, and imaging agents, to the nanoparticle surface [13].

Consequently, modified nanoparticles can be tailored for specific tasks, such as targeted drug delivery or molecular imaging. Fe_3O_4 are valued for their magnetic properties, which are crucial in applications like magnetic resonance imaging (MRI). Surface modification with amino acids can preserve or even enhance these magnetic properties, making them ideal for improving the performance of contrast agents used in medical imaging. They are pivotal in tailoring these nanoparticles for specific applications, particularly in the fields of medicine and nanotechnology. The advantages include biocompatibility, stability, and the ability to attach various functional groups, enhancing their value in drug delivery, diagnostics, imaging, and other areas of scientific and technological advancement [13].

2.5. CHOOSING AMINO ACID - GLYCINE AS A SURFACE MODIFIER

Glycine is an amino acid that holds significant importance in biomedical applications due to its diverse roles and functions in biological systems. Glycine acts as a neurotransmitter in the central nervous system, where it plays a crucial role in transmitting inhibitory signals. It helps to regulate neuronal excitability and is involved in motor control and the processing of sensory information [14]. As one of the 20 standard amino acids, glycine is an essential amino acid for protein synthesis. It is a building block for various proteins, including enzymes, receptors, and structural components of cells [15]. It is a vital component of collagen, the most abundant protein in the human body. Collagen provides structural support to tissues, including skin, tendons, ligaments, and blood vessels. Thus, glycine is essential for wound healing and tissue repair [16]. It is a key component in the synthesis of glutathione, a powerful antioxidant. Glutathione helps protect cells from oxidative stress and plays a crucial role in detoxification processes within the body [17]. It has an anti-inflammatory properties and can modulate the immune response. It is being studied for its potential in managing inflammatory diseases and conditions [18].

It has been investigated for its neuroprotective effects and potential in the treatment of neurodegenerative diseases, such as Alzheimer's and Parkinson's disease [19]. It is involved in various metabolic pathways, including the one-carbon metabolism cycle. It contributes to the synthesis of DNA, RNA, and various metabolites, making it important for cell growth and division [20]. It has been studied for its potential role in improving sleep quality. It may help individuals fall asleep more quickly, stay asleep longer, and experience better sleep quality [21]. Due to its involvement in collagen production and tissue repair, glycine is considered important in the healing of wounds, burns, and surgical incisions [22]. Emerging research suggests that glycine and glycine receptors may be implicated in neuropsychiatric disorders like schizophrenia and bipolar disorder, opening up new avenues for therapeutic interventions [23]. It is available as a dietary supplement and

is commonly used to promote overall health and well-being, particularly for its potential calming and anti-anxiety effects [22].

Therefore, glycine plays a multifaceted role in various biological processes and has significant relevance in biomedical applications. Its involvement in neurotransmission, protein synthesis, collagen formation, antioxidant defenses, and metabolic regulation underscores its importance in maintaining health and addressing a range of medical conditions. Researchers continue to explore and uncover the potential therapeutic benefits of glycine in the field of biomedicine. Hence, the glycine was chosen as a surface modifier of Fe_3O_4 to carry out different biomedical applications further.

2.6. SIGNIFICANCE OF SYNTHESIS OF GLYCINE-MODIFIED IRON OXIDE NANOPARTICLES (glycine@Fe_3O_4)

Glycine-modified iron oxide nanoparticles (glycine@Fe_3O_4) hold major significance in biomedical applications due to their unique properties and versatility such as biocompatibility, stability, dispersion, etc. These nanoparticles may offer a wide range of applications, including gene delivery, imaging, biosensing, and targeted therapies, making them valuable tools for addressing various biomedical challenges. The chapter focuses on synthesis of glycine@Fe_3O_4 by chemical co-precipitation method and further the synthesized particles were characterized for the validation of synthesis.

2.7. EXPERIMENTAL

2.7.1. MATERIALS

Ferric ($FeCl_3.6H_2O$) and ferrous ($FeCl_2.4H_2O$) chlorides, Sodium hydroxide (NaOH), and Glycine ($C_2H_5NO_2$) were purchased from Himedia Pvt. Ltd. Double distilled water (DDW) was used for all processes. Absolute ethanol (C_2H_6O) was purchased from the local market. *Klebsiella pneumoniae* (*K. pneumoniae*) strain and breast cancer MCF-7 cells were collected from Dr. D. Y. Patil Medical College, Hospital and Research Centre, Kolhapur, India and National Centre for Cell Science (NCCS), Pune, India for biological characterizations of synthesized material, respectively. Dulbecco's modified

eagle medium (DMEM), fetal bovine serum (FBS), trypsin, and antibiotics (penicillin, streptomycin) were purchased from Himedia Pvt. Ltd. for cell culture experiments. 3-(4,5-dimethylthiazol-2-yl)-2,5-diphenyl-2H-tetrazolium bromide (MTT) assay kit was purchased from Himedia Pvt. Ltd.

2.7.2. INSTRUMENTATION

Scanning electron microscopy (SEM, JSM-7900F, JEOL, Japan), XRD instrument (Rigaku miniflex diffractometer), X-ray photoelectron spectroscopy (XPS, K alpha plus), transmission electron microscopy (TEM, JEM-2010, JEOL, Japan. 200 kV), and Raman spectroscopy (Model: Flex G, Tokyo Instruments) were used for physicochemical characterizations of synthesized nanoparticles.

2.7.3. METHODOLOGY

The chemical co-precipitation synthesis of glycine@Fe_3O_4 was conducted in this study. Ferric ($FeCl_3.6H_2O$) and ferrous ($FeCl_2.4H_2O$) in 2:1 molar ratio were dissolved in a double distilled water (DDW). Simultaneously, glycine solution with 0.16 M was added in the solution which acted as a surface modifier. 2 M sodium hydroxide (NaOH) was prepared and added drop wise to the iron precursor solution. The addition of the base solution initiated the precipitation process. The reaction mixture was vigorously stirred using a magnetic stirrer to promote homogeneous mixing at 250 rpm for 2 hours to allow sufficient time for nucleation and growth of the nanoparticles. The washing process was repeated until the supernatant became clear, indicating the removal of contaminants. Finally, the synthesized glycine@Fe_3O_4 were dried at room temperature to remove any residual solvent. The dried nanoparticles were stored in a suitable container for further characterizations.

2.7.4. PHYSICO-CHEMICAL CHARACTERIZATIONS

Crystal structure and phase composition of synthesized material were determined by X-ray diffraction (XRD) analysis. The dried glycine@Fe_3O_4 nanoparticles were ground to a fine powder. The powdered

sample was then carefully loaded onto a glass slide, ensuring uniform distribution. The XRD analysis was performed using a X-ray diffractometer with Cu Kα radiation (λ = 1.5406 Å). The instrument was operated at a voltage of 40 kV and a current of 40 mA. The scanning range was set from 3° to 80° (2θ). The diffraction peaks were matched with standard reference patterns available in the Joint Committee on Powder Diffraction Standards (JCPDS) database.

The scanning electron microscopy (SEM) images of the glycine@Fe_3O_4 were examined in this study. The purpose was to analyze the morphology and surface characteristics of the nanoparticles. The SEM images were captured using a scanning electron microscope (SEM, JSM-7900F, JEOL, Japan), and the samples were prepared by depositing a thin layer of glycine@Fe_3O_4 onto a conductive substrate.

A drop of glycine@Fe_3O_4 suspension was placed onto a carbon-coated copper grid and allowed to air dry for transmission electron microscopy (TEM) analysis. This step ensured glycine@Fe_3O_4 adhered to the grid surface and formed a thin, dispersed layer suitable for TEM imaging. The TEM analysis was performed using a transmission electron microscope operating at an acceleration voltage of 200 kV. The carbon-coated copper grid with glycine@Fe_3O_4 sample was loaded onto the specimen holder of the microscope. The instrument was carefully aligned, and the objective aperture was adjusted for optimal imaging. Multiple images were captured at various magnifications to obtain a representative view of the nanoparticle morphology and size distribution. Particle size distribution was determined by measuring the diameters of individual nanoparticles in the images. At least 20 nanoparticles were measured to ensure statistical significance. The images were also examined to assess the overall morphology and shape of the nanoparticles.

The surface composition and chemical states of magnetic nanoparticles can be estimated using X-ray Photoelectron Spectroscopy (XPS) analysis. The XPS analysis was conducted using a high-resolution XPS instrument (Thermo scientific K-Alpha +). The glycine@Fe_3O_4 sample was

loaded into the analysis chamber, and the pressure inside the chamber was reduced to an appropriate level. The instrument was calibrated and aligned to ensure accurate measurements. Monochromatic X-rays were used to excite the sample and the emitted photoelectrons were detected and analyzed. A survey scan was performed to obtain an overview of the elemental composition present on the nanoparticle surface. High-resolution scans were performed to analyze the chemical states of the detected elements. The XPS instrument focused on specific energy ranges associated with each element of interest. Narrow energy windows were scanned to obtain detailed information about the bonding environments and oxidation states. The binding energies of the observed peaks were determined by referencing to the appropriate energy standard.

Dynamic Light Scattering (DLS) is a widely employed technique for studying the size distribution and stability of nanoparticles in solution by measuring the fluctuations in light intensity caused by their Brownian motion. Glycine@Fe_3O_4 sample was obtained for the analysis. The dispersion was carefully prepared by adding the glycine@Fe_3O_4 to the cell culture medium with continuous sonication to ensure uniform mixing. The dispersion was allowed to equilibrate for a specific period to ensure stable glycine@Fe_3O_4 nanoparticle suspension. Disposable cuvettes were cleaned and dried thoroughly to eliminate any contamination. The cuvette was filled with the prepared glycine@Fe_3O_4 dispersion. The cuvette was placed inside the sample holder of the DLS instrument, ensuring that it was properly aligned. The measurement parameters, including temperature and measurement duration, were set as per the instrument specifications and the desired experimental conditions. The DLS analysis was initiated and the instrument recorded the scattered light intensity as a function of time. After completing the measurements, the cuvette was removed from the instrument. The glycine@Fe_3O_4 nanoparticle dispersion was discarded properly and the cuvette was cleaned thoroughly for subsequent use. The data obtained from the DLS instrument were saved for further analysis.

Zeta potential is a parameter that provides information about the surface charge and stability of nanoparticles in a dispersion. The

glycine@Fe_3O_4 sample was dispersed in a distilled water at a predetermined concentration 1 mg/mL. The dispersion was prepared by adding the glycine@Fe_3O_4 to the solvent while continuous sonication for 6-8 hours to ensure uniform mixing. The cuvette was filled with the prepared nanoparticle dispersion using a pipette, taking care not to introduce air bubbles. The cuvette was placed inside the sample holder of the zeta potential analyzer, ensuring proper alignment. The zeta potential analysis was initiated, and the instrument measured the electrophoretic mobility of the nanoparticles.

Raman spectroscopy is a powerful technique for characterizing the vibrational modes and chemical composition of materials. The sample was placed on a clean and dry sample holder. The sample was spread evenly and thinly on the sample holder to ensure a uniform layer of glycine@Fe_3O_4. The sample holder with the glycine@Fe_3O_4 was positioned on the stage of the Raman spectrometer. The Raman spectra obtained were saved for further analysis.

2.7.5. BIOLOGICAL PROPERTIES

2.7.5.1. CYTOTOXICITY ASSAY

Assessing the cytotoxicity assay of glycine@Fe_3O_4 is crucial for their safety and potential in biomedical applications. The glycine@Fe_3O_4 nanoparticles were prepared for the *in-vitro* cytotoxicity analysis. Breast cancer MCF-7 cells were used to examine cytotoxicity of glycine@Fe_3O_4. The cell culture medium – high glucose Dulbacco's modified eagle media (DMEM) was prepared according to standard manufacturer's protocol {Himedia Pvt. Ltd. (AL251)}. Cell culture plates were labeled and filled with DMEM. The cells were seeded onto the plates at a predetermined cell density of 1×10^5 cells/mL. The plates were incubated at appropriate conditions (37°C temperature and 5% CO_2 levels) to allow cell attachment and growth. After the cells reached the desired confluence, different concentrations (0-100 µg/mL) of both pristine Fe_3O_4 and glycine@Fe_3O_4 nanoparticles were added individually to the cells-containing wells followed by incubation for 30 minutes. The cells were washed gently with sterile phosphate-buffered

saline (PBS) to remove any residual nanoparticles or medium. Further, 3-(4,5-dimethylthiazol-2-yl)-2,5-diphenyl tetrazolium bromide (MTT) reagent was added into the plates and incubated for 1 hour. After the incubation, the MTT reagent was carefully aspirated from the wells. The formazan crystals were solubilized by adding an appropriate volume of dimethyl sulfoxide (DMSO) to each well. The absorbance of each well was measured using a UV-visible spectrometer at the 620 nm.

2.7.5.2. ANTIMICROBIAL GROWTH KINETICS ASSAY

Nutrient broth (SUK: M002) and agar media (SUK: M001) were prepared by following standard protocols of Himedia Pvt. Ltd. The microbial strain (*Klebsiella pneumoniae*) was cultured in the sterile nutrient broth to obtain a pure culture. Sterile test tubes were labeled and filled with a suitable volume of nutrient agar media. Pristine Fe_3O_4 and glycine@Fe_3O_4 nanoparticles were weighed accurately with the concentration of 100 µg/mL. A series of dilutions of the nanoparticles were prepared in sterile centrifuge tubes to obtain different concentrations within the range of 0 to 100 µg/mL. A predetermined volume (100 µL) of the microbial inoculum was added to each tube containing the pristine and glycine@Fe_3O_4, and ensuring proper mixing. The tubes were incubated at an appropriate temperature (37°C) and for 24 hours for the microbial growth. After the incubation period, UV-visible absorbance at 600 nm of bacterial (*Klebsiella pneumoniae*) suspension was taken, allowing the antimicrobial activity of the magnetic nanoparticles to take effect. The antimicrobial activity was assessed by comparing the absorbance with control samples (e.g., bacteria treated with standard antibiotic).

2.8. RESULTS AND DISCUSSION

The glycine@Fe_3O_4 nanoparticles were synthesized by chemical co-precipitation method. To identify the significance of surface modification of Fe_3O_4 with glycine, prepared nanoparticles (glycine@Fe_3O_4) were compared with pristine Fe_3O_4 nanoparticles. These nanoparticles were characterized and their biological properties were tested.

2.8.1. X-RAY DIFFRACTOMETER ANALYSIS (XRD)

XRD patterns of pristine Fe_3O_4 and glycine@Fe_3O_4 are represented in **Figure 2.2**. The diffraction peaks are assigned to (220), (311), (400), (422), (511), (440), and (533) crystallographic planes with space group Fd3m. The observed planes correspond to cubic crystal structure with lattice parameter of a= 8.31 Å, b= 8.31 Å, and c= 8.31 Å and peaks are matching with JCPDS card no. 75-0449.

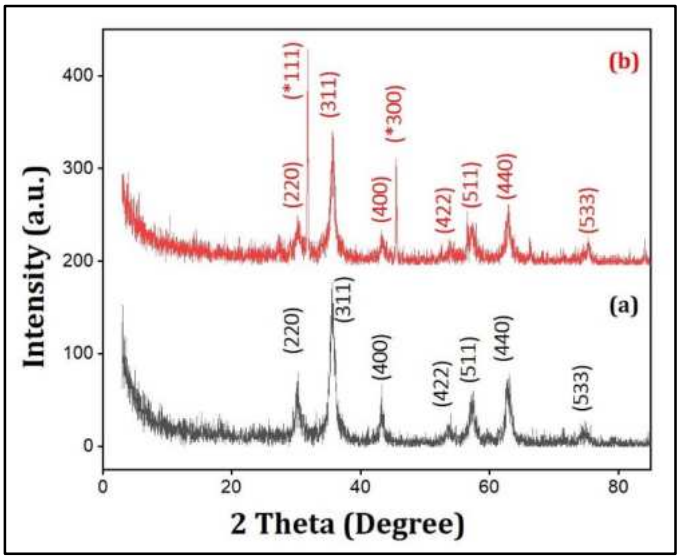

Figure 2.2. X-ray diffractometer (XRD) analysis of synthesized (a) pristine Fe_3O_4, and (b) glycine@Fe_3O_4 nanoparticles.

Interestingly, the XRD patterns of glycine@Fe_3O_4 show additional sharp diffraction peaks (marked by *) at (111) and (300), which are not present in pristine Fe_3O_4. These relatively sharper diffraction peaks may be attributed by the presence of glycine in glycine@Fe_3O_4 [24]. It is noteworthy that the addition of glycine did not affect the diffraction pattern of pristine Fe_3O_4 suggesting the successful surface modification of glycine onto the Fe_3O_4.

2.8.2. SCANNING ELECTRON MICROSCOPY (SEM)

SEM images were taken to obtain surface morphology and surface characterization. **Figure 2.3 a** shows SEM image of pristine Fe_3O_4 nanoparticles which have majority of the nanoparticles with nearly cuboidal (or hybrid) shape at 30 kX magnification. Further, **Figure 2.3 b** shows SEM image of glycine@Fe_3O_4 nanoparticles with morphology same as pristine

Fe_3O_4. Hence, SEM micrographs interpret that morphology of Fe_3O_4 remains unaffected after glycine modification.

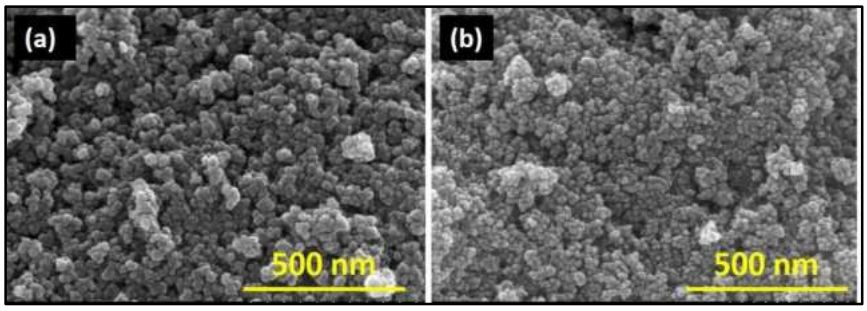

Figure 2.3. Scanning electron microscopy (SEM) photographs of (a) pristine Fe_3O_4 at 30kX magnification, and (b) glycine@Fe_3O_4 at 30kX magnification.

2.8.3. TRANSMISSION ELECTRON MICROSCOPY (TEM)

Figure 2.4 a shows pristine Fe_3O_4 with distorted size distribution and nearly cuboidal morphology same as glycine@Fe_3O_4 in **Figure 2.4 b.** It may be concluded that, Fe_3O_4 remains unaffected after surface modification with glycine.

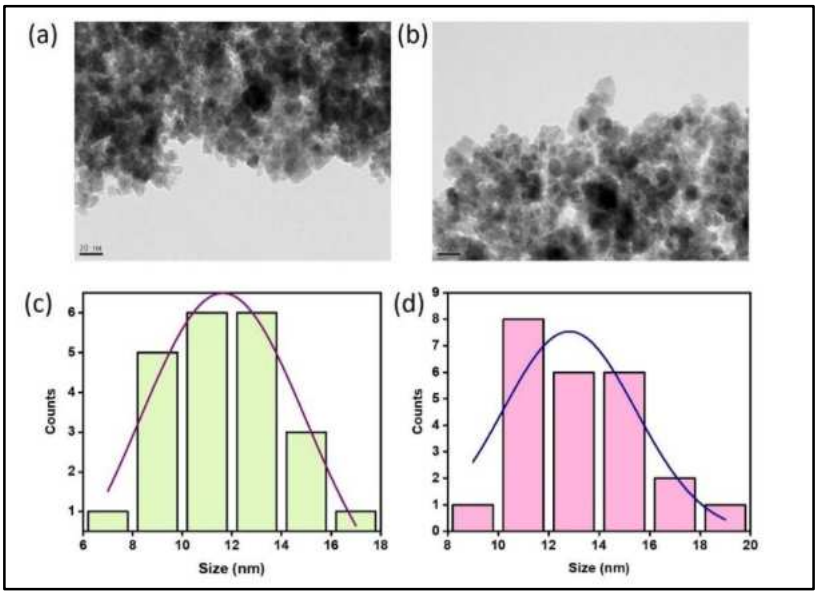

Figure 2.4. Transmission electron microscopy (TEM) photographs at 100kX magnification of (a) pristine Fe_3O_4, (b) glycine@Fe_3O_4 and histograms of (c) pristine Fe_3O_4, and (d) glycine@Fe_3O_4.

Further, the size count of pristine Fe_3O_4 and glycine@Fe_3O_4 nanoparticles is performed manually using Image J software in **Figure 2.4 c and d,** respectively. TEM histograms have size of 11.63 ± 0.28 nm and 12.82 ± 0.74 nm for pristine Fe_3O_4 and glycine@Fe_3O_4 nanoparticles, respectively.

The slight increase in size is observed in glycine@Fe_3O_4 than that of pristine Fe_3O_4, which may conclude the addition of glycine onto the Fe_3O_4 nanoparticles.

2.8.4. X-RAY PHOTOELECTRON SPECTROSCOPY ANALYSIS (XPS)

The XPS shows the presence of iron and carbon on the surface of Fe_3O_4 in **Figure 2.5 a**. The iron spectrum exhibited peaks correspond to Fe2p2 and Fe2p1 at binding energies of 709.21 and 723.40 eVs, respectively. The oxygen peak corresponds to 539.5 eV and the carbon peak corresponds to C1s at 284.6 eV binding energies. The XPS results confirmed the successful synthesis of Fe_3O_4 with surface composition primarily consisting of iron and oxygen. In **Figure 2.5 b**, iron peaks correspond to Fe2p2 and Fe2p1 at binding energies of 709.21 and 723.4 eVs, respectively. The oxygen peak corresponds to 539.5 eV and the carbon peak corresponds to C1s at 284.6 eV. The nitrogen peak at 495 eV indicates presence of nitrogen at the surface [25].

The glycine@Fe_3O_4 nanoparticle contains additional peak of nitrogen than that of pristine Fe_3O_4. The chemical formula of glycine is $C_2H_5NO_2$. This provides evidence for the glycine modification of Fe_3O_4.

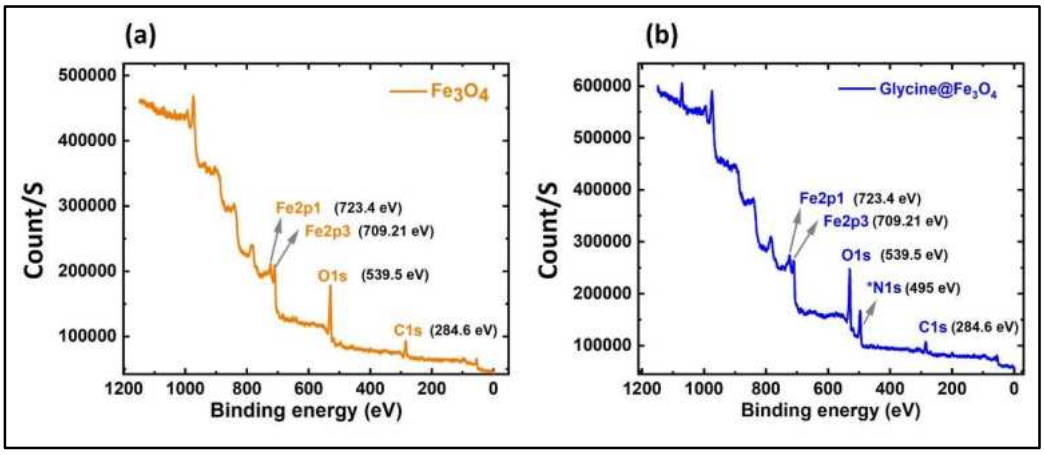

Figure 2.5. XPS analyses of (a) pristine Fe_3O_4 depicting the presence of Fe, O and C in the sample, and (b) glycine@Fe_3O_4 depicting the presence of Fe, O, N and C in the sample.

2.8.5. DYNAMIC LIGHT SCATTERING ANALYSIS (DLS)

The hydrodynamic size of pristine Fe_3O_4 and glycine@Fe_3O_4 through DLS was determined to be around 18 ± 3.57 and 70 ± 9.77 nm in **Figure 2.6 a and b**, respectively. The hydrodynamic size of glycine@Fe_3O_4 has been increased. The hydrodynamic size is measured because all experiments in the thesis have been carried out in an aqueous solution. The DLS gives overall size of particle in liquid state as particles behave differently in liquid medium due to electrostatic and non-electrostatic interactions present at the surface of the particles [26].

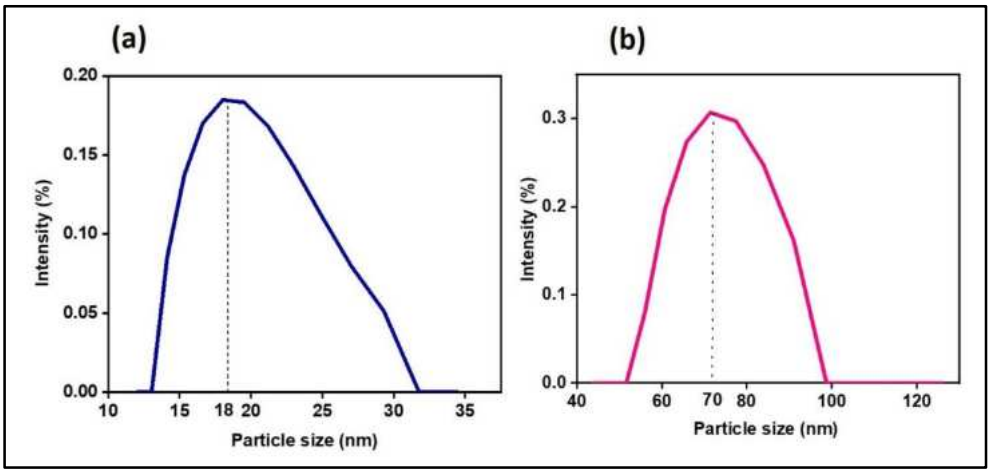

Figure 2.6. DLS analysis of (a) pristine Fe_3O_4, and (b) glycine@Fe_3O_4 nanoparticles.

2.8.6. ZETA POTENTIAL ANALYSIS

The zeta potential of pristine Fe_3O_4 and glycine@Fe_3O_4 is -27 and +35 mV, respectively as shown in **Figure 2.7**. It is considered that if the zeta potential is in between the range of -30 to +30 mV, the particles remain stable in the respective medium [27, 28]. Both the particles are stable in the cell culture medium which provides a promise for further applications. The surface charge for pristine Fe_3O_4 is negative while it is positive for glycine@Fe_3O_4, which confirms the presence of positively charged glycine on the surface of the Fe_3O_4 nanoparticles.

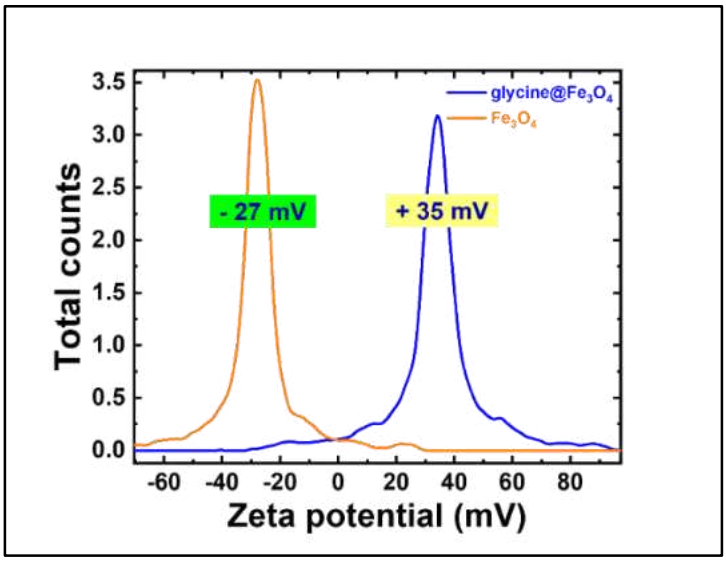

Figure 2.7. Zeta potential analysis of pristine Fe_3O_4 (orange color) shows negative surface charge with the value –27 mV, and glycine@Fe_3O_4 (blue color) shows positive surface charge with the value + 35 mV.

2.8.7. RAMAN SPECTROSCOPY ANALYSIS

In **Figure 2.8 a**, pristine Fe_3O_4 nanoparticles have a distinct peak near 650 nm, confirming the magnetite phase of the synthesized material (Fe_3O_4) [29]. The lack of additional peaks demonstrates that Fe_3O_4 is a weak Raman scatterer. With the addition of NH, OH, and CH_2 stretchings, pristine glycine exhibits the Raman scattering effect over a broad range (**Figure 2.8 b**). NH and OH-stretching can be seen in the peaks above 2000 cm^{-1} (3007, 2972, 2806, and 2595 cm^{-1}). The deformed carbon is represented by the peak at 1576 cm^{-1}. Peaks at 1412, 1320, 1143, 1033, and 899 cm^{-1} are stretchings of the CH_2 molecule. However, the interactions between the outer surface atoms of the glycine molecule and the water molecule (solvent) are indicated by the peaks at 700, 604, 501, 369, 200, 120, and 82 cm^{-1} [30]. The peak at 2146 cm^{-1} in **Figure 2.8 c** represents OH-stretching. Peaks at 672 and 613 cm^{-1} indicate the presence of Fe_3O_4, and the peak at 1318 cm^{-1} exhibits CH_2 stretching. Peaks at 404, 305, and 232 cm^{-1} are visible on the spectrum, indicating that the composite sample also contains traces of Fe_2O_3 [31-33].

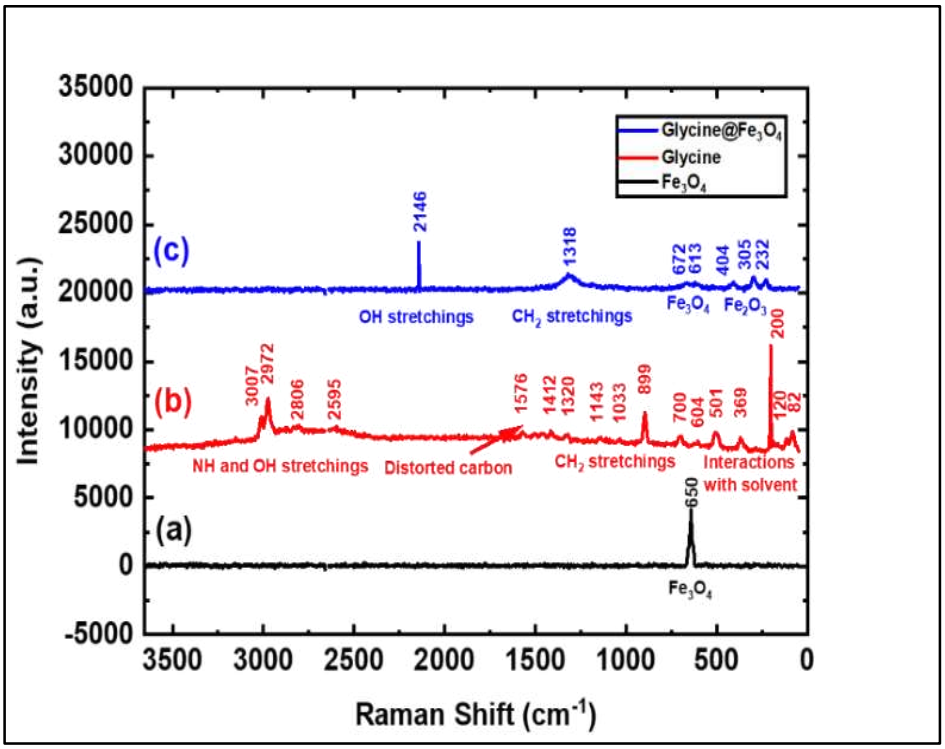

Figure 2.8. Raman spectroscopy analysis of (a) pristine Fe_3O_4, (b) pristine glycine, and (c) glycine@Fe_3O_4.

The significant Fe_3O_4 peak at 650 nm is absent in glycine@Fe_3O_4 nanoparticles. That means, whole surface of Fe_3O_4 is covered by glycine. The Raman analysis confirms the complete surface modification on Fe_3O_4 nanoparticles with the glycine molecule.

2.8.8. BIOLOGICAL PROPERTIES

2.8.8.1. CYTOTOXICITY ANALYSIS

In subsequent chapter, glycine@Fe_3O_4 nanoparticles need to be tested for DNA magnetofection inside the breast cancer cells (MCF-7). To employ safe DNA magnetofection, these prepared nanoparticles should not be toxic to the cells. Hence, cytotoxic potential of glycine@Fe_3O_4 along with the pristine Fe_3O_4 was assessed by using MTT cytotoxicity analysis.

This analysis reveals the impact of synthesized nanoparticles on cell viability as shown in **Figure 2.9**. Lesser cytotoxicity leads to the higher cell viability. 10-100 µg/mL nanoparticles (both pristine Fe_3O_4 and glycine@Fe_3O_4) concentrations were tested individually on breast cancer MCF-7 cells. Whereas 0 µg/mL concentration denotes positive control

(untreated cells). Results show that 97.00 ± 0.30 %, 94.30 ± 0.31 %, 87.42 ± 0.26 %, 87.24 ± 0.27 %, and 56.57 ± 0.38 % cell viability for the 10 µg/mL, 25 µg/mL, 50 µg/mL, 75 µg/mL, and 100 µg/mL glycine@Fe_3O_4 concentrations, respectively. Whereas, 70.50 ± 0.47 %, 61.90 ± 0.40 %, 48.75 ± 0.18 %, 37. 23 ± 0.38 %, and 33.70 ± 0.16 % cell viability is obtained for 10 µg/mL, 25 µg/mL, 50 µg/mL, 75 µg/mL, and 100 µg/mL pristine Fe_3O_4 concentrations, respectively. Data depicts glycine@Fe_3O_4 nanoparticles are more biocompatible than that of pristine Fe_3O_4.

Pristine Fe_3O_4 nanoparticles tend to be slightly toxic to the cells. Whereas, as mentioned in earlier chapter, glycine is already well-known for its biological activities and prominent presence in biological systems. Hence, it may be interpreted that the modification of Fe_3O_4 with glycine has provided biocompatibility.

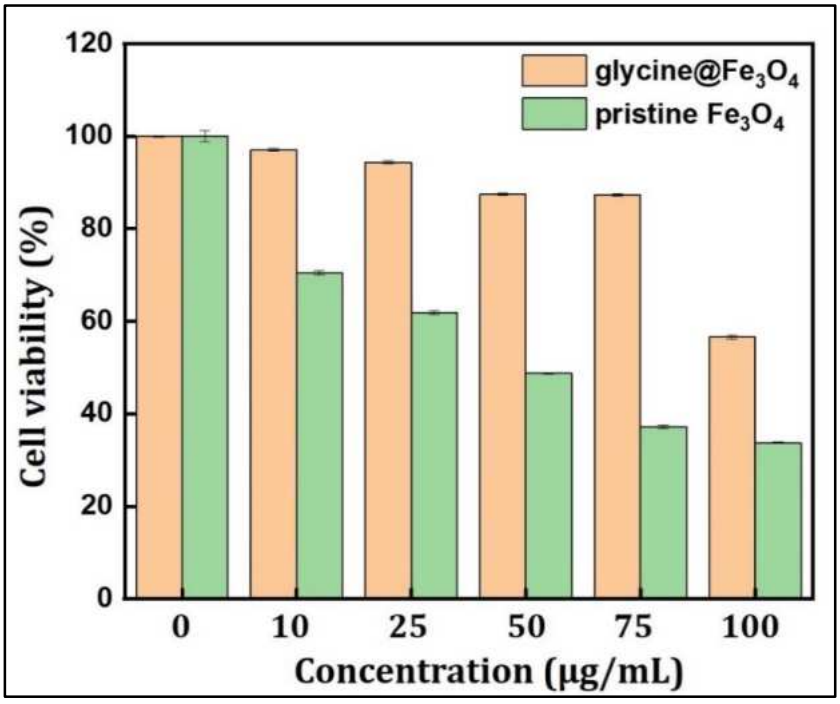

Figure 2.9. Cytotoxicity analysis of pristine Fe_3O_4 and glycine@Fe_3O_4 nanoparticles.

Hence, glycine@Fe_3O_4 nanoparticles are safe to use for further magnetofection study in the concentration range between 10 and 75 µg/mL as they are less cytotoxic and more biocompatible in this range.

2.8.8.2. ANTIMICROBIAL ANALYSIS

In subsequent chapter, glycine@Fe_3O_4 nanoparticles need to be tested for *Klebsiella pneumoniae* DNA separation. To employ safe DNA separation, these prepared nanoparticles should not be toxic to the bacterial (*Klebsiella pneumoniae*) cells. Hence, antimicrobial potential of pristine Fe_3O_4 and glycine@Fe_3O_4 was assessed by using *Klebsiella pneumoniae* growth kinetics assay.

The antimicrobial growth kinetics analysis reveals the effectiveness of pristine Fe_3O_4 and glycine@Fe_3O_4 nanoparticles against microbial strain *Klebsiella pneumoniae* in **Figure 2.10**. *Klebsiella pneumoniae* is a Gram-negative bacterium known to cause various infections, including pneumonia, urinary tract infections, and bloodstream infections. It possesses a protective outer membrane that can limit the effectiveness of certain antimicrobial agents.

Figure 2.10 a shows growth kinetics graph of *Klebsiella pneumoniae* to study antimicrobial nature of pristine Fe_3O_4 with concentration range 5 to 100 µg/mL. 0 µg/mL concentration denotes positive control (bacteria without addition of the nanoparticles). Whereas, **Figure 2.10 b** shows growth kinetics graph of *Klebsiella pneumoniae* to study antimicrobial nature of glycine@Fe_3O_4 with concentration range 5 to 100 µg/mL. 0 µg/mL concentration denotes positive control (untreated bacterial culture). The study run for the time period 0 to 24 hours. The results were compared with pristine Fe_3O_4 nanoparticles with the same experimental conditions.

The growth kinetic analysis does not demonstrate any significant concentration-dependent antimicrobial activity associated with both pristine Fe_3O_4 and glycine@Fe_3O_4 against the tested microorganism as shown in **Figure 2.10 a and b,** respectively.

The absence of concentration-dependent antimicrobial activity for the nanoparticle concentration range 5 to 100 µg/mL is observed in the growth kinetic analysis suggests that both pristine Fe_3O_4 and glycine@Fe_3O_4 nanoparticles may not possess antimicrobial properties up to 100 µg/mL nanoparticle concentration against the *Klebsiella pneumoniae* under the

conditions tested in this study. Hence, they are considered as microbe-compatible molecules up to 100 µg/mL to detect *Klebsiella pneumoniae* DNA in subsequent chapter.

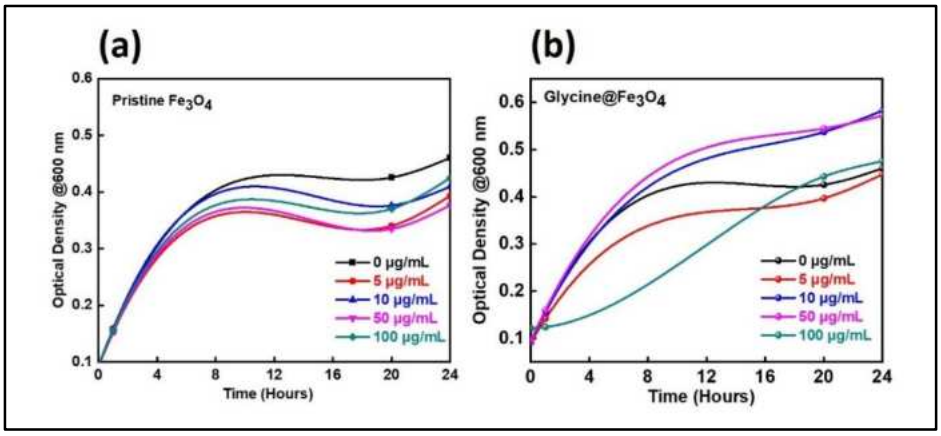

Figure 2.10. Antimicrobial assay of (a) pristine Fe_3O_4, and (b) glycine@Fe_3O_4 nanoparticles against *Klebsiella pneumoniae*.

2.9. CONCLUSIONS

In this study, glycine-modified iron oxide nanoparticles (glycine@Fe_3O_4) were synthesized by chemical co-precipitation method. Ferric ($FeCl_3$) and ferrous ($FeCl_2$) salt solutions were utilized in 2:1 molar ratio as precursor solutions. The incorporation of glycine as a surface modifier and stabilizing agent was enumerated for a range of potential applications. The synthesis of glycine-modified iron oxide nanoparticles resulted in well-defined black precipitate formation, which provides primary validation for successful synthesis of glycine@Fe_3O_4. The XRD analysis shows magnetite phase with JCPDS no. 75-0449. The SEM micrographs of pristine and glycine@Fe_3O_4 nanoparticles show cuboidal (or hybrid) shape. Presence of glycine did not affect the morphology. The TEM images depict ~12 nm size for glycine@Fe_3O_4 nanoparticles. The XPS analysis provides presence of Fe, O, N, and C elements. Later, the DLS provides ~70 nm hydrodynamic size for glycine@Fe_3O_4 nanoparticles. The Zeta potential values of -27 and +35 mV are observed for pristine Fe_3O_4 and glycine@Fe_3O_4 nanoparticles which give negative and positive surface charges, respectively. Raman spectroscopy confirms complete modification of Fe_3O_4 with glycine.

Biological properties (cytotoxicity and antimicrobial analysis) of glycine@Fe_3O_4 nanoparticles were checked to carry out biomedical applications in the subsequent chapters. glycine@Fe_3O_4 nanoparticles are more biocompatible than that of pristine Fe_3O_4 in the concentrations between 10 and 75 µg/mL. Hence, the glycine@Fe_3O_4 nanoparticles from the range 10-75 µg/mL are safe to use for DNA magnetofection in breast cancer MCF-7 cells experiments.

Further, no significant concentration-dependent antimicrobial activity was observed for both pristine Fe_3O_4 and glycine@Fe_3O_4 nanoparticles up to 100 µg/mL nanoparticle concentration, paving the way for safe *K. pneumoniae* DNA separation in subsequent chapter.

2.10. REFERENCES

[1] S. O. Aisida, P. A. Akpa, I. Ahmad, T. Kai Zhao, M. Maaza, F. I. Ezema. **Bio-inspired encapsulation and functionalization of iron oxide nanoparticles for biomedical applications**. Eur. Polym. J. 2020; 122(1): 109371.

[2] K. Q. Jabbar, A. A. Barzinjy, S. M. Hamad. **Iron oxide nanoparticles: preparation methods, functions, adsorption, and coagulation/flocculation in waste water treatment**. Environ. Nanotechnol. Monit. 2022; 17: 100661.

[3] T. Arredonodo-Ochoa, G. A. Silva-Martinez. **Microemulsion-based nanostructures for drug delivery**. Front. Nanotechnol. 2022; 3(1): 753947.

[4] G. Song, X. Shi, K. Sun, C. Li, C. Uher, J. R. Baker Jr, M. Mark, B. Holl, G. Bradford. **Facile hydrothermal synthesis of iron oxide nanoparticles with tunable magnetic properties**. J. Phys. Chem. C. 2009; 113(31): 13593.

[5] M. Unni, A. M. Uhl, S. Savliwala, B. H. Dhavalikar, N. Garraud, D. P. Arnold, L. F. Kourkoutis, J. S Andrew, C. Rinaldi. **Thermal decomposition synthesis of iron oxide nanoparticles with diminished magnetic dead layer by controlled addition of oxygen**. ACS Nano. 2017; 11(2): 2284.

[6] L. Zhanfeng, J. Dong, H. Zhang, Y. Zhang, H. Wang, X. Cui, Z. Wang. **Sonochemical catalysis as a unique strategy for the fabrication of nano-/micro-structured inorganics**. Nanoscale Adv. 2021; 3(1): 41.

[7] Sunde, T. O. Loveng, T. Grande, M. A. Einarsrud. **Modified pechini synthesis of oxide powders and thin films**. Handbook of solgel technology,

2016.

[8] B. Dmitry, A. T. Jalil, S. Chupradit, W. Suksatan, M. J. Ansari, I. H. Shewael, G. H. Valiev, E. Kianfar. **Nanomaterial by sol-gel method: synthesis and application.** Adv. Mater. Sci. Eng. 2021; 2021: 1.

[9] R. P. Gambhir, S. Kale, T. Dongale, S. Patil, D. Malavekar, A. P. Tiwari. **Green synthesized magnetic nanoparticles for selective inhibition of osteosarcoma cancer**. 2023; 25(4): 83.

[10] A. Ali, H. Zafar, M. Zia, I. Ul Haq, A. R. Phull, J. S. Ali, A. Hussain. **Synthesis, characterization, applications, and challenges of iron oxide nanoparticles**. Nanotechnol. Sci. Appl. 2016; 9: 49.

[11] M. O. Besenhard, A. P. Lagrow, A. Hodzic, M. Krienchbaum, M. Panarielli, L. Bais, G. Loizou, K. Damilos, M. M. Cruz, N. T. K. Thanh, A. Gavriilidis. **Co-precipitation synthesis of stable iron oxide nanoparticles with NaOH: new insights and continuous production via flow chemistry**. J. Chem. Eng. 2020; 399:125740.

[12] N. Ajinkya, X. Yu, P. Kaithal, J. Luo, P. Somani. S. Ramakrishna. **Magnetic iron oxide nanoparticle (IONP) synthesis to applications: present and future**. Materials. 2020; 13(20): 4644.

[13] H. M. Yang, C. W. Park, T. Ahn, B. Jung, B. K. Seo, J. H. Park, J. D. Kim. **A direct surface modification of iron oxide nanoparticles with various poly (amino acids) for use as magnetic resonance probes**. J. Colloid Interface Sci. 2013; 391: 158.

[14] R. Salceda. **Glycine neurotransmission: its role in development**. Front. Neurosci. 2022; 16: 947563.

[15] A. Alves, A. Bassot, A. L. Bulteau, L. Pirola, B. Morio. **Glycine metabolism and its alterations in obesity and metabolic diseases**. Nutrients. 2019; 11(6): 1356.

[16] P. de Paz-Lugo, J. A. Lupianez, E. Melendez-Hevia. **High glycine concentration increases collagen synthesis by articular chondrocytes in-vitro: acute glycine deficiency could be an important cause of osteoarthritis**. Amino acids. 2018; 50(10): 1357.

[17] M. F. McCarty, J. H. Okeefe, J. J. Dinicolantonio. **Dietary glycine is rate-limiting for glutathione synthesis and may have broad potential for health protection**. Oshsner. 2018; 18: 81.

[18] K. A. Aguayo-ceron, F. S. Munoz, R. A. Gutierrez-rojas, L. N. Acevedo-villavicencio, A. V. Flores-zarate, F. Huang, A. Giacoman-martinez. **Glycine: the smallest anti-inflammatory micronutrient**. Int. J. Mol. Sci. 2023; 24(14): 11236.

[19] R. Ullah, M. H. Jo, M. Riaz, S. I. Alam, K. Saeed, W. Ali, I. U. Rehman, M.

Ikram, M. O. Kim. **Glycine, the smallest amino acid, confers neuroprotection against D-galactose-induced neurodegeneration and memory impairment by regulating c-jun N-terminal kinase in mouse brain**. J. Neuroinflammation. 2020; 17(1): 1.

[20] Locasale, W. Jason. **Serine, glycine and one carbon units: cancer metabolism in full circle**. Nat. Rev. Cancer. 2013; 13(8): 572.

[21] W. Yamadera, K. Inagawa, S. Chiba, M. Bannai, M. Takahashi, K. Nakayama. **Glycine ingestion improves subjective sleep quality in human volunteers, correlating with polysomnographic changes**. Sleep Biol. Rhythms. 2007; 5: 126.

[22] M. A. Razak, P. S. Begum, B. Vishwanath, S. Rajagopal. **Multifarious beneficial effect of non-essenstial amino acid, glycine: a review**. Oxiv. Med. Cell. Longev. 2017; 2017: 1716701.

[23] J. C. Pei, D. Z. Luo, S. S. Gau, C. Y. Chang, W. S. Lai. **Directly and indirectly targeting the glycine modulatory site to modulate NMDA receptor function to address unmet medical needs of patients with schizophrenia**. Front psychiatry. 2021; 12: 742058.

[24] S. A. Azhagan, S. Ganesan. **Growth and characterization of gamma glycine single crystal from ammonium sulfate as solvent**. Recent Research in Science and Technology. 2010; 2(6): 107.

[25] L. Schio, C. Li, S. Monti, P. Salén, V. Yatsyna, R. Feifel, M. Alagia, R. Richter, S. Falcinelli, S. Stranges, V. Zhaunerchyk. **NEXAFS and XPS studies of nitrosyl chloride**. Phys. Chem. Chem. Phys. 2015; 17(14): 9040.

[26] D. D. Postnov, J. Tang, S. E. Erdener, K. Kılıç, D. A. Boas. **Dynamic light scattering imaging**. Science advances. 2020; 6 (45): 4628.

[27] N. Chandrasekar, K. Kumar, K. S. Balasubramnian, K. Karunamurthy, R. Varadharajan. **Facile synthesis of iron oxide, iron-cobalt and zero valent iron nanoparticles and evaluation of their anti-microbial activity, free radicle scavenging activity and antioxidant assay**. DJNB. 2013, 8(2): 765.

[28] A. P. Tiwari, R. K. Satvekar, S. S. Rohiwal, V. A. Karande, A. V. Raut, P. G. Patil, P. B. Shete, S. J. Ghosh, S. H. Pawar. **Magneto-separation of genomic deoxyribose nucleic acid using pH responsive Fe_3O_4@silica@chitosan nanoparticles in biological samples**. Rsc Advances. 2015; 5: 8463.

[29] P. C. Panta, C. P. Bergmann. **Raman spectroscopy of iron oxide of nanoparticles (Fe_3O_4)**. J. Mater. Sci. Eng. 2015; 5(1): 1000217.

[30] I. V. Krauklis, A. V. Tulub, A. V. Golovin, V. P. Chelibanov. **Raman Spectra of Glycine and Their Modeling in Terms of the Discrete–Continuum Model of Their Water Solvation Shell**. Opt. Spectrosc. 128(10): 1598.

[31] S. Biswal, D. S. Bhaskaram, G. Govindaraj. **α-Fe_2O_3/reduced graphene oxide nanocomposite: Interfacial effect on the magnetic property**. Journal of Superconductivity and Novel Magnetism. 2020; 33: 1629.

[32] N. Kirik, A. Krylov, A. Boronin, S. Koshcheev, L. Solovyov, E. Rabchevskii, N. Shishkina, A. Anshits. **The relationship between the structural characteristics of α-Fe_2O_3 catalysts and their lattice oxygen reactivity regarding hydrogen**. Materials. 2023; 16 (12): 4466.

[33] K. Kiskira, S. Papirio, M. C. Mascolo, C. Fourdrin, Y. Pechaud, E. D. van Hullebusch, G. Esposito. **Mineral characterization of the biogenic Fe (III)(hydr) oxides produced during Fe (II)-driven denitrification with Cu, Ni and Zn**. Science of the total environment. 2019; 687: 401.

Chapter 3

Preparation of glycine-modified iron oxide nanoparticle – deoxyribonucleic acid (DNA) conjugates

3.1. INTRODUCTION

Nucleic acids (NA) mainly deoxyribonucleic acid (DNA) and ribonucleic acid (RNA) are significant molecules present in biological systems. These nucleic acids are hereditary material of living cells which reserve, code, and transfer genetic information to DNA and other organelles of cells. Further, RNA acts as a mediator messenger to carry out routinely essential biological activities of a living cell [1]. Hence, detecting or separating nucleic acids from biological samples is a remarkable step in disease diagnosis as well as therapeutics [2, 3].

The concept of adsorption and desorption of nucleic acids involves the interaction and separation of nucleic acids using specific materials or nanoparticles. Adsorption refers to the attachment or binding of nucleic acids to the surface of a material or nanoparticle through various interactions, such as electrostatic, hydrogen bonding, or base pairing. This process allows for the selective capture and quantification of nucleic acids from a sample. Desorption, on the other hand, refers to the release or removal of the bound nucleic acids from the surface, typically achieved by altering the environmental conditions or introducing competitive molecules or enzymes. Understanding and optimizing the adsorption/binding and desorption/elution processes are crucial for applications such as nucleic acid extraction, purification, and targeted delivery in various fields, including biotechnology, medicine, and molecular biology [4].

There are several ways to detect and separate deoxyribonucleic acids (DNA) as mentioned in **Table 3.1**. Each method has distinct advantages and disadvantages. The efficient detection and separation of DNA from biological samples need rapid developments as they face multiple challenges. Simplification of protocol, effective specificity and sensitivity, easy availability of reagents, inexpensive point-of-care devices, patient-friendly and rapid diagnosis as well as therapies need to be recommended.

Table 3.1. DNA separation and detection methods, their advantages and disadvantages

No.	Method	Advantages	Disadvantages
1	DNA Hybridization	Southern and northern blotting help in detection and separation of specific sequences of nucleic acids. DNA can be separated at chromosome level.	Complex procedure, limited applicability, time consuming, cost, complex purification, and energy intensive.
2	Loop mediated isothermal amplification (LAMP)	Target DNA is detected and amplified at specific temperature. Simple screening assay for detecting bacteria and viruses.	Less sensitive than PCR. Requires heat-treated samples. Less effective for crude biological samples.
3	Reverse transcriptase polymerase chain reaction (RT-PCR)	Control over particle properties, versatility, high purity, cost-effective, and scalability.	Reaction requires alternative thermal cycles which make overall cost of diagnosis higher. Requires primers of desired DNA sequence. False negative results
4	Microarray based	Evaluate genetic expressions. Comparatively cheaper. Less computational power is required.	Reliance upon literature. Cross contamination. Limited detection range.
5	Clustered regulatory interspaced short palindromic repeats and CRISPR-associated sequences (CRISPR-Cas)	Powerful and accurate diagnosis. Identify and cleave specific DNA targets. Detection at any stage of infection.	Specialized equipment, Skilled labors, safety concern. Ethical and regulatory issues.
6	Next generation sequencing	Detects thousands of DNA sequences in short duration at the same time.	More often used in research than clinics and requires specialized equipment.
7	**Nanoparticles-based**	**Sustainable, low energy consumption, and cost effective.**	**Variable product quality and scale-up challenges.**

In remote and resource-poor nations, DNA detection and separation technologies that are easy to use, quick, inexpensive, and adaptable are especially important for laboratories and clinical applications.

3.2. IMPORTANCE OF IRON OXIDE NANOPARTICLE–DNA (Fe_3O_4-DNA) CONJUGATION

The optimization of the conjugation process between Fe_3O_4 and DNA holds paramount importance in the field of nanotechnology, particularly in the context of biomedical applications. Optimizing the conjugation process aims to improve the efficiency of the binding between Fe_3O_4 and DNA [5]. This efficiency is essential for ensuring a higher yield of well-formed conjugates, minimizing wastage of materials, and maximizing the utilization of resources. The optimization process considers the biocompatibility of the resulting conjugates. Ensuring that the conjugation is conducted under conditions that are compatible with biological systems is vital for potential applications in medicine [6].

Biocompatible conjugates are more likely to exhibit minimal toxicity and favorable interactions with biological entities. The stability of the formed conjugates is critical for their successful application in various fields, especially in biological environments [7]. Optimizing the process helps in creating conjugates that are more stable over time, reducing the chances of aggregation or degradation. This increased stability is crucial for the sustained functionality of the nanoparticles in biomedical applications [8]. The size, shape, and surface properties of Fe_3O_4 play a significant role in their interactions with DNA and, consequently, their performance in various applications [9]. Optimization allows researchers to exert control over these characteristics, tailoring the conjugates to meet specific requirements for targeted delivery, imaging, or therapeutic purposes. Optimizing the conjugation process ensures the reproducibility of the results. This is essential for the scalability and reliability of the production process, allowing researchers and manufacturers to consistently generate conjugates with the desired properties [10]. Reproducibility is a fundamental aspect of translating laboratory findings into practical applications. Different

biomedical applications may require unique features from the Fe_3O_4-DNA conjugates [11].

Optimization contributes to cost-effectiveness by minimizing the use of reagents and resources, reducing the experimental failures, and facilitating the scaling-up of production processes. Economic considerations are essential for the practical implementation of these conjugates in real-world applications.

3.3. PARAMETERS AFFECTING IRON OXIDE NANOPARTICLE-DNA (Fe_3O_4-DNA) CONJUGATION

The formation of Fe_3O_4-DNA conjugates is a complex process influenced by various parameters. Understanding and carefully controlling parameters like pH are essential for achieving successful and reproducible conjugation. The size of Fe_3O_4 significantly influences their surface area and the amount of available binding sites for DNA. Smaller nanoparticles (< 20 nm) may offer a higher surface area but can pose challenges related to stability and aggregation [12].

The surface charge of nanoparticles, often expressed by zeta potential; which plays a crucial role in electrostatic interactions with DNA. Negatively charged DNA can electrostatically bind to positively charged nanoparticles, facilitating conjugate formation. The length and structural features of nucleic acids, such as DNA or RNA; impact their interactions with nanoparticles [13]. Longer nucleic acid sequences may require different optimization parameters than shorter ones. Secondary structures of nucleic acids can affect the accessibility of binding sites.

The pH of the reaction environment can influence the ionization state of functional groups on both nanoparticles and DNA [14]. Optimal pH conditions must be determined to facilitate effective conjugation while avoiding unwanted side reactions or degradation. Reaction temperature affects reaction kinetics, binding affinities, and the stability of formed conjugates. Optimal temperature conditions should be established to ensure efficient and controlled conjugation [15]. Addition of stabilizing agents or

ligands to the nanoparticle surface can enhance stability, prevent aggregation, and improve the conjugation efficiency. Additionally, ligands provide specific functional groups for covalent bonding with nucleic acids. The concentration of Fe_3O_4 in the reaction mixture influences the availability of binding sites. Low concentration of nanoparticles may result in incomplete coverage of DNA, while excessively high concentrations can lead to aggregation. The concentration of DNA is crucial for achieving the desired ratio with nanoparticles. Optimizing concentrations is essential to avoid waste and ensure efficient conjugation.

The duration of the reaction (incubation time) plays a critical role in determining the extent of conjugation. Insufficient reaction time may result in incomplete binding, while excessively long reaction times may lead to non-specific interactions or degradation. The choice of solvent and the overall reaction environment can impact the stability and reactivity of both Fe_3O_4 and DNA. Compatibility with biological systems is essential for applications in medicine. Stirring or agitation during the conjugation process can influence the mixing of reactants, affecting the kinetics of the reaction and the uniformity of the formed conjugates. The purity of both the Fe_3O_4 and DNA is critical. Impurities can interfere with conjugation reactions, leading to undesired by-products or reduced efficiency. Understanding and optimizing these parameters are crucial steps in developing a robust protocol for the formation of Fe_3O_4-DNA conjugates, ensuring their applicability in various biomedical fields, including drug delivery, imaging, and diagnostics.

3.4. CHALLENGES IN Fe_3O_4-DNA CONJUGATE FORMATION

The formation of Fe_3O_4-DNA conjugates is a complex process that presents several challenges. Aggregation of Fe_3O_4 may occur during the conjugation process, leading to non-uniform distributions and altered properties. Aggregation can limit the accessibility of binding sites and affect the stability and functionality of the conjugates [16]. Proper surface modification, the addition of stabilizing agents, and optimizing reaction

conditions can minimize aggregation. Ensuring an appropriate nanoparticle size and surface charge is also crucial. Stability issues may arise due to the interaction between nanoparticles and DNA [17]. Unstable conjugates may experience degradation, detachment of DNA, or changes in their physicochemical properties over time. Utilizing stabilizing agents, optimizing reaction conditions for enhanced stability, and employing suitable storage conditions are key strategies to address stability concerns. Achieving consistent results across different experiments can be challenging, leading to issues with the reproducibility of conjugation processes. Variability in nanoparticle characteristics, DNA properties, or experimental conditions can contribute to this challenge [18-21].

3.5. OVERALL SIGNIFICANCE OF CHAPTER

The significance of this chapter lies in its exploration of the conjugation between glycine@Fe_3O_4 and DNA, which could have several important implications in biomedical research. This conjugation can be utilized in various applications such as targeted pathogen detection and magnetofection. Utilizing glycine@Fe_3O_4-DNA conjugates can improve target specificity and sensitivity, aiding in early disease detection and monitoring. The conjugation of DNA with glycine@Fe_3O_4 can facilitate the development of novel therapeutic strategies, such as targeted gene editing or silencing, potentially offering more precise and effective treatments for various diseases.

This chapter shows experimental methods, results, and interpretation to elucidate the process of forming conjugates between glycine@Fe_3O_4 and DNA, shedding a light on their potential applications across various biomedical domains.

3.6. EXPERIMENTAL

Previous literature shows optimized parameters for surface modified Fe_3O_4-DNA conjugate formation [15, 22-24]. Depending upon the interactions and stabilizing/surface functionalizing material the parameter

conditions are varied. As discussed earlier, glycine@Fe_3O_4 have been used for glycine@Fe_3O_4-DNA conjugation. These interactions are possibly due to electrostatic forces between glycine and DNA (possible mechanism of interaction is described further). As isoelectric pH (PI) of glycine is 6 [23]. That means, in medium with pH > 6 glycine gains surface negative charge and in pH < 6 glycine possesses surface positive charge. The initial adsorption experiments are carried out in acidic conditions (pH < 6). According to the previous data, the mentioned conjugates are prepared with the incubation time 30 min [15]. Hence, the initial experiment of effect of DNA concentration on glycine@Fe_3O_4-DNA conjugation is performed with the same incubation time. Further, all the experiments are carried out at room temperature (~25°C). Also, the glycine@Fe_3O_4 concentration was kept constant with the value 50 µg/mL. DNA concentration was optimized with respect to the glycine@Fe_3O_4 concentration. Later on, pH and incubation time were optimized to prepare glycine@Fe_3O_4-DNA conjugates.

3.6.1. MATERIALS

Standard DNA (calf thymus) was purchased from Sigma Aldrich Pvt. Ltd. Phosphate buffered saline (PBS), sodium hydroxide (NaOH), and sodium chloride (NaCl) were purchased from Himedia Pvt. Ltd.

3.6.2. METHODOLOGY

3.6.2.1. DNA ADSORPTION ON GLYCINE-MODIFIED IRON OXIDE NANOPARTICLE-DNA (Fe_3O_4-DNA) CONJUGATION

The adsorption of standard DNA onto the glycine@Fe_3O_4 was performed in sterile PBS of 1 mL using standard DNA solution of 100 µg/mL (1 mL) batch-wise for optimization of parameters (pH, DNA concentration and incubation time). **Table 3.2** depicts details of the studied parameters for the conjugation of glycine@Fe_3O_4 and DNA.

Table 3.2. Details of parameters for optimization of glycine@Fe_3O_4-DNA conjugation

No.	Parameter	Optimization values
1	pH	3, 4, 5, 6, 7, 8, 9, and 10
2	DNA concentration	10, 25, 50, 75, and 100 µg/mL
3	Incubation time	10, 20, 30, 40, and 50 min

Later on, adsorption capacity of glycine@Fe_3O_4 was calculated with the UV-visible spectroscopy analysis at 260 nm. "Best" obtained values were considered as an optimum parameter for glycine@Fe_3O_4-DNA conjugate formation.

3.6.2.2. DNA DESORPTION FROM GLYCINE@Fe_3O_4

The DNA desorption process was carried out for glycine@Fe_3O_4 at 25°C for 30 min using 0.5 M NaCl solution (1 mL) batch-wise. Amount and rate of desorption was calculated by following equations.

DNA concentration = (A_{260} – A_{320}) x dilution factor x A_{260} of 1 **... 3.1**

Wherein, DNA concentration is desorbed DNA in µg/mL, A_{260} is absorbance at 260 nm, A_{320} is absorbance at 320 nm, and A_{260} of 1.0 is 50 µg/mL.

Rate of desorption = (amount of DNA desorbed/ total DNA) x 100 **... 3.2**

Wherein, rate of desorption is in percentage (%).

3.7. RESULTS AND DISCUSSION

3.7.1. MECHANISM OF GLYCINE-MODIFIED IRON OXIDE NANOPARTICLE-DNA (glycine@Fe_3O_4–DNA) CONJUGATION

As discussed earlier, genetic information is passed down through generations mainly through DNA molecules. These structures are made up of several nucleosides that have a phosphate backbone with nucleic acid bases that can form double helices. These characteristics, along with the exceptional qualities of surface modified glycine@Fe_3O_4, enable the fabrication of glycine@Fe_3O_4-DNA conjugates [24-26].

Evidences suggest that DNA binds to amino acids through various coupling agents via covalent immobilization. Amino, sulfhydryl, carboxyl,

and azido coupling agents are initially attached to glycine@Fe_3O_4 to further adsorption of DNA. Likewise, glycine@Fe_3O_4-DNA conjugates can be interacted with each other through electrostatic interactions, physical adsorption, Van der waal's forces, and non-covalent interactions. As proven already, amino acids link with each other through hydrogen bonds, disulphide bonds, hydrophilic, hydrophobic interactions and ionic bonds [24-26].

As glycine is an amino acid, it contains free amino group. Also, it acts as a zwitter ion at neutral, cation in acidic, and anion in basic pH [27]. This powerful pH influence of the charge state reflects to change their properties and sensitivity towards the DNA. pH-dependent DNA adsorption takes place through interactions between amino group of glycine and phosphate backbone of DNA. Protonated amino group of glycine contains positive charge whereas phosphate backbone of DNA holds strong negative charge. Hence, charge-specific attractive interactions take place to form glycine@Fe_3O_4-DNA conjugates.

The interaction is computationally supportive through **Figure 3.1**. It can be interpreted that cationic glycine and anionic DNA make a conjugate at chemical level. Glycine-DNA interactions develop a conjugate when studied computationally; the study where computer-aided interactions of different biomolecules are predicted. The computational study (docking analysis) of glycine-DNA conjugate was carried out by different softwares like PyRx, Discovery studio 2021, and Pymol. Docking analysis is the study in computational biology where possible bond formations are predicted when two biomolecules come in vicinity. Here, DNA and glycine biomolecule conjugation was studied as a function of their conjugate formation. DNA model was built by providing (5'TTTCGTGTCGCCCTTATTCC3') standard DNA sequence using Discovery studio 2021. Protein data bank (PDB) model of glycine was taken from PDB database. Further, in PyRx 0.8, glycine and DNA macromolecule models were prepared for docking by minimizing their energy and the molecules were docked. The docked image was directly obtained after the process is done in **Figure 3.1 a**, where the glycine molecule seen to be docked inside the DNA with

binding energy around – 6 Kcal/mol (calculated by PyRx 0.8 software). Negative binding energy provides the natural binding interactions between molecules. Further, the obtained model was visualized in Pymol software shown in **Figure 3.1 b**. The figure significantly shows the glycine@Fe_3O_4-DNA conjugate formation.

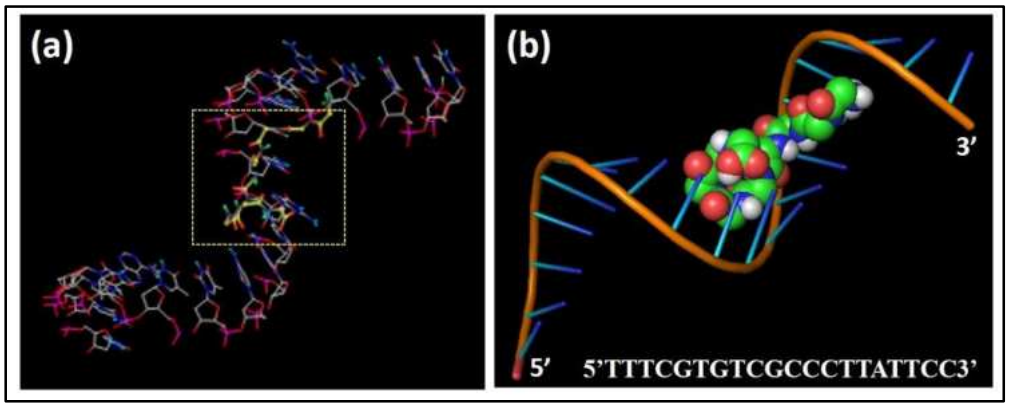

Figure 3.1. Glycine@Fe_3O_4-DNA conjugation computational study; (a) glycine-DNA docking with PyRx 0.8, and (b) glycine-DNA conjugate visualization by Pymol software.

3.7.2. DNA ADSORPTION ON GLYCINE-MODIFIED IRON OXIDE NANOPARTICLE-DNA (Fe_3O_4-DNA) CONJUGATION

Formation of glycine@Fe_3O_4-DNA conjugate was studied by varying three major parameters (DNA concentration, pH and incubation time). To evaluate the contribution of glycine in the conjugate formation, the parameters were tested on pristine Fe_3O_4 as well using UV-visible spectroscopy and DNA quantification. UV-visible spectroscopy is a widely utilized technique for the detection and quantification of NA, particularly DNA and RNA. One of the key features of nucleic acids that makes them amenable to UV-visible spectroscopy is their ability to absorb light in the ultraviolet (UV) region, particularly around 260 nanometers (nm). The principle behind glycine@Fe_3O_4-DNA conjugate formation using UV-visible spectroscopy is based on the absorption of UV light by the nitrogenous bases present in DNA and RNA. NA contains aromatic heterocyclic bases such as adenine, guanine, cytosine, thymine (in DNA), and uracil (in RNA), which absorb UV light at specific wavelengths. Among these bases, the purine bases (adenine and guanine) and pyrimidine bases (cytosine, thymine, and uracil)

absorb UV light most strongly at approximately 260 nm. The absorption of UV light at 260 nm is primarily due to the presence of conjugated double bonds in the aromatic rings of these bases.

Hence successful glycine@Fe_3O_4-DNA conjugation is directly proportional to the absorbance peak at 260 nm. The absorbance of the sample is measured using a UV-visible spectrophotometer set to a wavelength of 260 nm. The spectrophotometer measures the amount of light absorbed by the nucleic acid molecules in the prepared conjugate sample. The absorbance value obtained from the sample is then compared to a standard curve or established extinction coefficient to determine the concentration of nucleic acid present in the sample. The Beer-Lambert law, which relates absorbance to concentration, is often used for this purpose.

Effect of DNA concentration, pH, and incubation time on glycine@Fe_3O_4-DNA conjugate formation was investigated with respect to constant glycine@Fe_3O_4 concentration (50 µg/mL) at room temperature (25°C). Above mentioned parameters were varied as an individual experiment to optimize glycine@Fe_3O_4 conjugate formation.

3.7.2.1 EFFECT OF DNA CONCENTRATION ON GLYCINE-MODIFIED IRON OXIDE NANOPARTICLE-DNA (Fe_3O_4-DNA) CONJUGATION

Effect of DNA concentration is studied at first to obtain glycine@Fe_3O_4-DNA conjugate formation **(Figure 3.2).** As mentioned earlier, glycine@Fe_3O_4 concentration was considered constant with the value of 50 µg/mL and DNA concentration was varied in the range of 10 to 100 µg/mL to study glycine@Fe_3O_4-DNA conjugation.

Figure 3.2 a depicts at 50 µg/mL DNA concentration, the DNA peak absorbance is greater. Only DNA (without any conjugation) and only glycine@Fe_3O_4 nanoparticles (without any conjugation) are considered as positive and negative controls, respectively. The figure shows 1:1 (50 µg/mL: 50 µg/mL) glycine@Fe_3O_4 and DNA ratio is optimum for the better glycine@Fe_3O_4-DNA conjugation as it provides DNA peak as close as positive control.

Furthermore, pristine Fe_3O_4 does not provide Fe_3O_4-DNA conjugation as there is absence of DNA peak at 260 nm in **Figure 3.2 b**. Effect of pristine Fe_3O_4 is studied with the same experimental conditions as that of glycine@Fe_3O_4 to understand the pH-responsive role of glycine in this conjugation. Only DNA (without any conjugation) and only glycine@Fe_3O_4 nanoparticles (without any conjugation) are considered as positive and negative controls, respectively. Pristine Fe_3O_4 graph does not show DNA peak at 260 nm and hence, there is no glycine@ Fe_3O_4-DNA conjugate formation in case of pristine Fe_3O_4.

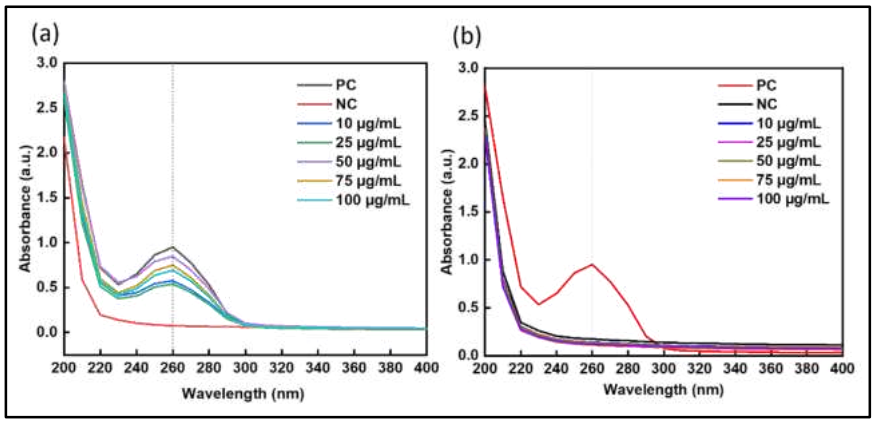

Figure 3.2. Effect of DNA concentration by UV-visible spectroscopy on; (a) glycine@Fe_3O_4-DNA conjugation, and (b) pristine Fe_3O_4-DNA conjugation.
pH < 6 (~5.8), temperature = 25°C, nanoparticles = 50 µg/mL, time = 30 min.

Furthermore, the quantification of adsorbed DNA on glycine@Fe_3O_4 and pristine Fe_3O_4 is depicted in **Figure 3.3**. Highest DNA adsorption (79.56 ± 0.15 µg/mL) is obtained for glycine@Fe_3O_4 at DNA concentration 50 µg/mL (**Figure 3.3 a**). The obtained values for different DNA concentrations are present in **Table 3.3**. However, no DNA is quantified for pristine Fe_3O_4 (**Figure 3.3 b**). Hence, 50 µg/mL DNA concentration condition remains suitable for glycine@Fe_3O_4-DNA conjugation.

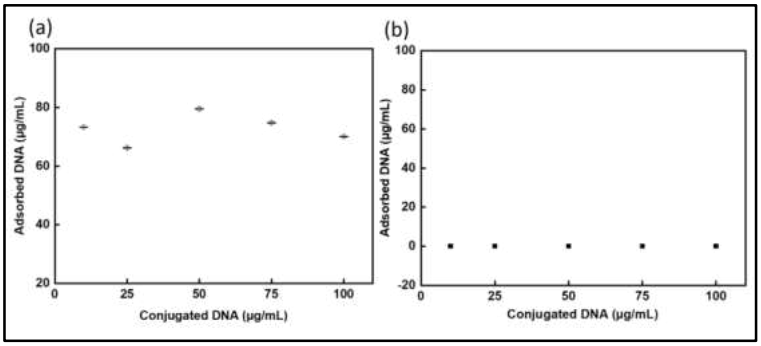

Figure 3.3. Effect of DNA concentration by UV-visible spectroscopy on; (a) glycine@Fe_3O_4-DNA conjugation, and (b) pristine Fe_3O_4-DNA conjugation.
pH < 6, temperature = 25°C, nanoparticles = 50 µg/mL, time = 30 min.

Table 3.3. Quantification of adsorbed DNA on glycine@Fe_3O_4 by influencing DNA concentration conditions

No.	DNA concentration (µg/mL)	Adsorbed DNA (µg/mL)
1.	10	73.34 ± 0.06
2.	25	66.22 ± 0.11
3.	50	79.56 ± 0.15
4.	75	74.76 ± 0.16
5.	100	70.03 ± 0.15

3.7.2.2. EFFECT OF pH ON GLYCINE-MODIFIED IRON OXIDE NANOPARTICLE-DNA (Fe_3O_4-DNA) CONJUGATION

As discussed earlier, glycine is a zwitter ion and tends to change its surface charge according to the pH of solution [27]. Hence, it is important to discuss an influence of pH on glycine@Fe_3O_4-DNA conjugate formation. **Figure 3.4** provides UV-visible spectroscopy analysis of glycine@Fe_3O_4-DNA conjugates at different pH (3 to 10) for glycine@Fe_3O_4 (a) and pristine Fe_3O_4 (b). **Figure 3.4 a** shows spectra of glycine@Fe_3O_4 which enumerates highest peak (260 nm) of DNA adsorption at pH 5. It is important to describe that isoelectric pH of glycine is 6. That means below pH 6, it possesses strong positive charge (cation) [28]. Since DNA contains strong negative charge due to their phosphate backbones, it can be predicted that pH 5 conditions remain suitable for conjugation. The figure also shows low intensity of DNA peak below pH 5. Though conjugation needs acidic environment, strong acidic pH disturbs the composition of DNA and that reason might have influenced the conjugation at low pH conditions. Later on, in the same figure

DNA peaks at basic pH (8 to 10) conditions are showing low intensity. As mentioned earlier, glycine gains negative charge at basic conditions and hence there is strong repulsion in between glycine@Fe_3O_4 and DNA due to same surface charge. Effect of pristine Fe_3O_4 on DNA conjugation is observed in **Figure 3.4 b**. No DNA conjugation appears at any pH condition when compared with control DNA peak. Our previous study shows that pristine Fe_3O_4 (-30 mV zeta potential) contains negative charge. Hence due to same charge repulsion, no DNA conjugation occurs with pristine Fe_3O_4. This shows the importance of surface modification of Fe_3O_4 with glycine to carry out glycine@Fe_3O_4-DNA conjugate applications. Hence, pH 5 condition remains suitable for glycine@Fe_3O_4-DNA conjugation.

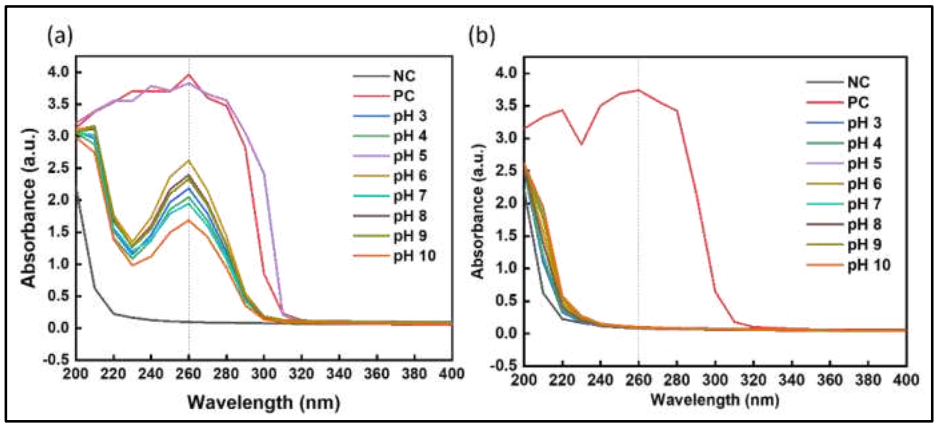

Figure 3.4. Effect of pH by UV-visible spectroscopy on; (a) glycine@Fe_3O_4-DNA conjugation, and (b) pristine Fe_3O_4-DNA conjugation.
DNA = 50 µg/mL, temperature = 25°C, nanoparticles = 50 µg/mL, time = 30 min.

Furthermore, the quantification of adsorbed DNA on glycine@Fe_3O_4 and pristine Fe_3O_4 is depicted in **Figure 3.5**. Highest DNA adsorption (78.74 ± 0.33 µg/mL) is obtained for glycine@Fe_3O_4 at pH 5 (**Figure 3.5 a**). The obtained values for different pH are present in **Table 3.3**. However, no DNA is quantified for pristine@Fe_3O_4 (**Figure 3.5 b**). Hence, pH 5 condition remains suitable for glycine@Fe_3O_4-DNA conjugation.

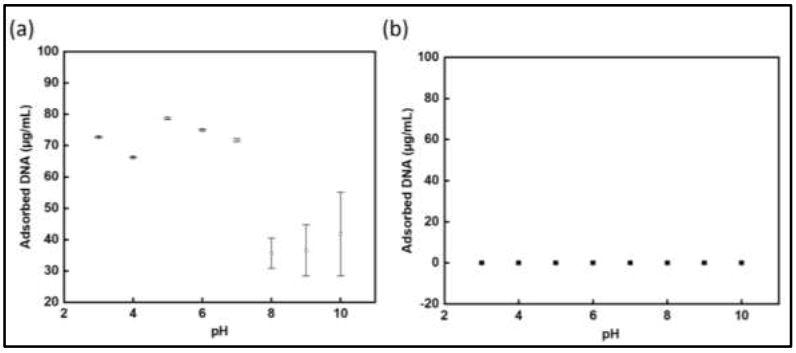

Figure 3.5 Effect of pH by UV-visible DNA quantification on (a) glycine@Fe_3O_4-DNA conjugation, and pristine Fe_3O_4-DNA conjugation.
DNA = 50 µg/mL, temperature = 25°C, nanoparticles = 50 µg/mL, time = 30 min.

Table 3.4 Quantification of adsorbed DNA on glycine@Fe_3O_4 by influencing pH conditions

No.	pH	Adsorbed DNA (µg/mL)
1.	3	72.72 ± 0.16
2.	4	66.29 ± 0.15
3.	5	78.74 ± 0.33
4.	6	75.00 ± 0.27
5.	7	71.73 ± 0.47
6.	8	35.68 ± 4.84
7.	9	36.53 ± 8.12
8.	10	41.77 ± 13.37

3.7.2.3 EFFECT OF INCUBATION TIME ON GLYCINE-MODIFIED IRON OXIDE NANOPARTICLE-DNA (Fe_3O_4-DNA) CONJUGATION

Incubation time of interaction is optimized to obtain glycine@Fe_3O_4-DNA conjugate formation **(Figure 3.6).** Here, glycine@Fe_3O_4 concentration was considered constant with the value of 50 µg/mL. **Figure 3.6 a** depicts at incubation time 30 min, the DNA peak absorbance is greater. Further no DNA peak is obtained for pristine Fe_3O_4 which shows no Fe_3O_4-DNA conjugation in **Figure 3.6 b**.

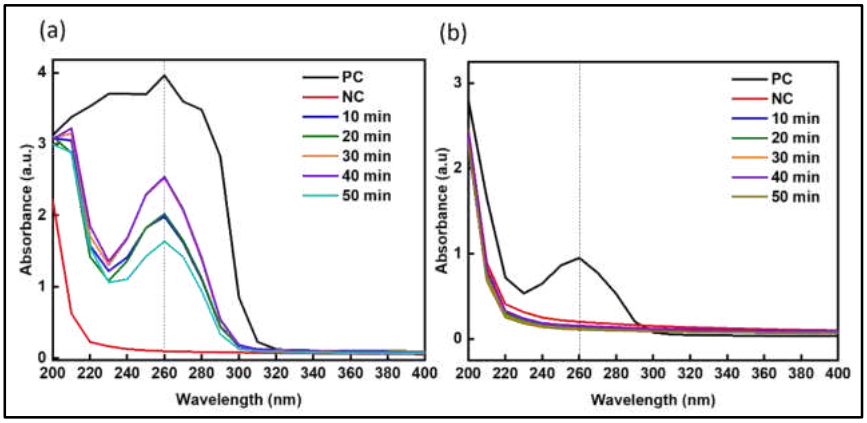

Figure 3.6. Effect of incubation time by UV-visible DNA quantification on (a) glycine@Fe_3O_4-DNA conjugation, and pristine Fe_3O_4-DNA conjugation.
DNA = 50 µg/mL, temperature = 25°C, nanoparticles = 50 µg/mL, pH = 5.

Furthermore, the quantification of adsorbed DNA on glycine@Fe_3O_4 and pristine Fe_3O_4 is depicted in **Figure 3.7**. Highest DNA adsorption (77.24 ± 0.71 µg/mL) is obtained for glycine@Fe_3O_4 in 30 min (**Figure 3.7 a**). The obtained values for different incubation time are present in **Table 3.4**. However, no DNA is quantified for pristine@Fe_3O_4 (**Figure 3.7 b**). Hence, 30 min incubation condition remains suitable for glycine@Fe_3O_4-DNA conjugation.

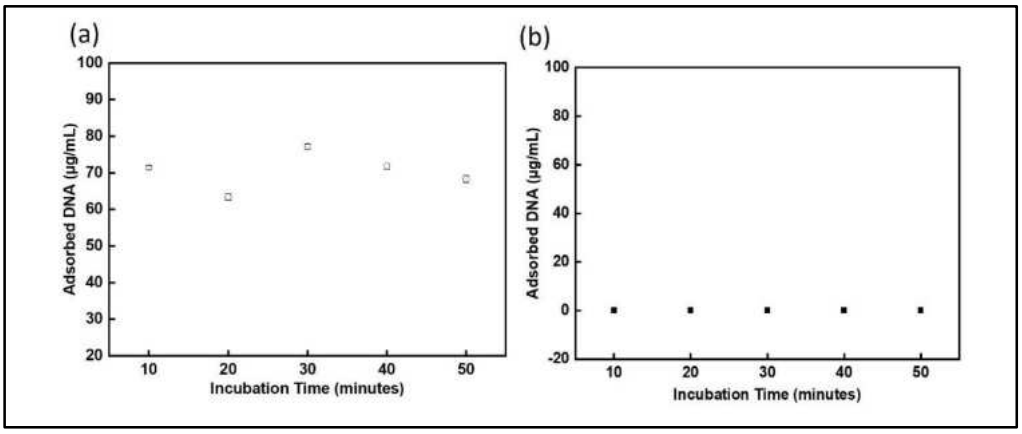

Figure 3.7 Effect of incubation time by UV-visible DNA quantification on; (a) glycine@Fe_3O_4-DNA conjugation, and (b) pristine Fe_3O_4-DNA conjugation.
DNA = 50 µg/mL, temperature = 25°C, nanoparticles = 50 µg/mL, pH = 5.

Table 3.5. Quantification of adsorbed DNA on glycine@Fe_3O_4 by influencing incubation time conditions.

No.	Incubation time (min)	Adsorbed DNA (µg/mL)
1.	10	71.46 ± 0.56
2.	20	63.40 ± 0.83
3.	30	77.24 ± 0.71
4.	40	71.91 ± 0.92
5.	50	68.37 ± 0.93

3.7.3. DNA DESORPTION FROM GLYCINE-MODIFIED IRON OXIDE NANOPARTICLE-DNA (Fe_3O_4-DNA) CONJUGATION

Desorption of DNA from glycine@Fe_3O_4 was occurred in presence of desorption agent with pH 8 (29) with 250 rpm for 30 min at room temperature. **Figure 3.8** shows desorption of DNA from glycine@Fe_3O_4 using UV-visible spectroscopy analysis. The desorption rate obtained from equations 1 and 2 is 96.9 ± 2.65 % of total adsorbed DNA. Here, only DNA (without conjugation) is considered as a positive control (PC).

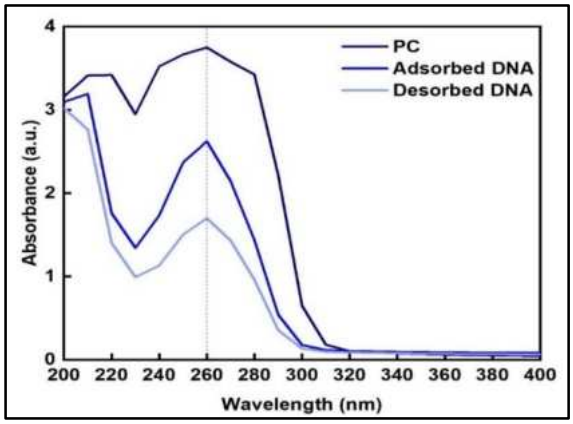

Figure 3.8. UV-visible spectra scan of desorbed DNA from glycine@Fe_3O_4.
DNA = 50 µg/mL, temperature = 25°C, glycine@Fe_3O_4 = 50 µg/mL, pH = 7, time = 30 min.

Validation of desorption of DNA from glycine@Fe_3O_4 was carried out through agarose gel electrophoresis as depicted in **Figure 3.9**. This figure shows standard DNA band in well 1 considered as positive control. Wells 2 to 5 show adsorbed and desorbed DNA with 600 and 100 kb fragments. Well 6 contains reference DNA ladder of 1000 kb unit. Further, well 7 depicts no

DNA band as it is negative control. The figure clearly represents the DNA adsorption and desorption on and from the glycine@Fe_3O_4, respectively.

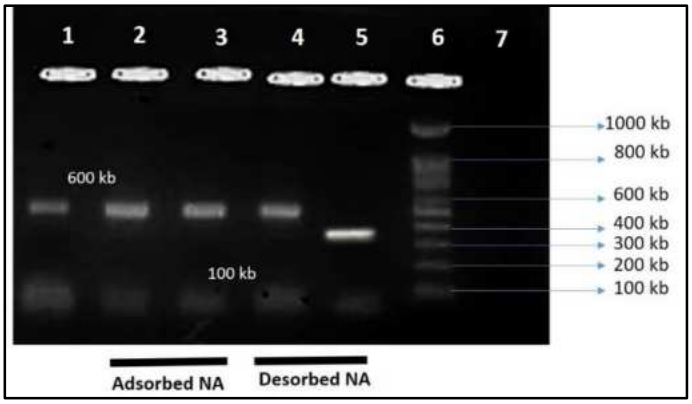

Figure 3.9. Desorption of DNA from glycine@Fe_3O_4 by agarose gel electrophoresis. Well 1 shows standard DNA bands. Whereas, wells 2-3 show adsorbed and wells 4-5 show desorbed DNA bands. Wells 6 and 7 show reference DNA ladder and negative control, respectively.

3.7.4. ZETA POTENTIAL MEASUREMENTS

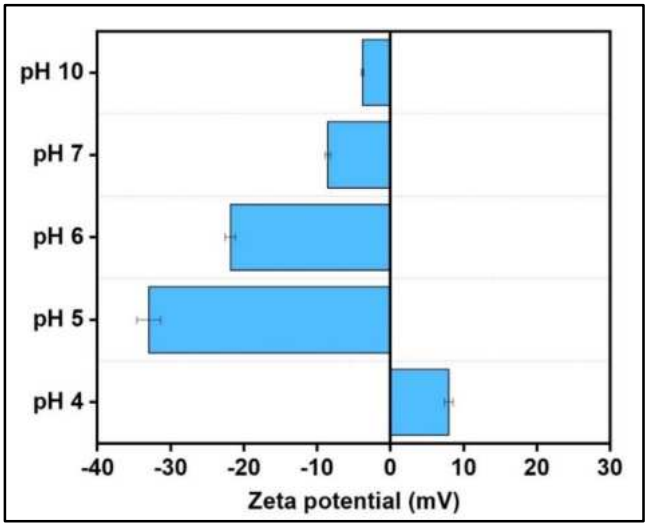

Figure 3.10. Zeta potential of glycine@Fe_3O_4-DNA conjugates at different pH.

Zeta potential analysis of glycine@Fe_3O_4-DNA conjugates at different pH provides surface charge values in **Figure 3.10**. At pH 4, the positive surface charge is present on the glycine@Fe_3O_4-DNA conjugates with the value of 7.99 ± 0.55 mV. At pH 5, stable conjugate formation occurs as the surface charge on conjugate is – 32.97 ± 1.63. At pH 6, 7, and 8 negative surface charges are present with the values - 21.85 ± 0.69, - 8.54 ± 0.38, -

3.82 ± 0.18 mV, respectively. It is considered that if the zeta potential is in between the range of -30 to +30 mV, the particles remain stable in the respective medium (30, 31).

3.8. CONCLUSIONS

Present chapter denotes the conjugation of iron oxide nanoparticle and DNAs by simple means. In previous chapter, glycine-modified iron oxide nanoparticles were synthesized by chemical co-precipitation method and named as glycine@Fe_3O_4. This chapter highlights the importance of glycine in DNA conjugation, possible interactions of glycine@Fe_3O_4 and DNA conjugation, and experimental study. To obtain efficient glycine@Fe_3O_4–DNA conjugates, following parameters were optimized – DNA concentration, pH, and incubation time. Adsorption and desorption studies of DNA on and from glycine@Fe_3O_4 proved glycine@Fe_3O_4 an efficient candidate for biomedical applications like pathogen detection, DNA separation, or gene delivery. pH-influenced electrostatic interactions are responsible for glycine@Fe_3O_4-DNA conjugate formation. Computational analysis additionally proves the proposed conjugation. Optimized conditions, 50 µg/mL DNA, pH 5, and 30 min incubation time was confirmed to make glycine@Fe_3O_4-DNA conjugates. Further, 96.9 ± 2.65 % of total adsorbed DNA was desorbed from glycine@Fe_3O_4. Further, zeta potential analysis of glycine@Fe_3O_4-DNA conjugates showed stable conjugation with the strong negative surface charge, – 32.97 ± 1.63 at pH 5. These results suggest adsorption and desorption of DNA on and from glycine@Fe_3O_4, respectively.

3.9. REFERENCES

[1] F. Wang, P. Li, H. C. Chu, P. K. Lo. **Nucleic acids and their analogues for biomedical applications**. Biosensors. 2022; 12(2): 93.

[2] R. Paul, E. Ostermann, Q. Wei. **Advances in point-of-care nucleic acid extraction technologies for rapid diagnosis of human and plant diseases**. Biosens. Bioelectron. 2020; 169: 112592.

[3] L. Z. Kong, S. M. Kim, C. Wang, S. Y. Lee, S. C. Oh, S. Lee, S. Jo, T. D. Kim. **Understanding nucleic acid sensing and its therapeutic applications**. Exp. Mol. Med. 2023: 1.

[4] L. Abarca-Cabrera, P. Fraga-García, S. Berensmeier. **Bio-nano interactions: binding proteins, polysaccharides, lipids and nucleic acids onto magnetic nanoparticles.** Biomater. Res. 2021; 25: 1.

[5] J. R. Sosa-Acosta, C. Iriarte-Mesa, G. A. Ortega, A. M. Díaz-García. **DNA-iron oxide nanoparticles conjugates: Functional magnetic nanoplatforms in biomedical applications**. Surface-modified nanobiomaterials for electrochemical and biomedicine applications. 2020:19-47.

[6] N. M. Noah, P. M. Ndangili. **Green synthesis of nanomaterials from sustainable materials for biosensors and drug delivery**. Sensors International. 2022; 3: 100166.

[7] R. Abbasi, G. Shineh, M. Mobaraki, S. Doughty, L. Tayebi. **Structural parameters of nanoparticles affecting their toxicity for biomedical applications: a review**. J. Nanopart. Res. 2023; 25(3): 43.

[8] I. Khan, K. Saeed, I. Khan. **Nanoparticles: Properties, applications and toxicities.** Arabian journal of chemistry. 2019; 12(7): 908.

[9] U. S. Ezealigo, B. N. Ezealigo, S. O. Aisida, F. I. Ezema. **Iron oxide nanoparticles in biological systems: Antibacterial and toxicology perspective**. JCIS Open. 2021; 4: 100027.

[10] S. Kim, Y. H. No, R. Sluyter, K. Konstantinov, Y. H. Kim, J. H. Kim. **Peptide-nanoparticle conjugates as a theranostic platform**. Coordination Chemistry Reviews. 2024; 500: 215530.

[11] S. J. Shepherd, D. Issadore, M. J. Mitchell. **Microfluidic formulation of nanoparticles for biomedical applications**. Biomaterials. 2021; 274: 120826.

[12] N. Desai. **Challenges in development of nanoparticle-based therapeutics**. AAPS journal. 2012; 14(2): 282.

[13] S. Eljack, S. David, A. Faggad, I. Chourpa, E. Allard-Vannier. **Nanoparticles design considerations to co-deliver nucleic acids and anti-cancer drugs for chemoresistance reversal.** Int. J. Pharm: X. 2022: 100126.

[14] F. Wang, P. Li, H. C. Chu, P. K. Lo. **Nucleic acids and their analogues for biomedical applications**. Biosensors. 2022; 12(2): 93.

[15] K. Köse. **Nucleotide incorporated magnetic microparticles for isolation of DNA**. Process Biochemistry. 2016; 51(10): 1644.

[16] J. Zhang, T. Zhang, J. Gao. **Biocompatible iron oxide nanoparticles for targeted cancer gene therapy: A review.** Nanomaterials. 2022; 12(19): 3323.

[17] G. Sanità, B. Carrese, A. Lamberti. **Nanoparticle surface functionalization: how to improve biocompatibility and cellular internalization**. Front. Mol. Biosci. 2020; 7: 587012.

[18] J. H. Min, M. K. Woo, H. Y. Yoon, J. W. Jang, J. H. Wu, C. S. Lim, Y. K. Kim**. Isolation of DNA using magnetic nanoparticles coated with dimercaptosuccinic acid**. Anal. Biochem. 2014; 447: 114.

[19] L. S. Arias, J. P. Pessan, A. P. Vieira, T. M. Lima, A. C. Delbem, D. R. Monteiro. **Iron oxide nanoparticles for biomedical applications: A perspective on synthesis, drugs, antimicrobial activity, and toxicity**. Antibiotics. 2018; 7(2): 46.

[20] Li X, Wang L, Fan Y, Feng Q, Cui FZ. **Biocompatibility and toxicity of nanoparticles and nanotubes**. J. Nanomater. 2012; 2012: 6.

[21] C. J. Taylor, A. Pomberger, K. C. Felton, R. Grainger, M. Barecka, T. W. Chamberlain, R. A. Bourne, C. N. Johnson, A. A. Lapkin. A **Brief Introduction to Chemical Reaction Optimization**. Chem. Rev. 2023; 123(6): 3089.

[22] T. Tanaka, R. Sakai, R. Kobayashi, K. Hatakeyama, T. Matsunaga. **Contributions of phosphate to DNA adsorption/desorption behaviors on aminosilane-modified magnetic nanoparticles.** Langmuir. 2009; 25(5): 2956.

[23] C. Leppin, A. Langhoff, H. F. Poggemann, A. S. Gödde, D. Johannsmann. **Fast and slow EQCM response of zwitterionic weak electrolytes to changes in the electrode potential: a pH-mediated mechanism**. Analyst. 2021; 146(19): 6005.

[24] Z. M. Saiyed, C. Bochiwal, H. Gorasia, S. D. Telang, C. N. Ramchand. **Application of magnetic particles (Fe_3O_4) for isolation of genomic DNA from mammalian cells**. Analytical Biochemistry. 2006; 356(2): 306.

[25] K. Smerkova, S. Dostalova, M. Vaculovicova, J. Kynicky, L. Trnkova, M. Kralik, V. Adam, J. Hubalek, I. Provaznik, R. Kizek. **Investigation of interaction between magnetic silica particles and lambda phage DNA fragment**. J. Pharm. Biomed. Anal. 2013; 86: 65.

[26] S. Kumar, A. Sindhu, T. Vasantha, I. Khoiroh, N. Devunuri, P. Venkatesu. **Preferential and competitive role of hydrophilic/hydrophobic interactions quantifying amino acid-based ILs for papain stabilization.** J. Mol. Liq. 2022; 363: 119920.

[27] R. Herboth, G. Gopakumar, C. Caleman, M. Wohlert. **Charge state dependence of amino acid propensity at water surface: mechanisms elucidated by molecular dynamics simulations**. J. Phys. Chem. A. 2021; 125(22): 4705.

[28] X. Dou, Y. M. Jung, Z. Q. Cao, Y. Ozaki. **Surface-enhanced Raman scattering of biological molecules on metal colloid II: effects of aggregation of gold colloid and comparison of effects of pH of glycine solutions between gold and silver colloids**. Appl. spectrosc. 1999; 53(11): 1440.

[29] A. G. Pérez, E. González-Martínez, C. R. Águila, D. A. González-Martínez, G. G. Ruiz, A. G. Artalejo, H. Yee-Madeira. **Chitosan-coated magnetic iron oxide nanoparticles for DNA and rhEGF separation**. Colloids Surf. 2020; 591: 124500.

[30] N. Chandrasekar, K. Kumar, K. S. Balasubramnian, K. Karunamurthy, R. Varadharajan. **Facile synthesis of iron oxide, iron-cobalt and zero valent iron nanoparticles and evaluation of their anti-microbial activity, free radicle scavenging activity and antioxidant assay**. DJNB. 2013, 8(2): 765.

[31] A. P. Tiwari, R. K. Satvekar, S. S. Rohiwal, V. A. Karande, A. V. Raut, P. G. Patil, P. B. Shete, S. J. Ghosh, S. H. Pawar. **Magneto-separation of genomic deoxyribose nucleic acid using pH responsive Fe_3O_4@silica@chitosan nanoparticles in biological samples**. Rsc Advances. 2015; 5: 8463.].

Chapter 4

Klebsiella pneumoniae DNA separation based on glycine-modified iron oxide nanoparticle–DNA conjugate formation

4.1. INTRODUCTION

Bacteria pose a significant threat to human health, causing a wide range of diseases with varying degree of severity. Bacterial infections are caused by invasion and proliferation of bacteria within the body. Bacteria are single celled organisms that can be found everywhere, including soil, water, air, and within the living organisms [1].

The bacterial DNA separation allows diagnostic testing, identification of bacterial species, genomic analysis, antibiotic resistance monitoring, vaccine development, and environmental studies. It is a fundamental step in a wide range of scientific and clinical applications, enabling researchers and healthcare professionals to study bacterial biology, diagnose infections, develop treatments and monitor bacterial populations for public health purposes [2]. *K. pneumoniae* is a leading cause of hospital-acquired pneumonia, particularly in the individuals with compromised immune systems or underlying medical conditions. The chapter particularly focuses on the *Klebsiella pneumoniae* DNA separation by using glycine@Fe_3O_4 nanoparticles.

4.2. METHODS OF BACTERIAL DNA SEPARATION

Scientists have made extraordinary progress in designing extraction methods that are more reliable, easier and faster to perform, more cost-effective and produces a higher yield from the first DNA separation performed by Friedrich Miescher in 1869 [3]. The classic liquid-liquid DNA extraction method involves the use of organic and inorganic reagents such as phenol-chloroform which pose a toxic threat to humans. Many newer methods are now based on physical extraction, which have significantly contributed to developing simpler methods for DNA handling, such as extraction using magnetic beads and cellulose-based filter paper. With the advent of gene-editing and personalized medicine, there has been an increase in the demand for reliable and efficient DNA separation methods that can yield adequate quantities of high-quality DNA with minimal impurities [5]. Widely used bacterial DNA separation methods have been discussed below.

4.2.1. CHROMATOGRAPHY-BASED DNA SEPARATION

DNA can be isolated from biological material using chromatography-based DNA extraction techniques. Size exclusion chromatography (SEC) and ion-exchange chromatography (IEC) are two extensive types of the mentioned procedure. An organic solvent is employed in SEC to separate molecules based on their shapes and sizes at the molecular level. Porous beads made of polyacrylamide, dextran, or agarose are present in the column. Smaller molecules, such mRNA and proteins, enter through the tiny pores and channels of the beads when the sample is added on top and transported through the column, however DNA is prevented from entering the beads and eludes the matrix with its higher hydrodynamic volume. As a result, DNA elutes from the column more quickly than smaller molecules. SEC works well with materials that are sensitive to pH and metal ion concentration changes.

IEC is another chromatography-based method for extracting DNA. A solution containing DNA anion-exchange resin is used to bind DNA with its positively charged diethylaminoethyl cellulose (DEAE) group in order to initially equilibrate the column. Other biological elements such as proteins, lipids, carbohydrates, metabolites, and RNA are eluted with medium-salt buffers while DNA remains in the column. The pH can then be lowered or high salt can be used to recover DNA. When compared to other DNA extraction methods that produce high-quality DNA, including CsCl-gradient centrifugation, this procedure is comparatively easy to carry out [4].

However, only a trained individual is capable of operating the chromatographic apparatus. Instruments used in chromatography are expensive. The overload of the samples leads to an error. The expensive and fragile components of chromatography equipment must be handled carefully. To separate the DNA, some procedures demand an additional solvent. Periodic upkeep and replacement parts are required. Some chromatographic techniques have large power requirements. To achieve effective separation, a high operational pressure may be needed.

4.2.2. GRADIENT CENTRIFUGATION-BASED DNA SEPARATION

Inorganic solvents like cesium chloride (CsCl) are first combined with DNA, and the mixture is then ultra-centrifuged at a high speed for more than 10 h (10,000–12,000 rpm). DNA separates from the other materials using centrifugation based on its density. Upon reaching the isopycnic point, one or more DNA bands may be visible depending on the density-varying DNA types. Supercoiled DNA can accumulate at lower densities because the intercalating chemical ethidium bromide (EtBr) is integrated into non-supercoiled DNA molecules more frequently than supercoiled DNA molecules. Under ultraviolet light, the DNA's location is clearly visible. EtBr and CsCl are eliminated before DNA is precipitated with ethanol. It is possible to utilize this procedure to extract DNA from bacteria, although a significant quantity of the original material source is needed. Furthermore, this approach requires a lengthy period of high-speed ultra-centrifugation, which makes it difficult, time-consuming, and expensive [5].

4.2.3. PHENOL-CHLOROFORM EXTRACTION

The process of phenol-chloroform based DNA separation involves vigorous mixing of sample with the phenol-chloroform solution followed by the mixture centrifuging. As phenol partially inhibit the RNase action, alcohol and chloroform solutions are being added to maintain the pure DNA separation. A high concentration of salt and ethanol or isopropanol can be used to separate the upper (aqueous) phase holding the DNA from the lower (organic) phase containing denatured proteins after centrifugation. The last step is to collect the target DNA by dissolving it in TE buffer or sterile distilled water after washing with 70% ethanol to eliminate any leftover ethanol or isopropanol. By using guanidinium isothiocyanate concurrently, this technique is also employed for RNA extraction. After separating the upper phase (total RNA) from the bottom phase (total DNA and proteins), the total RNA is recovered by precipitation with isopropanol. The phenol-chloroform method albeit more easier than CsCl/EtBr and very effective for extracting nucleic acids, presents difficulties for the clinical microbiology laboratory

since phenol has significant drawbacks because it is poisonous, caustic, and flammable [6] .

4.2.4. SOLID PHASE SEPARATION

DNA can be efficiently and quickly purified using solid-phase separation instead of liquid extraction, which has drawbacks like inadequate phase separation. Solid-phase separation uses a spin column driven by centrifugal force. One of the most used methods for separating nucleic acids today uses silica in a solid-phase extraction. Positively charged silica aggressively interacts with negatively charged DNA, allowing for quick, accurate, and quantitative purification. It works with clinical specimens, DNA, and bacteria and requires minimal time. The steps in the solid-phase extraction procedure are cell lysis, nucleic acid adsorption, washing, and elution. The process of conditioning a column involves employing a buffer with a specific pH. After cell lysis and decanting of lysis buffer into the column, the nucleic acid will be liberated. A chaotropic salt solution is used for the adsorption of nucleic acids. A competitive agent is present in washing buffers, which can remove impurities like proteins and salts. Elution involves adding TE buffer to the column to release pure nucleic acid. However, the process requires ample amount of chemicals and skilled labors. Also, the process is time consuming with variable ration of purity [7].

4.2.5. POLYMERASE CHAIN REACTION (PCR)-BASED DNA SEPARATION

Polymerase chain reaction (PCR) represents reliable method to selectively separate and amplify a specific DNA region. On a thermocycler, PCR is carried out in three steps: (1) dsDNA template denaturation at 92–95°C, (2) primer annealing at 50–70°C, and (3) dsDNA molecule extension at around 72°C. There are 30–40 repetitions of these stages performed. $MgCl_2$, buffer (pH: 8.3–8.8), Deoxynucleoside triphosphates (dNTPs), PCR primers, target DNA, and thermostable DNA polymerase are a few of the chemical elements of PCR. The sequence in the DNA template that will be amplified by PCR is known as the target sequence. In order to initiate DNA synthesis in PCR, single-stranded DNA primers must match the sequences at the ends of or within the

target DNA. These primers are typically 18–25 nucleotides long [8]. However, the method is tedious and time-consuming. The PCR detection apparatus is huge and expensive, and the users require specialized training. Therefore, it is crucial to create quick and affordable nucleic acid detection tools and technology.

4.3. GLYCINE-MODIFIED IRON OXIDE NANOPARTICLES (glycine@Fe_3O_4)-BASED NUCLEIC ACID SEPARATION

In the field of molecular biology and biotechnology, the separation and purification of nucleic acids, such as DNA and RNA, are essential for numerous applications, including genetic analysis, diagnostics, and therapeutic development. Magnetic iron oxide nanoparticles (Fe_3O_4) have emerged as a powerful tool for nucleic acid separation due to their unique properties, including high surface area, tunable size, and super-paramagnetism. Various magnetic nanoparticles-based strategies are employed for nucleic acid separation, highlighting their advantages and potential applications [9].

4.3.1. INCORPORATION OF IRON OXIDE NANOPARTICLES (Fe_3O_4) FOR DNA SEPARATION

Magnetic iron oxide nanoparticles (Fe_3O_4) are nanoscale particles with magnetic properties, typically consisting of a magnetic core and a functionalized surface. The most commonly used magnetic materials in Fe_3O_4 are iron oxide-based compounds, such as magnetite (Fe_3O_4) and maghemite (γ-Fe_2O_3). These nanoparticles exhibit superparamagnetic behavior, which means they become magnetic in the presence of an external magnetic field but lose their magnetization when the field is removed. This property allows for efficient separation and manipulation of MNPs using external magnetic fields [9].

4.3.2. SURFACE MODIFICATION OF IRON OXIDE NANOPARTICLES (Fe_3O_4)

The surface of Fe_3O_4 can be modified with various molecules, such as polymers, surfactants, antibodies, or nucleic acid probes, biological entities, to impart specific functionalities. These functionalized or modified Fe_3O_4 enable selective binding and separation of DNA from complex biological samples. For

example, specific oligonucleotide probes can be immobilized onto the Fe_3O_4 surface to capture complementary DNA sequences [10].

4.3.3. METHODS FOR DNA SEPARATION USING IRON OXIDE NANOPARTICLES (Fe_3O_4)

Magnetic Bead-Based Separation:

This strategy involves the immobilization of DNA-specific probes on Fe_3O_4. When the modified Fe_3O_4 are added to a sample containing DNA, the complementary sequences bind to the probes, allowing for selective isolation. By applying an external magnetic field, the Fe_3O_4, along with the bound DNA, can be easily separated from the solution, enabling efficient purification [11].

Solid-Phase Extraction:

Fe_3O_4 can be functionalized with solid supports, such as silica, to create a solid-phase extraction system. The nucleic acids (DNA or RNA) present in a sample can be selectively adsorbed onto the Fe_3O_4, followed by washing steps to remove impurities. Finally, the Fe_3O_4 are collected using a magnet, and the purified nucleic acids can be eluted for downstream applications [12].

Microfluidic-Based Separation:

Fe_3O_4 are also integrated into microfluidic devices to achieve efficient DNA separation. Microfluidic channels are designed with specific binding regions coated with Fe_3O_4. When the sample is introduced into the device, the target nucleic acids selectively bind to the Fe_3O_4 within the microfluidic channel. The application of an external magnetic field facilitates the separation of the Fe_3O_4 and the bound nucleic acids, allowing for high-throughput and rapid purification [13].

4.3.4. ADVANTAGES AND APPLICATIONS

The utilization of Fe_3O_4 in nucleic acid separation offers several advantages over conventional methods. Fe_3O_4 provide fast and efficient separation due to their high surface area, allowing for a higher binding capacity and reduced processing time. The functionalization of Fe_3O_4 with specific probes enables selective binding and separation of target nucleic acids,

even in complex samples. Magnetic separation can be easily scaled up for processing larger sample volumes, making it suitable for various applications, including clinical diagnostics, genomics research, and environmental monitoring. Magnetic nanoparticles-based nucleic acid separation strategies have revolutionized the field of molecular biology by offering rapid, efficient, and selective methods for separation and purification of nucleic acids [14].

4.3.5. LIMITATIONS OF BACTERIAL DNA SEPARATION USING IRON OXIDE NANOPARTICLES (Fe_3O_4)

Bacterial infections pose a significant threat to human health, requiring efficient and accurate diagnostic methods for timely detection and treatment. One promising approach is the use of Fe_3O_4 for bacterial DNA separation. Fe_3O_4, due to their unique magnetic properties, can be employed to isolate and concentrate bacterial DNA from complex clinical samples. While this method holds great potential, it also has certain limitations that need to be addressed for its successful application. Following are the limitations associated with bacterial nucleic acid separation using magnetic nanoparticles [15].

Overcoming the challenges of selectivity, bacterial diversity, sample complexity, DNA integrity, scalability, and cost will contribute to the wider application and adoption of magnetic nanoparticle-based separation methods in clinical settings. Continued research and technological advancements are necessary to improve the performance and overcome the limitations associated with bacterial DNA separation using magnetic nanoparticles. Hence, present chapter tries to improve some mentioned limitations using electrochemical DNA separation and enhance the bacterial DNA separation research.

4.4. EXPERIMENTAL

4.4.1. MATERIALS

Analytical grade (AR grade 99.9%) phosphate buffer saline (PBS) was purchased from Himedia Pvt. Ltd. Three electrode system (Ag/AgCl, platinum and glassy carbon electrodes) was purchased from PSP biological, Nashik, MS, India. Electrochemical workstation (Biologic VSP) was used from Dr. T. D.

Dongale's laboratory, Department of Nanoscience, Shivaji University, Kolhapur, MS, India. *Klebsiella pneumoniae* cultures and DNA samples were obtained from the Dr. D. Y. Patil Medical College, Hospital and Research Centre, Kolhapur, MS, India.

4.4.2. MODIFICATION OF ELECTRODE WITH GLYCINE-MODIFIED IRON OXIDE NANOPARTICLES (glycine@Fe_3O_4)

Previously prepared glycine@Fe_3O_4 were incorporated for *Klebsiella pneumoniae* DNA separation using an electrochemical detection setup. The synthesized nanoparticle (glycine@Fe_3O_4, 1 mg/mL in double distilled water) solution was drop cast on the silica-activated glassy carbon electrode (GCE) and left at room temperature while keeping it vertical. On GCE, a well-adhered black-colored glycine@Fe_3O_4 thin layer was seen to develop and was directly employed for further applications.

4.4.3. ELECTROCHEMICAL MEASUREMENTS

Three electrode cell system in 1 M PBS (Phosphate buffer saline) electrolyte was used to conduct the electrochemical DNA separation using glycine@Fe_3O_4 electrode. Ag/AgCl, platinum plate, and synthesized glycine@Fe_3O_4 GCE were used as the working electrode, counter electrode, and reference electrode, respectively.

The working electrode (glycine@Fe_3O_4) was first stabilized for a limited number of cyclic voltammogram (CV) cycles in 1 M PBS electrolyte, within the 0 to 0.5 V potential window at a scan rate of 50 mV/s, until the steady state of the voltammogram was attained. By gradually adding various (or identical) DNA concentrations in 1 M PBS at a fixed (0.5 V versus Ag/AgCl) potential, the electrochemical properties of DNA separation were investigated. The electrolyte (1 M PBS) was continually swirled at 250 rpm to reduce mass transfer interference. By monitoring CV at various scan rates - 20, 40, and 60 mV/s, it was possible to ascertain the nature of the redox reaction occurring with the GCE electrode. EIS measurements were performed for DNA separation after DNA samples were introduced to the electrolyte.

4.4.4. VALIDATION OF DNA SEPARATION

DNA quantification and polymerase chain reaction (PCR)-associated agarose gel electrophoresis were employed to evaluate the DNA separation efficiency.

4.5. RESULTS AND DISCUSSION

4.5.1. MECHANISM OF BACTERIAL DNA SEPARATION

In the current study, electrochemical conjugation mechanism of *Klebsiella pneumoniae* DNA and glycine@Fe_3O_4 to form a glycine@Fe_3O_4–DNA conjugate on the electrode surface is used to separate DNA from *Klebsiella pneumoniae*. Glycine is an amino acid with simple carbon chain. It conducts the positive charge on the surface at pH 5 and hence attracts negatively charged DNA present in the electrolyte. As a result, specific electrostatic ionic interactions take place on the electrode surface that enable electrochemical separation of the *Klebsiella pneumoniae* DNA.

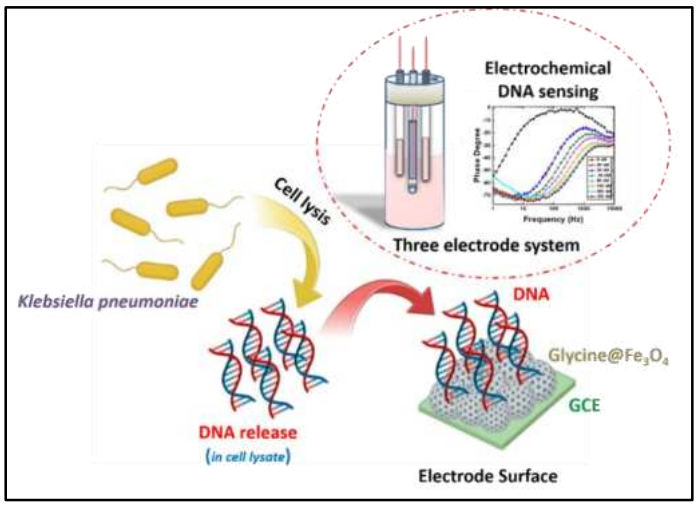

Figure 4.1. Electrochemical *Klebsiella pneumoniae* DNA separation using glycine-modified iron oxide nanoparticles (glycine@Fe_3O_4) electrode.

Figure 4.1 illustrates a DNA separation method used in this study. The above-mentioned conjugation reaction occurs on the electrode surface without addition of any particular enzyme or aptamers, causing higher selectivity towards *Klebsiella pneumoniae* DNA and repelling other non-specific biomolecules like proteins, cells, etc. from the electrode surface. Therefore, in the present work, a non-enzymatic label-free DNA separation methodology was established by using glycine@Fe_3O_4 electrode.

At the electrode surface, the glycine@Fe_3O_4 interact with DNA through various mechanisms, primarily driven by the functional groups present on both the nanoparticles and the DNA molecules.

Glycine molecules on the Fe_3O_4 nanoparticles possess hydrogen bonding sites in the amino and carboxyl groups. DNA bases contain hydrogen bonding sites (nitrogen and oxygen atoms in the bases). Hydrogen bonding interactions occur between the functional groups of glycine and the nitrogenous bases of the DNA, contributing to the stabilization of the DNA on the electrode surface [16, 17]. Both glycine and DNA bases contain aromatic rings capable of engaging in π-π stacking interactions. π-π stacking interactions occur between the π-electron systems of the aromatic rings, further enhancing the binding affinity between the nanoparticles and the DNA molecules [18].

The sequence-specific binding between the DNA bases allows for selective recognition of target DNA sequences by the glycine@Fe_3O_4 nanoparticles. This specific binding enables the capture and separation of target DNA, such as *Klebsiella pneumoniae* DNA, from complex samples on the electrode surface.

Overall, at the electrode surface, the interaction between the glycine@Fe_3O_4 nanoparticles and DNA involves a combination of electrostatic forces, hydrogen bonding, π-π stacking interactions, and sequence-specific binding. These interactions drive the adsorption and selective capture of DNA molecules on the electrode surface, facilitating efficient DNA separation and analysis.

4.5.2. ELECTROCHEMICAL MEASUREMENTS

Electrochemical validation of mentioned DNA separation was carried out by cyclic voltammetry (CV) and electrochemical impedance spectroscopy (EIS) techniques. A working electrode was constructed by simply drop casting 100 µg/mL glycine@Fe_3O_4 over glassy carbon electrode (GCE) with 0.05 cm^2 active surface area and air dried it for 15 min at ambient temperature. Then cyclic voltammetry was implemented with a three-electrode system (GCE,

Ag/AgCl, and platinum wire) for sensing the particular DNA in 1 M PBS electrolyte.

Figure 4.2 depicts a cyclic voltammogram of electrochemical sensing of glycine@Fe_3O_4-modified GCE at various concentrations of standard DNA in PBS (1 M) electrolyte. The cyclic voltammogram suggested a very minute difference in peak current for 20 nM to 300 nM DNA concentration in the electrolyte. The peak observed at - 0.2 V is associated with the interaction between glycine@Fe_3O_4 and DNA which does not appear in the 0 nM concentration of DNA in the electrolyte. The cyclic voltammogram of various DNA concentrations at 20, 40, and 60mV/s scan rates are shown in **Figure 4.2 a**, **b,** and **c,** respectively.

In cyclic voltammetry (CV), the scan rate refers to the rate at which the potential is swept linearly across a range of values during the experiment. It is usually expressed in volts per second (V/s) or millivolts per second (mV/s). The scan rate affects the speed at which the redox reactions occur at the electrode surface and influences the current response observed during the experiment. Higher scan rates lead to faster potential sweeps, resulting in shorter experiment times but may also cause mass transport limitations and other kinetic effects. Conversely, lower scan rates allow more time for reactions to occur and can provide greater sensitivity to slow processes but may require longer experiment times. That means 20 mV/s scan rate provides greater sensitivity to DNA detection. Hence, **Figure 4.2 d** depicts the magnified potential window of cyclic voltammogram at 20 mV scan rate for 0, 100, and 300 nM DNA concentrations.

Based on the cyclic volumetric study, it can be seen that some oxidation reactions are varying at the oxidation area which predict the surface-level interactions at GCE. It can be observed that in absence of DNA (0 nM) no redox peak appears for modified GCE. Whereas, after adding DNA into the solution, small characteristic redox peaks appear, indicating the efficient electron transfer due to interactions between glycine@Fe_3O_4 and DNA. The increase in concentration of DNA shows the more efficient electron transfer at oxidation peak. The limited accessibility of the glycine@Fe_3O_4 to the electrode surface, potentially caused by the rigidity of the double-stranded DNA, may be

contributing to the presence of smaller peaks by hindering efficient electron transfer.

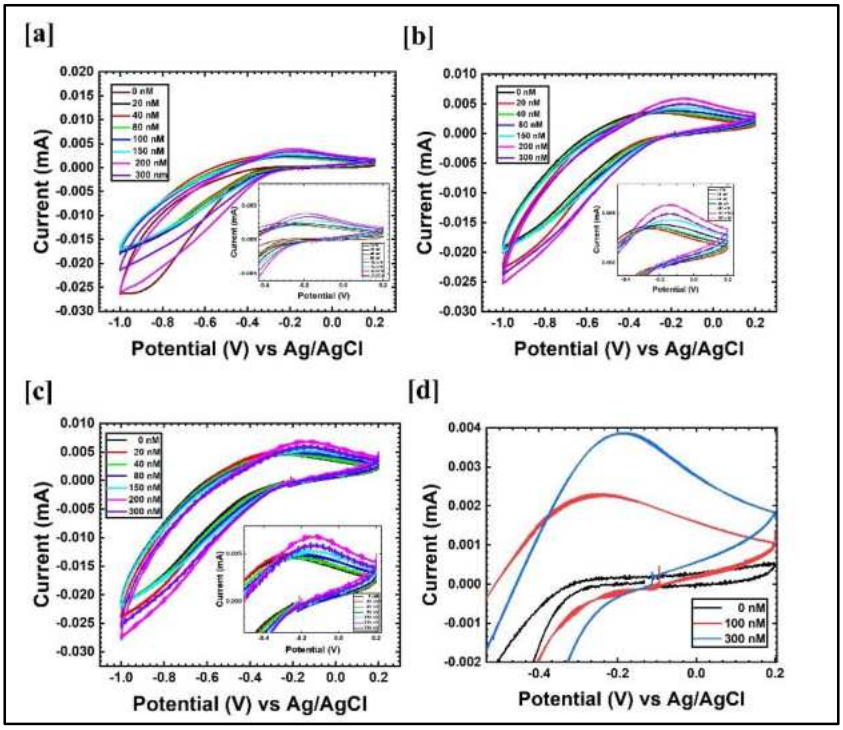

Figure 4.2. Cyclic voltammetry curves of glycine@Fe_3O_4-modified electrodes with the DNA concentration range from 0 to 300 nM; (a) at 20 mV/s, (b) at 40 mV /s, (c) at 60 mV/s, and (d) the magnified potential window at 20 mV/s showing DNA separation in 1 M PBS electrolyte.

The glycine@Fe_3O_4 nanoparticles may participate in redox reactions with DNA. These nanoparticles in their oxidized form (at pH 5), may accept electrons from electron donors. DNA can serve as a reducing agent, donating electrons to glycine@Fe_3O_4 nanoparticles. When glycine@Fe_3O_4 nanoparticles accept electrons from DNA, they undergo reduction, forming the glycine@Fe_3O_4-DNA conjugate. Glycine present on the glycine@Fe_3O_4 nanoparticles becomes oxidizing agent with the protonated NH_3^+ ends and hence tend to accept electrons (e^-) and donate proton (H^+) to the PO_4^- ends of DNA. Thereby, prominent redox reactions occur at the surface of GCE.

However, cyclic Voltammetry does not significantly distinguish the electrochemical response between the glycine@Fe_3O_4 and DNA. Therefore, Electrochemical Impedometric approach is carried out to examine *Klebsiella pneumoniae* DNA separation.

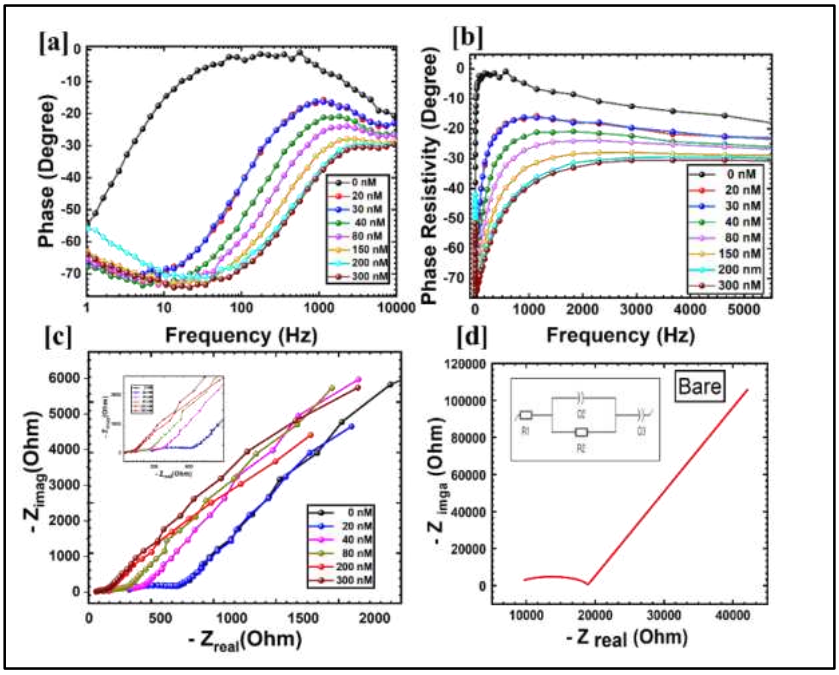

Figure 4.3. Electrochemical impedance spectrometry (EIS) responses of glycine@Fe_3O_4-based DNA sensing with DNA concentration range 0 to 300 nM; (a) Bode plot, (b) Phase resistivity spectrum, (c) and (d) Nyquist plots showing significant concentration-dependent DNA separation.

In **Figure 4.3 a**, the Bode plot typically consists of two plots: magnitude (amplitude) versus frequency and phase angle versus frequency. In this context, the Bode plot likely shows the magnitude and phase of the impedance response of the sensing system vary with frequency. The Bode plot provides information about the DNA dependent impedance behavior of the system and how it changes in response to different DNA concentrations. In this approach, the impedance is measured over a frequency range of 10 mHz to 100KHz. **Figure 4.3 a** depicts the bode plot of 0 to 300 nM concentration range of *Klebsiella pneumoniae* DNA separation in 1 M PBS electrolyte. It is found that bode plots significantly show the variation in peak position frequency (shifted towards higher frequency) as per increase in the DNA concentration. In this figure, concentration dependent frequency shift is observed. 0 nM concentration peak provides absence of DNA in the electrolyte. When DNA is added into the solution, frequency shift takes place in ascending manner. The concentration-dependent DNA separation is analyzed based on the obtained values of bode plot.

In **Figure 4.3 b**, the phase resistivity spectrum refers to the variation of phase angle (phase shift) across different frequencies. This spectrum indicates how the phase difference between the input and output signals changes with frequency. For better analysis, the frequency Vs phase resistivity degree graph is plotted as shown **Figure 4.3 b**. This graph significantly distinguishes the various concentrations of the DNA. It is observed that the Phase Resistivity Degree is directly proportional to the interaction between the DNA and glycine@Fe_3O_4. Also, it is inversely proportional to the concentration of DNA. The decrease in phase resistivity degree is found as the DNA content increased.

For further investigation, the Nyquist plot is made which is frequently employed for impedometric detection. **Figure 4.3 c** shows Nyquist plots for 0 to 300 nM DNA concentrations is depicted. In Figure 4.3c and d, Nyquist plots are typically used to represent impedance data in complex plane form, where the real part of impedance is plotted against the imaginary part. The Nyquist plots likely show the impedance response of the DNA separation system at different DNA concentrations. Changes in the shape, size, and position of Nyquist plots with varying DNA concentration can reveal information about the kinetics of DNA binding, charge transfer processes, and the overall sensitivity of the sensing system. 0 nM (Bare GCE without DNA) DNA concentrations and the corresponding equivalent circuit is depicted in the inset of **Figure 4.3 d**. The equivalent circuit consists of solution resistance (Rs) in series with the parallel combination of constant phase element (Q2) and charge transfer resistance (Rct) and constant phase element (Q3).

The interpretation of the **Figure 4.3** involves understanding the results obtained from electrochemical impedance spectroscopy (EIS) experiments conducted on a glycine@Fe_3O_4-based DNA separation system over a range of DNA concentrations from 0 to 300 nM. Overall, the figure suggests that the electrochemical impedance spectroscopy responses of the glycine@Fe_3O_4-based DNA separation system which exhibit significant concentration-dependent behavior. This implies that the impedance characteristics of the sensing system change noticeably in response to different DNA concentrations,

indicating the potential for sensitive DNA separation and detection using this system.

Table 4.1 contains values of circuit elements obtained from EIS measurements for *Klebsiella pneumoniae* (*K. pneumoniae*) DNA separation at different DNA concentrations. In this case, it includes "Bare" (without DNA) and various concentrations of *K. pneumoniae* DNA ranging from 20nM to 300nM. Rs (Ω) represents the solution resistance, which is the resistance of the electrolyte solution between the working and reference electrodes. It reflects the ionic conductivity of the solution. Q2 (Fs^{-1}) and α2 represent the constant phase element (CPE) parameters associated with the double-layer capacitance at the electrode interface. Q2 represents the CPE constant, and α2 represents the exponent of the CPE. These parameters describe the non-ideal behavior of the double-layer capacitance. Rct (Ω) represents the charge transfer resistance, which is the resistance associated with the transfer of charge across the electrode-electrolyte interface. It reflects the kinetics of the redox reaction or DNA binding process. Q3 (Fs^{-1}) and α3 are similar to Q2 and α2, these columns represent the CPE parameters associated with any additional capacitance or processes occurring at the electrode interface. The table shows that as the DNA concentration increases from 20nM to 300nM, there are changes in the values of the circuit elements. Generally, the solution resistance (Rs) tends to decrease with increasing DNA concentration, possibly due to changes in the ionic strength or conductivity of the solution. The charge transfer resistance (Rct) shows variable behavior with DNA concentration, suggesting changes in the kinetics of the DNA sensing process. The CPE parameters (Q2, α2, Q3, α3) also exhibit variations with DNA concentration, indicating changes in the non-ideal behavior of the double-layer capacitance or additional processes occurring at the electrode interface. The values of the solution resistance (Rs) go on the decrease (from 8480 to 47.9Ω**)** with an increase in the DNA concentration, suggesting increasing the conductivity of the electrolyte. The curvature of the semicircle, which is correlated with the charge transfer resistance (Rct), reduced (10372 to 48) as DNA content increased, indicating that the electrode (glycine@Fe_3O_4) was more interacting

with DNA [19]. The value of the α parameter for CPE indicates the dominance of the capacitive or resistive effect within the electrochemical cell. The value of α is 0 for pure resistive behavior and 1 for optimum capacitive behavior. All values for Q2 and Q3 are above 0.75 indicating that the capacitive effect is dominated at lower frequencies [20]. The table provides valuable information about the electrical properties and behavior of the DNA sensing system under different DNA concentrations, which is essential for separating and detecting *K. pneumoniae* DNA.

Table 4.1. Values of circuit elements for *K. pneumoniae* DNA separation

DNA (nM)	Rs (Ω)	Q2 (Fs^{-1})	α2	Rct (Ω)	Q3 (Fs^{-1})	α3
0 (Bare)	8480	$3.499*10^{-6}$	0.9498	10372	$5.036*10^{-6}$	0.8623
20	263	$0.1489*10^{-6}$	0.9546	343.8	$6.08*10^{-6}$	0.8345
30	263	$0.1508*10^{-6}$	0.9544	322.7	$6.698*10^{-6}$	0.8144
40	133.7	$0.2944*10^{-6}$	0.9272	191.2	$6.715*10^{-6}$	0.8153
80	95.04	$0.4164*10^{-6}$	0.9270	121.2	$7.397*10^{-6}$	0.8024
150	68.23	$0.3201*10^{-6}$	1.0000	68.7	$8.285*10^{-6}$	0.7873
200	50.59	$0.3734*10^{-6}$	1.0000	40.7	$10.19*10^{-6}$	0.7560
300	47.9	$0.589*10^{-6}$	0.9598	48.0	$7.627*10^{-6}$	0.8004

Based on the Bode plot **(Figure 4.3 a)** a calibration curve is plotted as shown in **Figure 4.4 a**. Here, peak position frequency of 0 nM bode plot is considered as f_i and for 10, 20, 40, 80, 150, 200, and 300 nM as f_1-f_7, respectively. The difference between f_i and f_{1-7} is considered as Δf for each concentration. The linear fitting of the calibration plot indicates the linear increment in peak position frequency as an increase with DNA concentration (0-300 nM). For isolated unknown clinical sample concentration simply measured electrochemical impedance spectroscopy (EIS) and plotted a Bode plot for it. The peak position frequency difference (Δf) is calculated by comparing with the bare peak position frequency **(Figure 4.4 b),** which is found to be Δf = 993.13. Finally, Δf is compared with the calibration curve and

found that a separated unknown concentration of *Klebsiella pneumoniae* DNA from the clinical culture is around 20 nM in the presence of other biomolecules present in the clinical culture.

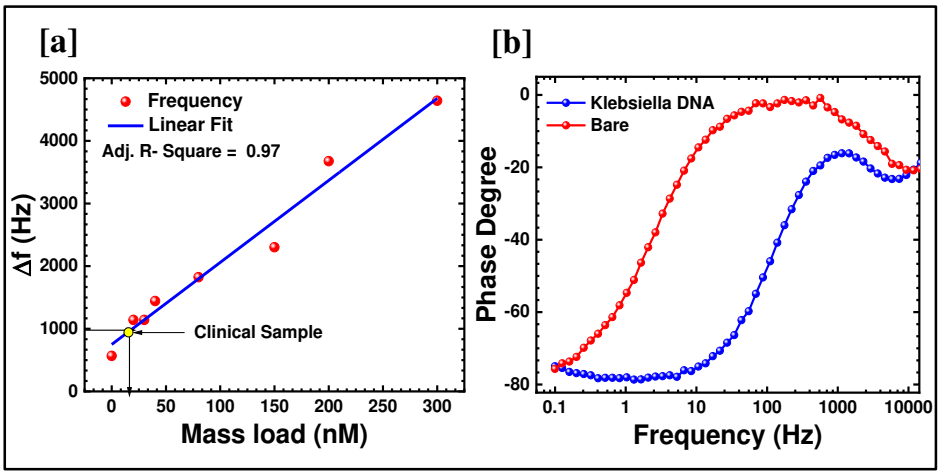

Figure 4.4. Calibration plots for DNA separation; (a) Relationship between DNA mass load and frequency shift provides the R^2 value 0.97, and (b) Bode plot for DNA separation from *Klebsiella pneumoniae clinical* cultures (blue color).

To confirm the selectivity of the *Klebsiella pneumoniae* DNA for glycine@Fe_3O_4 electrode, the same electrochemical experiments such as cyclic voltammetry and electrochemical impedance spectroscopic technique (Bode plot) are performed in the presence of different biological entities like whole cell, protein, and bioanalyte.

Figure 4.5 depicts the cyclic voltammogram (**Figure 4.5 a, c, and e**) and Bode plots (**Figure 4.5 b, d, and f**) for the whole cell, protein, and bioanalyte with 0, 100, 200, and 300 nm concentration at 20 mV/s. These results indicate the minimal electrochemical interactions of other biomolecules viz. whole cell, protein, and bioanalyte with glycine@Fe_3O_4 and do not show any significant change or variation in peak current and peak position frequency in CV and Bode plots respectively. This suggests that the glycine@Fe_3O_4 has high selectivity toward the *Klebsiella* DNA present in the culture.

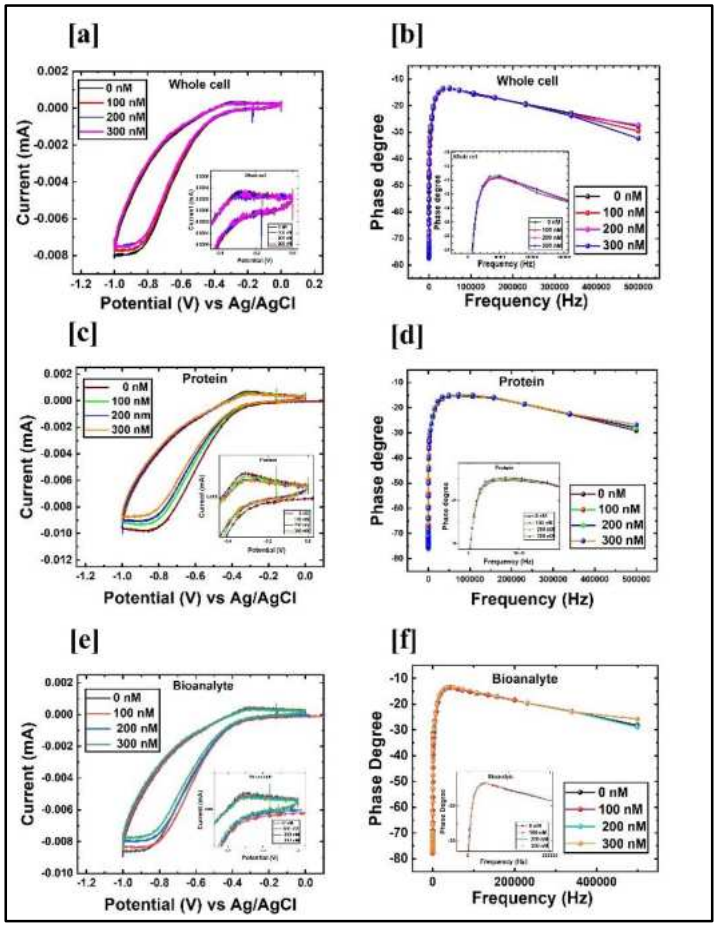

Figure 4.5. Cross reactivity analysis using (a, c, e) cyclic voltammogram, and (b, d, f) EIS responses of glycine@Fe_3O_4 electrode under the successful addition of whole cell, protein, and bioanalyte with the concentration range from 0 to 300 nM.

4.5.3. VALIDATION OF DNA SEPARATION

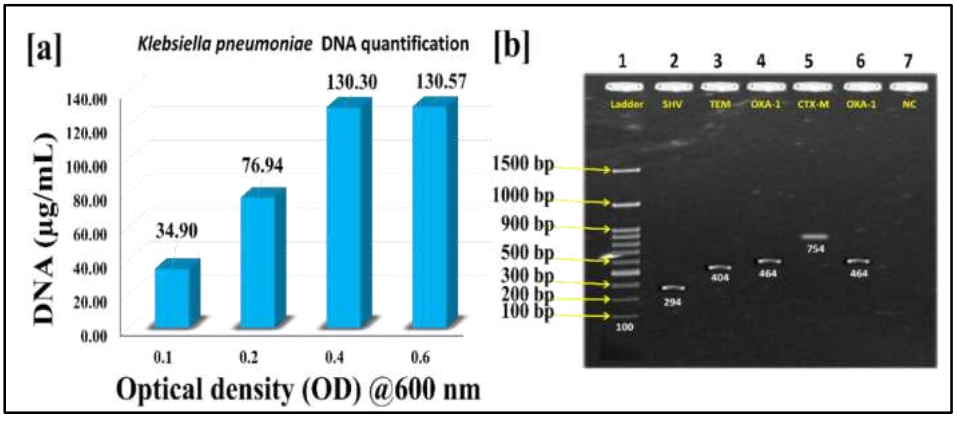

Figure 4.6. Validation of *Klebsiella pneumonia*e DNA separation; (a) UV-visible quantification of separated DNA at different bacterial concentrations (optical densities), and (b) PCR-based agarose gel electrophoresis of sensed DNA showing specific primers (SHV, TEM, OXA-1, CTX-M) of MD-resistant *Klebsiella pneumonia*e DNA fragments.

The above-mentioned DNA separation is validated with currently used DNA detection methods i.e. UV-Visible spectroscopy. The UV spectroscopy-based DNA quantification shows increase in DNA concentration with that of bacterial growth (**Figure 4.6 a**). Sensed DNA is separated from the glycine@Fe_3O_4 by ceasing the applied current; confirming the separated material is DNA. The UV-visible quantification of *Klebsiella pneumoniae* DNA at an optical density of 260 nm serves as a robust validation method for assessing the success of the DNA separation process. By quantifying the separated DNA, concentrations are determined at different bacterial densities, providing crucial evidence of the effectiveness of the separation. Higher absorbance values at 260 nm indicate higher DNA concentrations, suggesting the DNA separation. Therefore, based on the UV-visible quantification results, it is concluded that the DNA separation procedure for *Klebsiella pneumoniae* has been successfully validated, ensuring the reliability of subsequent analyses and experiments.

Also, the conventional PCR-based agarose gel electrophoresis is used for the validation of DNA separation as shown in **Figure 4.6 b.** The separated DNA was further PCR-amplified to detect the specific gene sequence of *K. pneumoniae* DNA. Qualitative PCR estimation of separated DNA [*K. pneumoniae*] from GCE was performed by 0.8 % agarose gel electrophoresis. 1st well represents reference 100-1000 base pairs (bp) DNA ladder. 2nd well represents the SHV gene with 294 bp. 3rd well represents the TEM gene with 404 bp. 4thand 6th wells represent OXA-1 gene with 464 bp. 5th well represents the CTX-M gene with 754 bp. 7th well represents negative control with nuclease-free water. After performing PCR-based agarose gel electrophoresis using specific primers targeting genes commonly associated with multiple drug resistance (MDR) in *Klebsiella pneumoniae*, including SHV, TEM, OXA-1, and CTX-M, successfully validated the DNA separation process. The visualization of amplified DNA fragments corresponds to these specific genes that confirms the presence of MDR-associated genetic elements in the *Klebsiella pneumoniae* DNA sample. This provides strong evidence that the DNA separation method effectively isolated DNA fragments of interest,

enabling their subsequent analysis and characterization. Therefore, based on the PCR results, it is concluded that the validation of *Klebsiella pneumoniae* DNA separation is successful, paving the way for further investigations into antibiotic resistance mechanisms and therapeutic strategies targeting MDR pathogens.

The obtained gene sequences in the present study are compared with the previous publications as described in **Table 4.2** [17]. The detailed PCR conditions given for *K. pneumoniae* DNA detection have been summarized in **Table 4.3**.

Table 4.2. Sensed Anti-microbial resistant gene sequences of Klebsiella pneumoniae DNA.

No.	DNA (Gene)	Primer	Amplicon
1	SHV	SHV-F: CGCCTGTGTATTATCTCCCT SHV-R: CGAGTAGTCCACCAGATCCT	294 bp
2	TEM	TEM-F: TTTCGTGTCGCCCTTATTCC TEM-R: ATCGTTGTCAGAAGTAAGTTGG	404 bp
3	CTX-M	CTX-M-F: CGCTGTTGTTAGGAAGTGTG CTX-M-R: GGCTGGGTGAAGTAAGTGAC	754 bp
4	OXA-1	OXA-1-F: ACACAATACATATCAACTTCGC OXA-1-R:AGTGTGTTTAGAATGGTGATC	464 bp

Table 4.3. Given PCR conditions for the K. pneumonia DNA detection.

Step	TEM	SHV	CT X-M	OXA-48
Initial denaturation	94˚C for 5 min	94˚C for 5 min	94˚C for 5 min	94˚C for 3 min
Denaturation	94˚C for 30 s	94˚C for 30 s	94˚C for 30 s	61.7˚C for 5 min
Annealing	65.5˚C for 30 s	60˚C for 30 s	60˚C for 30 s	61.7˚C for 30 s
Extension	72˚C for 50 s	72˚C for 50 s	72˚C for 50 s	72˚C for 1 min
Final extension	72˚C for 5 min	72˚C for 5 min	72˚C for 5 min	72˚C for 7 min
Cycles	35	35	35	35
Hold	4˚C	4˚C	4˚C	4˚C

4.6. CONCLUSIONS

Klebsiella pneumoniae is an opportunistic bacterium that typically target immune-compromised patients who are hospitalized and have serious underlying illnesses like diabetes mellitus or persistent lung obstruction which are known as nosocomial infections. The use of glycine-modified magnetic iron oxide nanoparticles (glycine@Fe_3O_4) for DNA separation from *Klebsiella pneumoniae* offers a promising approach with detection of nosocomial infection caused due to *K. pneumoniae*. This method enables rapid and accurate isolation of bacterial DNA, facilitating various downstream analyses such as diagnostics, genotyping, and pathogen detection. The glycine@Fe_3O_4 nanoparticles provide a versatile platform for selective separation, enrichment, and detection of target DNA from complex biological samples. Here, the glycine@Fe_3O_4 nanoparticles were utilized for the *Klebsiella pneumoniae* DNA separation from clinical samples. The glycine@Fe_3O_4 acted as bio-analogous receptors in the development of electrochemical DNA separation methodology for the detection of pathogens from clinical samples. The electrode surface serves as the site of reaction between the glycine@Fe_3O_4 and target (DNA). An electrochemical DNA separation works on the basic premise that biological reactions involving the nanoparticles and target can either make or consume ions or electrons, which alter the electric current, potential, or other electrical properties of the solution. The proposed methodology precisely responds to the DNA just in a few min. It separates as low as 20 nM DNA with high sensitivity towards the DNA from the other interfering biomolecules like whole cells, proteins, and bioanalytes in clinical samples. The present method is non-enzymatic and label-free. Thus, it achieves the goal of sensitive, labor-free, and low-cost DNA separation for nosocomial infections.

4.7. REFERENCES

[1] L. R. Johnson, M. Mangel. **Life histories and the evolution of aging in bacteria and other single-celled organisms**. Mechanisms of ageing and development. 2006; 127 (10): 786.

[2] M. H. Wright, J. Adelskov, A. C. Greene. **Bacterial DNA extraction using individual enzymes and phenol/chloroform separation**. Journal of microbiology & biology education. 2017; 18 (2): 10.

[3] R. Dahm. **Discovering DNA: Friedrich Miescher and the early years of nucleic acid research**. Human genetics. 2008; 122: 565.

[4] M. Dairawan, P. J. Shetty. **The evolution of DNA extraction methods**. Am. J. Biomed. Sci. Res. 2020; 8 (1): 39.

[5] E. L. Ibanez, C. Lässer, G. V. Shelke, R. Crescitelli, S. C. Jang, A. Cvjetkovic, A. García-Rodríguez, J. Lötvall. **DNA analysis of low-and high-density fractions defines heterogeneous subpopulations of small extracellular vesicles based on their DNA cargo and topology**. J. Extracell. vesicles. 2019; 8(1): 1656993.

[6] S. Köchl, H. Niederstätter, W. Parson. **DNA extraction and quantitation of forensic samples using the phenol-chloroform method and real-time PCR**. Forensic DNA typing Protoc. 2005; 1(1): 13.

[7] J. H. Shin. **Nucleic acid extraction techniques**. Adv. Tech. Diagnostic Microbiol. 2012; 209.

[8] N. Gupta. **DNA extraction and polymerase chain reaction**. J. Cytol. 2019; 36(2): 1.

[9] K. Niemirowicz, K. H. Markiewicz, A. Z. Wilczewska, H. Car. **Magnetic nanoparticles as new diagnostic tools in medicine**. Adv. Med. Sci. 2012; 57(2): 196.

[10] B. García-Merino, E. Bringas, I. Ortiz. **Synthesis and applications of surface-modified magnetic nanoparticles: Progress and future prospects**. Rev. Chem. Eng. 2022; 38(7): 821.

[11] Z. He, C. Tang, X. Chen, H. Liu, G. Yang, Z. Xiao, W. Li, Y. Deng, L. Jin, H. Chen, Z. Chen. **Based on magnetic beads to develop the kit for extraction of high-quality cell-free DNA from blood of breast cancer patients**. Mater. Express. 2019; 9(8): 956.

[12] M. Zhang, L. Li, B. Li, N. Tian, M. Yang, H. Zhang, C. You, J. Zhang. **Adsorption of DNA by using polydopamine modified magnetic nanoparticles based on solid-phase extraction**. Anal. Biochem. 2019; 579(1): 9.

[13] M. Zhang, L. Li, B. Li, N. Tian, M. Yang, Zhang H, You C, Zhang J. **Magnetic nanoparticles in microfluidic and sensing: From transport to detection**. Electrophoresis. 2020; 41(13): 1206.

[14] C. Tang, Z. He, H. Liu, Y. Xu, H. Huang, G. Yang, Z. Xiao, S. Li, H. Liu, Y. Deng, Z. Chen. **Application of magnetic nanoparticles in nucleic acid detection.** J. Nanobiotechnology. 2020; 18(1): 62.

[15] E. K. Schneider-Futschik, F. Reyes-Ortega. **Advantages and disadvantages of using magnetic nanoparticles for the treatment of complicated ocular disorders**. Pharmaceutics. 2021; 13(8): 1157.

[16] I. Y. Wong, N. A. Melosh. **An electrostatic model for DNA surface hybridization**. Biophysical journal. 2010; 98 (12): 2954.

[17] S. Huang, J. J. Zhu. **Linkage pathways of DNA–nanoparticle conjugates and biological applications**. Chemosensors. 2023; 11 (8): 444.

[18] T. Chen, M. Li, J. Liu. **π–π stacking interaction: a nondestructive and facile means in material engineering for bioapplications**. Crystal Growth & Design. 2018; 18 (5): 2765.

[19] T. Chakraborty, M. Das, C. Y. Lin, Y. Su, B. Yuan, C. H. Kao. **ZIF-8 Nanoparticles based electrochemical sensor for non-enzymatic creatinine detection**. Membranes (Basel). 2022; 12(2): 159.

[20] P. Vadhva, J. Hu, M. J. Johnson, R. Stocker, M. Braglia, D. J. Brett, A. J. Rettie. **Electrochemical impedance spectroscopy for all-solid-state batteries: Theory, methods and future outlook**. ChemElectroChem. 2021; 8(11): 1930.

[21] T. Sana, K. Rami, B. Racha, D. Fouad, A. Marcel, M. Hassan, H. Sani, H. Monzer. **Detection of genes TEM, OXA, SHV and CTX-M in 73 clinical isolates of Escherichia coli producers of extended spectrum Betalactamases and determination of their susceptibility to antibiotics**. Int. Arab. J. Antimicrob. Agents. 2011; 1(1): 5.

Chapter 5

DNA magnetofection in breast cancer cells based on quantum dot-labelled-glycine-modified iron oxide nanoparticle – DNA conjugate formation

5.1. INTRODUCTION

Breast cancer is a devastating disease affecting millions of women worldwide. Despite advancements in treatments, the development of effective therapies for breast cancer remains a significant challenge [1]. Commonly used treatment for breast cancer is surgery where tumor and surrounding healthy tissues are removed by operation [2]. Followed by, adjuvant therapy is given to treat breast cancer patient. Adjuvant therapy is a treatment given after surgery to reduce chances of reoccurrence of tumor and also to remove remaining cancer cells if any. Adjuvant therapy covers radiation, chemotherapy, targeted therapy, immune therapy, and hormonal therapy [3]. Most common one is chemotherapy where steroid drugs are given to the patient to destroy cancer cells. Following are some generic drugs given to patient in chemotherapy; taxens, vinorelbine, ixabepilone, and platinum agents. There are tremendous severe side effects occur due to these drugs, for example damage in nervous and limbic systems [4].

In current research, targeted gene (nucleic acid) delivery (transfection) in tumor-specific area has emerged as a promising strategy to overcome these challenges and enhance the treatment outcomes in breast cancer [5]. Transfection could be considered as one of the adjuvant therapies as it uses target specific detection and destruction of cancer cells. Magnetofection is one of the innovative and efficient transfection techniques which utilizes Fe_3O_4 to deliver therapeutic genes (nucleic acids) to breast cancer cells with precision and efficacy. Magnetofection represents a promising approach for targeted gene delivery in breast cancer cells. Its ability to achieve site-specific and high-efficiency gene delivery combined with its versatility and controllability, makes it a valuable tool in the development of innovative therapeutic strategies for breast cancer treatment. Further research and optimization of magnetofection techniques are necessary to fully exploit its potential and translate it into clinical applications that can improve the lives of breast cancer patients [6].

To achieve mentioned magnetofection process, Fe_3O_4-DNA conjugation is an extremely crucial step. On majority basis, Fe_3O_4 nanoparticles are considered for such applications over other magnetic nanoparticles due to their comparatively less cytotoxicity, easy availability and synthesis. Hence, iron oxide nanoparticle-nucleic acid conjugate remains attractive and feasible choice of researchers for magnetofection [7].

Based on the principle of IONP-DNA conjugation, standard DNA magnetofection in breast cancer cell (MCF-7) has been performed in this chapter and analyzed by a method of fluorescence spectroscopy. It is one of the first magnetofection studies interpreted by fluorescence spectroscopy as per the author's knowledge. As magnetic Fe_3O_4 do not possess property of fluorescence, the respective conjugates have been labelled with carbon quantum dots (QDs). Usually, magnetofection is performed with the help of fluorescent chemical entities like green fluorescent protein [8] and lipofectamine [9]. However, reports suggest that carbon QDs are sustainable, easy to prepare, cost-effective, less cytotoxic, highly fluorescent and biocompatible in nature [10]. Hence, here, carbon quantum dots-labelled iron oxide-nucleic acid conjugates attempted magnetofection with a unique fluorescence spectroscopy method. Detail description of every mentioned topic has been provided further.

5.2. ABOUT BREAST CANCER

Breast cancer is considered as most common malignancy among females globally. Till 1990 breast cancer was at fourth rank in India for most frequent cancers and now in 2023 it has become the first. Hence, early diagnosis, treatment modalities and other loopholes of Indian healthcare practices like, delayed diagnosis, limited funding, and human resources management cause difficult challenges for breast cancer patients. Globally, 2.3 million new cases have been added which represent 11.7% of total cancer cases. In India, 13.5% (1,78,361) cases have been reported till 2016 of total cancer cases. When compared to Western nations, India's breast cancer patient survival rate is lower due to young age at onset, advanced

symptoms at presentation, a delay in the commencement of definitive management, and insufficient treatment [11].

Hence, there is tremendous need in breast cancer research to initiate with innovative diagnostic and treatment strategies to reduce the suffering and death rates of breast cancer patients. The chapter is a small attempt to establish unique magnetofection method of standard DNA into the breast cancer cells so that it will provide a future platform to site-specific therapeutic nucleic acid/gene magnetofection in breast cancer cells and thereby the destruction of cancer cells.

5.3. IMPORTANCE OF MAGNETOFECTION

Traditional nucleic acid delivery (transfection) systems, such as viral vectors, liposomes, have demonstrated limitations such as low transfection efficiency, cytotoxicity, and lack of specificity as shown in **Figure 5.1**. These drawbacks necessitate the development of novel approaches to improve nucleic acid delivery (transfection) in breast cancer cells [13].

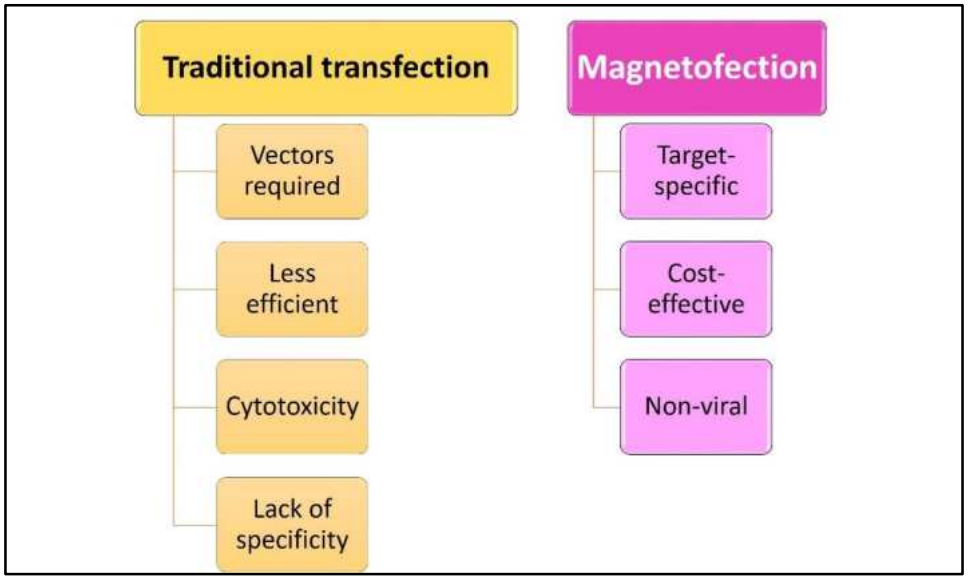

Figure 5.1. Advantages of magnetofection over traditional transfection.

Magnetofection has recently gained attention as a potential solution, offering several advantages over conventional transfection methods. The principle underlying magnetofection is based on the use of MNPs that are conjugated with nucleic acids and guided to specific target sites using an

external magnetic field. As noted earlier, majority of the times MNPs used in magnetofection are Fe_3O_4 nanoparticles [7]. One notable importance of magnetofection is its ability to achieve site-specific delivery. By applying an external magnetic field, nanoparticles can be directed to the desired target site, such as a tumor or specific regions within the breast tissue. This magnetic targeting approach enhances the accumulation of Fe_3O_4 in the vicinity of cancer cells, resulting in increased local concentration of therapeutic nucleic acid and reduces systemic toxicity. Researchers can modulate the uptake and release of therapeutic nucleic acids according to magnetic field. This flexibility allows targeted nucleic acid delivery process according to specific characteristics of breast cancer cells, such as receptor expression profiles or micro-environmental conditions. Additionally, magnetofection demonstrates high transfection efficiency due to the unique properties of Fe_3O_4. Their small size, large surface area, and magnetic behavior facilitate efficient cellular uptake and endosomal escape of nucleic acids. Moreover, the magnetic field applied during magnetofection induces mechanical forces on the cell membrane, further enhancing the internalization of Fe_3O_4 and improving nucleic acid delivery efficiency [14, 15]. Detailed description of types of magnetofection has been given below.

5.4. TYPES OF MAGNETOFECTION

Here are the types of magnetofection, each represents a different approach to achieve targeted magnetofection using MNPs:

5.4.1. COVALENT CONJUGATION MAGNETOFECTION

Covalent conjugation magnetofection involves the chemical attachment of nucleic acids to the surface of Fe_3O_4 through covalent bonds as shown in **Figure 5.2**. This approach typically requires the modification of nucleic acids with functional groups that can react with the surface chemistry of Fe_3O_4. Common coupling chemistries include amino-silane, carboxyl-amine, or thiol-maleimide reactions. The functionalized nucleic acids are then conjugated to the Fe_3O_4, forming stable covalent linkages. Covalent conjugation provides robust binding between the Fe_3O_4 and nucleic

acids, ensuring efficient loading and controlled release of the genetic material [16].

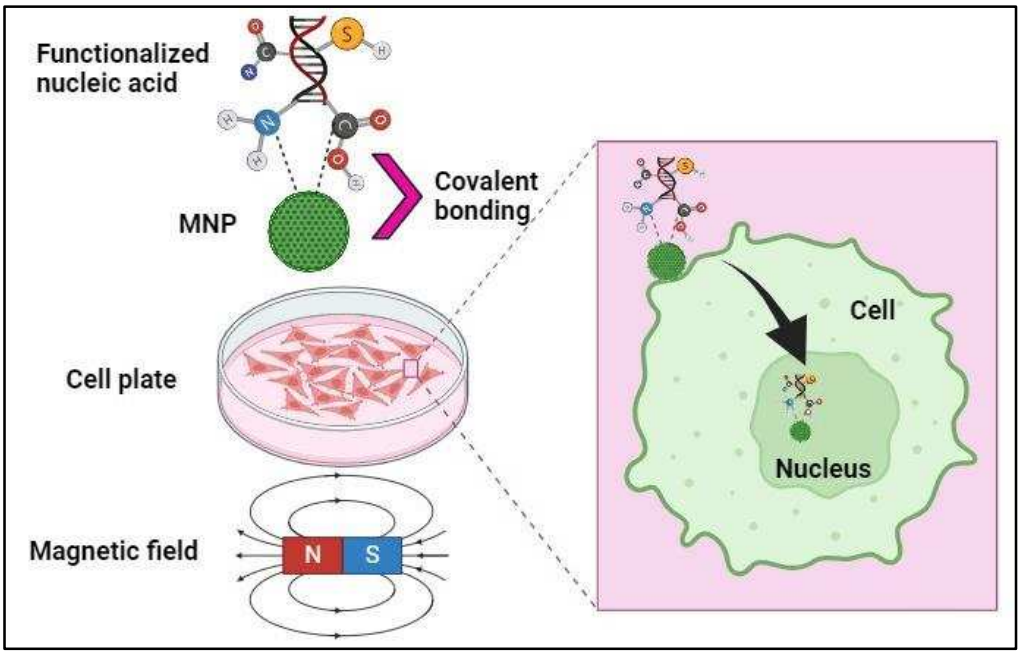

Figure 5.2. Covalent magnetofection of standard DNA in breast cancer cells.

5.4.2. NON-COVALENT MAGNETOFECTION

Non-covalent magnetofection involves the direct adsorption of nucleic acids onto the surface of Fe_3O_4. The Fe_3O_4 used in this approach are typically coated with biocompatible materials, such as dextran or polyethylene glycol (PEG), to enhance stability and prevent aggregation. The nucleic acids, such as plasmid DNA or siRNA, are conjugated with the Fe_3O_4, allowing them to adhere to the Fe_3O_4 surface through non-covalent interactions, such as electrostatic interactions or hydrophobic interactions. This simple and straightforward method allows for efficient loading of nucleic acids onto Fe_3O_4 without the need for complex chemical modifications [17].

Electrostatic complexation magnetofection involves the formation of electrostatic complexes between Fe_3O_4 and nucleic acids. In this method, the Fe_3O_4 are typically coated with positively charged polymers, such as polyethyleneimine (PEI) or poly-l-lysine (PLL), which can interact with negatively charged nucleic acids. The negatively charged nucleic acids, such as siRNA or plasmid DNA, are mixed with the positively charged Fe_3O_4,

leading to the formation of stable complexes through electrostatic interactions [18].

Present study (magnetofection in breast cancer cells) involves electrostatic adsorption method as shown in **Figure 5.3**. The figure describes direct adsorption of nucleic acid (standard DNA) on carbon quantum dot labelled-glycine-modified iron oxide nanoparticles (glycine@Fe_3O_4@QD) and further magnetofection in cell was carried out using an external magnetic field.

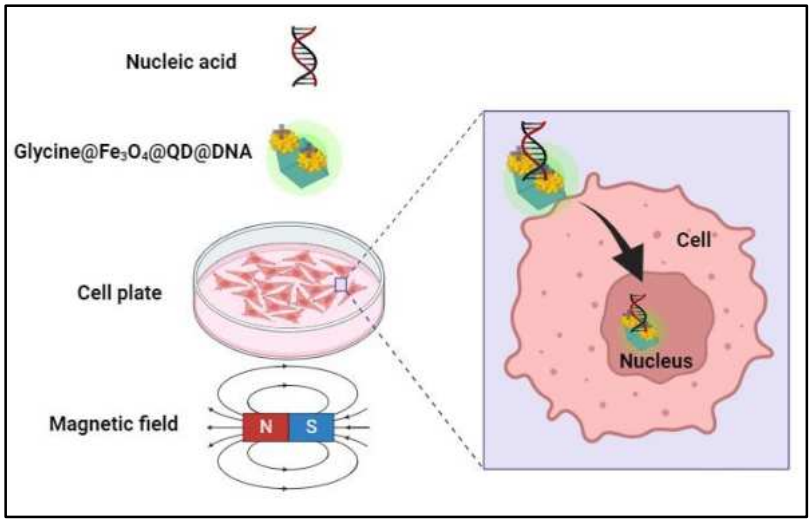

Figure 5.3. Non covalent magnetofection of standard DNA in breast cancer cells.

5.5. ADVANTAGES OF MAGNETOFECTION

One of the key advantages of magnetofection is its ability to achieve targeted and site-specific gene delivery, resulting in higher local concentrations of therapeutic genes and reduced off-target effects [19-21].

The magnetic field applied during magnetofection can induce mechanical forces on the cell membrane, promoting the internalization of Fe_3O_4 and improving gene delivery efficiency and facilitates the efficient delivery of nucleic acids into the target cells, increasing the chances of successful gene expression or gene silencing [22, 23].

Magnetofection can deliver various types of nucleic acids, including plasmid DNA, small interfering RNA (siRNA), microRNA, and antisense

oligonucleotides. This versatility allows researchers to utilize different gene-based therapeutic strategies [24-26].

5.6. EXPERIMENTAL

Standard DNA and Standard fluorescence agent – Fluorescein Isothiocyanate (FITC) were obtained from Sigma Aldrich Pvt. Ltd. MCF-7 cell line was purchased from National Centre for Cell Science, Pune, MS, India. Dulbecco's Modified Eagle Medium (DMEM), fetal bovine serum (FBS), penicillin-streptomycin solution, dimethyl sulfoxide (DMSO) and trypsin-ethylene diamine tetra acetic acid (EDTA) solution were purchased from Himedia Pvt. Ltd. All chemicals have been purchased from Himedia Pvt. Ltd. unless otherwise stated.

5.7. METHODOLOGY

5.7.1. PREPARATION OF QUANTUM DOT LABELLED GLYCINE-MODIFIED IRON OXIDE NANOPARTICLES (glycine@Fe_3O_4@QD)

The glycine@Fe_3O_4 nanoparticles were conjugated with carbon quantum dots (QDs) by incubating both at room temperature. The glycine@Fe_3O_4 nanoparticles (1 mg/mL) were prepared according to the previously established protocol (Chapter 2).

The fluorescent QDs were prepared by previously published method (27) and were added to the glycine@Fe_3O_4 nanoparticle suspension, with the glycine@Fe_3O_4-to-QD ratio optimized through preliminary experiments to achieve maximum labelling efficiency. The formed quantum dots-labelled glycine-modified iron oxide nanoparticles (glycine@Fe_3O_4@QDs) were characterized using fluorescence spectroscopy, UV-visible spectroscopy, and zeta potential analysis.

A stock solution (1 mg/mL) of the fluorescent dye – FITC (positive control) was prepared by dissolving it in a 5% DMSO solution, as per the manufacturer's instructions (Himedia Pvt. Ltd.). The dye solution was protected from light to prevent photobleaching. The stock solution was then diluted with distilled water to obtain the working dye concentration (50 µg/mL), ensuring thorough mixing for a homogeneous solution.

5.7.2. FORMATION OF QUANTUM DOTS LABELLED GLYCINE-MODIFIED IRON OXIDE NANOPARTICLES-DNA (glycine@Fe_3O_4@QD-DNA) CONJUGATE

The stock solution of glycine@Fe_3O_4@QD was vortexed briefly to ensure proper dispersion. The glycine@Fe_3O_4@QD nanoparticles were sonicated for 10 minutes. The standard DNA was diluted in a sterile phosphate buffer saline (PBS) to achieve the desired concentration (50 µg/mL). The desired volume of the DNA solution was pipetted into the microcentrifuge tube containing the glycine@Fe_3O_4@QD by maintaining 1:1 (v/v ratio). The tube was gently vortexed to ensure proper mixing of the glycine@Fe_3O_4@QD and DNA solution. The mixture was incubated at room temperature for 30 minutes to facilitate DNA adsorption onto the glycine@Fe_3O_4@QD. The glycine@Fe_3O_4@QD-DNA conjugates were stored at the appropriate temperature, typically 4°C, until further use.

5.7.3. CELL CULTURE

MCF-7 human breast cancer cells were cultured in high glucose DMEM supplemented with 10 % FBS and 1 % Pen-strep antibiotic. Cells were maintained in a 37°C humidified CO_2 incubator (5% CO_2).

5.7.4. MAGNETOFECTION

MCF-7 cells were allowed to reach approximately 70-80% confluence before proceeding with magnetofection. MCF-7 cells were seeded in sterile culture plates at a density suitable for the experiment (1 x 10^5 cells/mL), allowing them to attach overnight. Prior to magnetofection, the culture medium was carefully removed from the cells and gently washed with PBS.

50 µg/mL glycine@Fe_3O_4@QD-DNA conjugate solution was added directly into the cells, ensuring complete coverage. A clean magnet was positioned in close proximity to the culture plates, aligning it with the desired area for magnetofection. The cells were incubated in the presence of the magnetic field for 30-40 minutes to allow the glycine@Fe_3O_4@QD-DNA conjugate to interact with the cells. After every 10 minutes of the incubation,

the supernatant was carefully aspirated. The cells were washed twice with PBS to eliminate any remaining glycine@Fe_3O_4@QD-DNA conjugate.

5.7.5. AGAROSE GEL ELECTROPHORESIS

Aspirated supernatant centrifuged at 15000 rpm from magnetofected conjugates and pellet was added to 1 % agarose gel with time interval 10 to 40 minutes, and 30 V of electric potential was applied across the gel assembly for 30 minutes. Gel was previously stained with 0.5 g/mL ethidium bromide (etBr) dye and visualized using Gel Doc system (Applied biosystem e gel imager).

5.7.6. CELLULAR UPTAKE ANALYSIS

Magnetofected DNA was quantified from aspirated supernatant after the incubation with cells for 30 minutes.

5.7.7. CYTOTOXICITY ANALYSIS

3-(4, 5-dimethyl thiazol-2-yl)-2, 5-diphenyl tetrazolium bromide (MTT) assay was carried out according to manufacturer's standard instructions to study cytotoxicity of magnetofected nanoparticles.

5.8. RESULTS AND DISCUSSION

5.8.1. PREPARATION OF QUANTUM DOT LABELLED GLYCINE-MODIFIED IRON OXIDE NANOPARTICLES (glycine@Fe_3O_4@QDs)

The conjugation of glycine@Fe_3O_4 and QDs was studied by incubating both in varied ratio. The glycine@Fe_3O_4 nanoparticles amount was kept constant where the QD amount varied in 1 to 6 (v/v) ratio as shown in **Figure 5.4**. Fluorescence intensity was examined with mentioned conjugated samples with the help of fluorescence spectroscopy (JASCO Agilent Technologies, United States).

Fluorescence spectroscopy is a powerful analytical technique used to study the fluorescence properties of substances. The peak intensity in the fluorescence spectrum indicates the amount of fluorescence emitted by the sample at a particular wavelength. Higher intensity generally signifies a

higher concentration of fluorescent and better incorporation of quantum dots onto the glycine@Fe_3O_4. Here, only QDs (without any conjugation) were considered as positive control (PC) which emits highest fluorescence with the intensity >8000 a.u. For 1:4 glycine@Fe_3O_4:QD (v/v) conjugate the fluorescence intensity was emitted as close as positive control (~ 8000 a.u.). Therefore the same ratio was continued for further experiments.

The peak wavelength corresponds to the wavelength at which the maximum fluorescence emission occurs. Optimization involves determining the ideal conditions under which this peak wavelength aligns with the desired characteristics of the QDs. It has been reported that QDs emit fluorescence at 400 nm [27]. Here, glycine@Fe_3O_4@QD conjugates show prominent peaks at 400 nm, heading the way for effective conjugation. Only glycine@Fe_3O_4 nanoparticles (NP only) were used as a negative control.

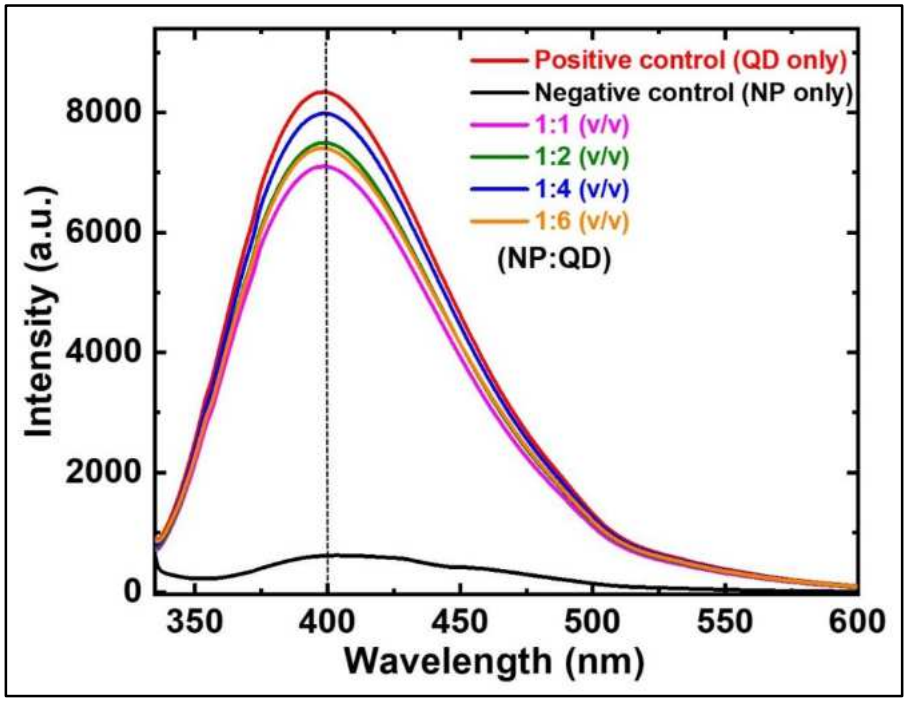

Figure 5.4. Fluorescence spectroscopy analysis for optimization of glycine@Fe_3O_4@QD formation.

Further, UV-Visible spectroscopy (Thermoscientific multiskan sky) was used to examine the formation of glycine@Fe_3O_4@QD nanoparticles as shown in **Figure 5.5**. The QDs presence is confirmed by the absorption peaks in the UV-Vis spectra that correspond to the QDs at 230 and 280 nm (27).

Fluorescence properties of formed material are visualised in **Figure 5.5 (inset)**. Figure shows blue fluorescence in glycine@Fe_3O_4@QD when compared with positive and negative controls.

Hence, with the help of fluorescence and UV-visible spectroscopy, the formation of glycine@Fe_3O_4@QD is confirmed.

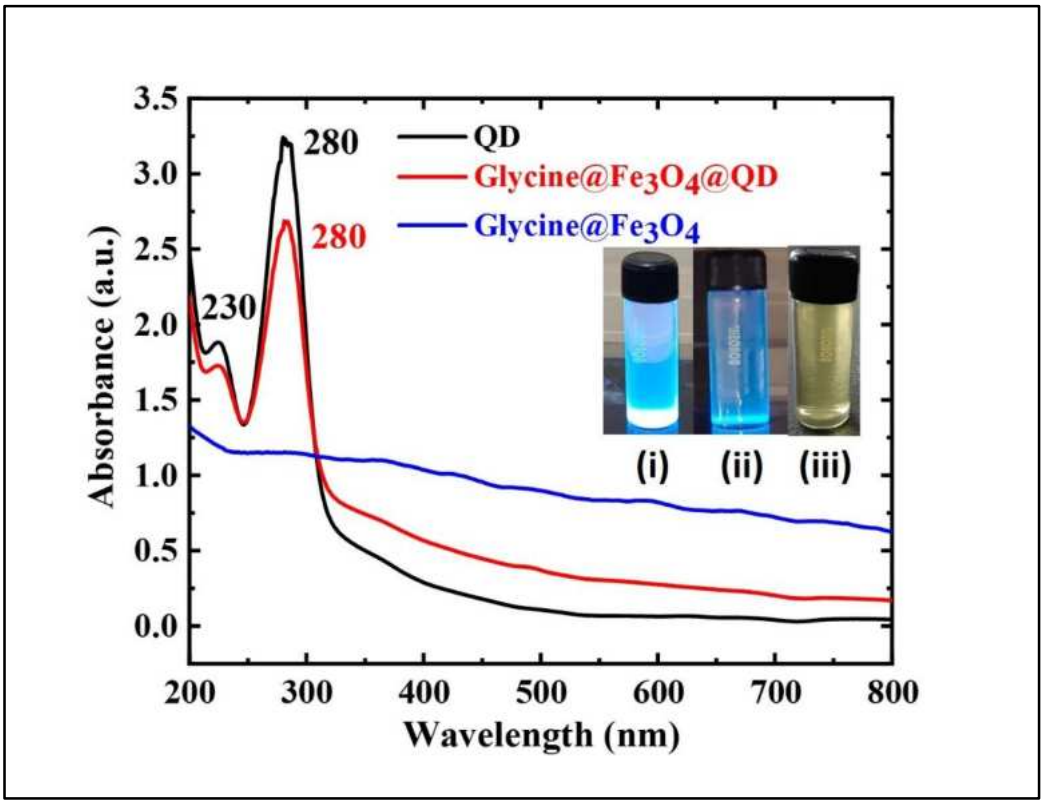

Figure 5.5. UV-visible spectroscopy analysis of glycine@Fe_3O_4@QD formation; Inset: (i) Only QDs, (ii) glycine@Fe_3O_4@QD, and (iii) only glycine@Fe_3O_4.

5.8.2. FORMATION OF QUANTUM DOT LABELLED GLYCINE-MODIFIED IRON OXIDE NANOPARTICLES-DNA CONJUGATE (glycine@Fe_3O_4@QD-DNA)

In this study, the conjugation of glycine@Fe_3O_4@QD with DNA was investigated with the help of UV-visible spectroscopy in **Figure 5.6**.

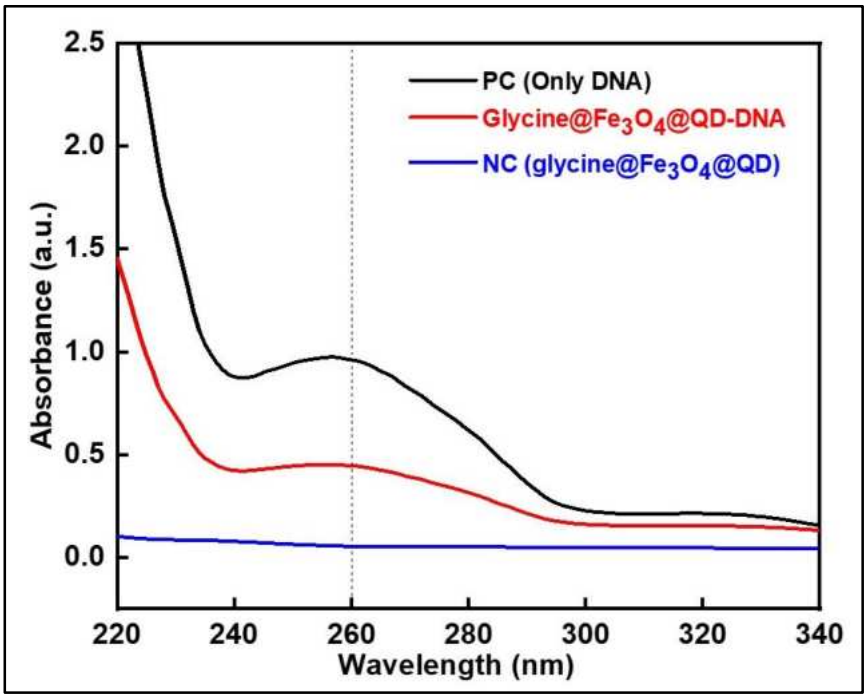

Figure 5.6. UV-visible spectroscopy analysis of glycine@Fe_3O_4@QD-DNA conjugate formation.

The glycine@Fe_3O_4@QD-DNA conjugates show a characteristic DNA peak at 260 nm when compared to standard DNA; confirmed the DNA conjugation. Standard DNA (without any conjugation) is considered as positive control. Whereas, glycine@Fe_3O_4@QD nanoparticles (without DNA conjugation) are considered as a negative control.

5.8.3. MAGNETOFECTION

Magnetofection is a specialized transfection technique that combines magnetic nanoparticles with genetic material (such as DNA or siRNA) labelled with fluorophores like FITC (Fluorescein Isothiocyanate). This approach allows for enhanced and targeted delivery of genetic material into specific cells through the use of magnetic fields and enables researchers to monitor transfection efficiency using the FITC label. Typically, the DNA or RNA of interest is labelled with FITC. This can be achieved by direct conjugation of FITC to the genetic material during synthesis or by using FITC-labelled nucleotides. The cationic transfection reagent on the nanoparticles binds to the negatively charged genetic material, forming the magnetofection complex. Researchers can then monitor transfection

efficiency by visualizing the FITC-labelled genetic material using fluorescence microscopy or flow cytometry. The green fluorescence from FITC indicates that the genetic material has been successfully taken up and expressed by the cells [9].

Here, FITC labels were replaced with sustainable quantum dots (QDs) to carry out the successful magnetofection. Also, the currently used techniques for analyzing magnetofection have been replaced by fluorescence spectroscopy assay.

To evaluate the magnetofection efficiency, a fluorescence spectroscopy analysis is carried out. It is a valuable approach to investigate various aspects of the transfection process and assess the efficiency of gene delivery into cells. The principle of this technique relies on the interaction between a fluorescently labelled nucleic acid (e.g., a fluorophore-labelled plasmid DNA) and internal components of the cells [28].

After the magnetofection, the fluorescence signal of the glycine@Fe_3O_4@QD-DNA conjugate is measured as shown in **Figure 5.7**. The fluorescence intensity is compared between the transfected cells and the control cells. The glycine@Fe_3O_4@QD-treated cells show highest intensity peak (~7000 a.u.). As glycine and sustainable QDs are present on the surface, they could have provided biocompatible environment and easily entered inside the cells. Further, glycine@Fe_3O_4@QD@DNA provides entry of DNA inside the cells in red spectrum with intensity ~3000 a.u. It is suggested that even after magnetofection of 30 minutes and several washing steps, fluorescence intensity is detected from the cells. When compared with negative (non-magnetofected cells) and positive (glycine@Fe_3O_4@QD-treated cells), it is interpreted that DNA is magnetofected inside the cells due to obtained fluorescence of ~3000 a.u. Interestingly, the fluorescence intensity of glycine@Fe_3O_4@QD-magnetofected cells (~3000 a.u.) is three times higher than that of FITC control (~1000 a.u.) which leads to high efficiency of glycine@Fe_3O_4@QDs as a magnetofecting agent inside the cells. Here, auto-fluorescence intensity of cells is collected (non-magnetofected

cells) to minimize the risk of false fluorescence which is <1000 a.u. Hence, mentioned graph provides detailed interpretation of magnetofection via fluorescent spectroscopy.

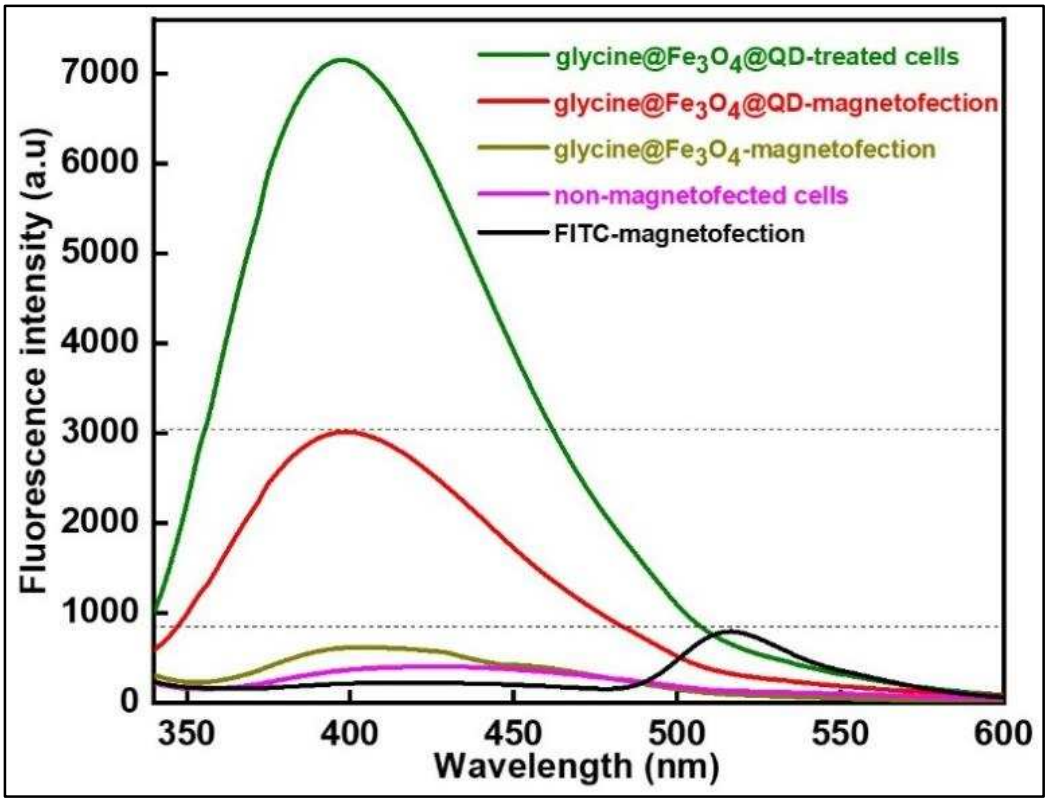

Figure 5.7. Fluorescence spectroscopy to study magnetofection of glycine@Fe_3O_4@QD-DNA in MCF-7 cells.

In order to validate the magnetofection efficiency of glycine@Fe_3O_4@QDs, fluorescence microscopy images are observed as shown in **Figure 5.8** at 60X magnification. **Figure 5.8 a** shows the untreated cells with no or minimal auto-fluorescence by MCF-7 cells. **Figure 5.8 b** shows control-treated cells (only QDs) which show fluorescence emitted by cells after entry of QDs inside the cells. QDs show fluorescence at around 400 nm. That leads to the blue light emission as observed in the below mentioned figure. Likewise, glycine@Fe_3O_4@QD-DNA-magnetofected cells show blue emission confirming the visual success of glycine@Fe_3O_4@QD-based DNA magnetofection inside the MCF-7 cells in **Figure 5.8 c**.

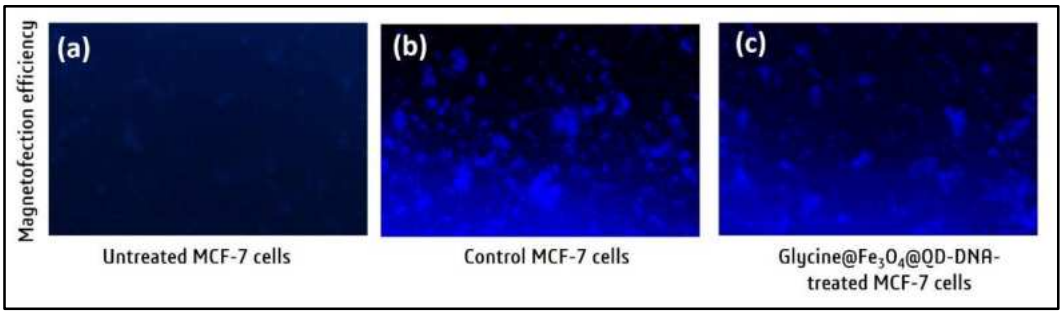

Figure 5.8. Detection of magnetofection by fluorescence microscopy of MCF-7 cells at 60x magnification; (a) untreated, (b) control (only QDs)-treated, and (c) glycine@Fe_3O_4@QD-DNA-magnetofected cells.

5.8.4. AGAROSE GEL ELECTROPHORESIS

Effective magnetofection was examined by agarose gel electrophoresis. Supernatant between 10 and 40 minutes of magnetofection was aspirated and individually run on the gel.

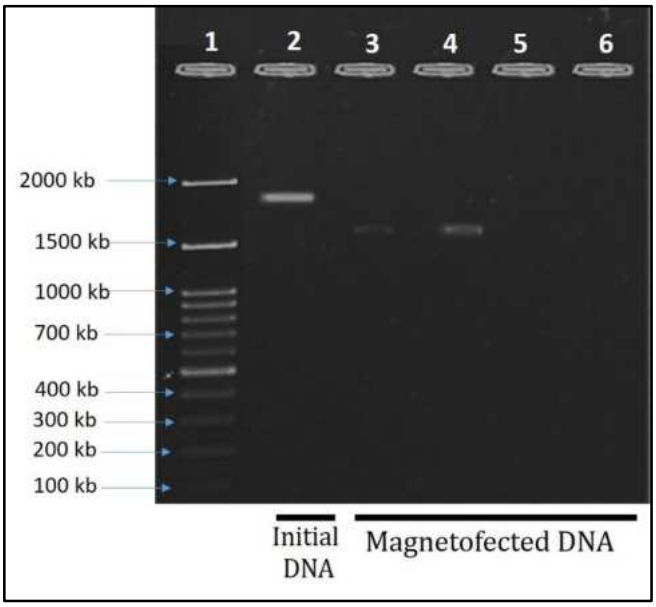

Figure 5.9. Agarose gel electrophoresis to study magnetofection of glycine@Fe_3O_4@QD@DNA in MCF-7 cells; well 1 – reference DNA ladder, wells 2, 3, 4, 5, and 6 represent magnetofected supernatant at 0, 10, 20, 30, and 40 minutes, respectively.

In **Figure 5.9**, well 1 represents the reference DNA ladder with the size 100-to-2000 kb. Well 2 represents initial supernatant at 0 minute of magnetofection which gives DNA band around 2000 kb. Well 3 represents magnetofected supernatant at 10 minutes, showing nearly blur band of around 1500 kb. Well 4 represents magnetofected supernatant at 20

minutes, again showing nearly blur band of around 1500 kb. Well 5 represents magnetofected supernatant at 30 minutes with no DNA band at all. This clearly states that DNA is magnetofected inside the cells completely after 30 minutes. Similarly, well 6 represents magnetofected supernatant at 40 minutes with no DNA band at all. This confirms successful magnetofection of DNA inside the cells.

5.8.5. CELLULAR UPTAKE ANALYSIS

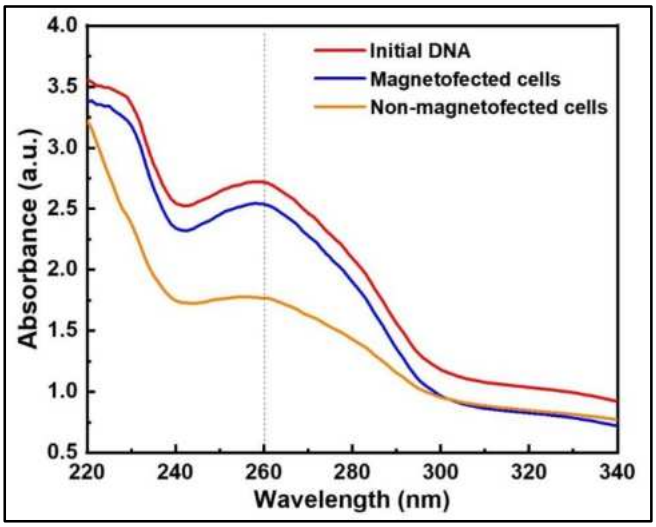

Figure 5.10. UV-visible spectroscopy analysis to study magnetofection of glycine@Fe_3O_4@QD@DNA in MCF-7 cells.

Figure 5.10 shows UV-visible spectroscopy analysis of magnetofected cells. DNA absorbance (at 260 nm) is raised in case of magnetofected cells when compared with non-magnetofected cells. This suggests the effective magnetofection of DNA into the MCF-7 cells. Further according to the standard equation **(Equation 5.1)**, 60.25 % of total DNA is adsorbed by the cells. **Table 5.1** depicts the values of magnetofected DNA.

Rate of DNA uptake =
(Amount of magnetofected DNA/ total DNA) x 100 **... (5.1)**

Wherein, rate of desorption is in percentage (%).

Table 5.1: Detection of magnetofection by DNA quantification.

No.	Cells	DNA uptake (µg/mL)
1.	Initial DNA	80.5 ± 1.13
2.	Magnetofected cells	48.5 ± 0.70
3.	Non-magnetofected cells	6.5 ± 0.87

5.8.6. CELL CYTOTOXICITY

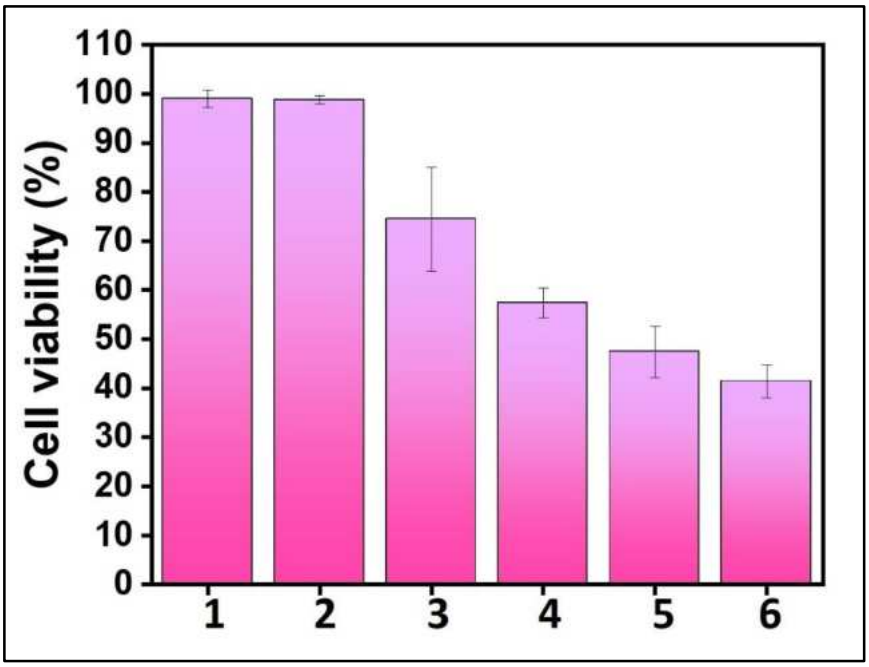

Figure 5.11. Cytotoxicity analysis of glycine@Fe_3O_4 nanoparticles in MCF-7 cells; (1) untreated, (2) only DNA-treated, (3) glycine@Fe_3O_4@QD@DNA-treated, (4) only glycine@Fe_3O_4@QD–treated, (5) FITC@DNA-treated, and (6) only glycine@Fe_3O_4–treated cells.

The magnetofection process itself can be cytotoxic to cells. Hence, cytotoxicity assay was conducted to assess the biocompatibility of the nanoparticles. It is found that the conjugates exhibit minimal cytotoxic effects, indicating their potential for safe and efficient nucleic acid delivery applications in **Figure 5.11**. High cell viability is observed in magnetofected cells (74 ± 10.6 %) than that of FITC@DNA-treated ones (46 ± 5.2 %). **Table 5.2** provides cell viability % of magnetofected cells along with controls. As QDs are environment-friendly and sustainable [27], the overall biocompatibility of nanoparticles is enhanced. Inset image in the Figure 5.10 indicates live Vs dead cells visualization with respect to color change. Color of MTT dye is yellow in nature. This dye gets converted into purple colored

molecule known as formazan when comes in contact with live cells. Hence, Purple color shows live cells due to conversion of MTT dye to formazan by mitochondrial succinate dehydrogenase enzyme. Dead cells (cells without mitochondrial enzymes) possess yellow color. Here, magnetofected cells show live purple color as compared to only glycine@Fe_3O_4-treated cells.

Table 5.2: Cell viability (%) values of magnetofected cells.

No.	Cells	Cell viability (%)
1.	Non-magnetofected cells	99.00 ± 1.73
2.	Only DNA-treated	98.76 ± 0.83
3.	Glycine@Fe_3O_4@QD-DNA-treated	74.44 ± 10.64
4.	Only glycine@Fe_3O_4@QD-treated	57.34 ± 3.07
5.	FITC@DNA-treated	47.42 ± 5.27
6.	Only glycine@Fe_3O_4-treated	41.36 ± 3.33

5.9. CONCLUSIONS

Breast cancer is considered as one of the most frequent cancers among the world. There is an urgent need of rapid diagnosis and treatments on breast cancer as patient survival rate is significantly low. To increase survival rate, several research efforts are being taken nowadays. Magnetofection is one of the treatment strategies need to be researched in depth. Sustainable and biocompatible magnetofecting agents are in demand for effective therapy.

Here, carbon quantum dots labelled-glycine modified-iron oxide nanoparticles (glycine@Fe_3O_4@QDs) were incorporated to study magnetofection of standard DNA in MCF-7 breast cancer cells. Amount of glycine@Fe_3O_4 and QDs was optimized as 1:4 (v/v) ratio for effective conjugation. UV-visible peaks at 230 and 280 nm confirmed the formation of glycine@Fe_3O_4@QD complex. Further, UV-visible peak at 260 nm confirmed the conjugation of glycine@Fe_3O_4@QD-DNA along with negative surface charge zeta potential (-8.55 ± 0.38 mV) due to presence of DNA phosphate backbone. These conjugates were further utilized for magnetofection study. High fluorescence intensity (~ 3000 a.u.) was obtained after magnetofection at 30 minutes. Non-magnetofected cells showed auto-fluorescence with relatively negligible intensity (<1000 a.u.). Fluorescence microscopy

analysis showed the visual success of glycine@Fe_3O_4@QD-based DNA magnetofection inside the MCF-7 cells by emission of blue light. Further, agarose gel electrophoresis showed effective magnetofection at 30 minutes by complete disappearance of DNA bands in aspirated supernatant. 60.25 % of total DNA uptake by magnetofected cells was calculated as an evidence of effective magnetofection. Moreover, 74 ± 10.6 % cell viability was observed after magnetofection. These results indicate that glycine@Fe_3O_4@QD nanoparticles have significant potential to act as a magnetofecting agent in breast cancer cells.

5.10. REFERENCES

[1] Sun, Y. Sheng, Z. Zhao, Z. N. Yang, F. Xu, H. Lu, Z. Zhu, W. Shi, J. Jiang, P. Yao, Han. Zhu. **Risk factors and preventions of breast cancer.** Int. J. Biol. Sci. 2017; 13(11): 1387.

[2] A. G. Waks, E. P. Winer. **Breast cancer treatment**. Jama. 2019; 321(3): 316.

[3] I. Jatoi, W. F. Anderson, J. H. Jeong, C. K. Redmond. **Breast cancer adjuvant therapy: time to consider its time-dependent effects.** J. Clin. Onc. 2011; 29(17): 2301.

[4] C. Zhang, C. Xu, X. Gao, Q. Yao. **Platinum-based drugs for cancer therapy and anti-tumor strategies.** Theranostics. 2022; 12(5): 2115.

[5] C. Katsura, I. Ogunmwonyi, H. K. Kankam, S. Saha. **Breast cancer: presentation, investigation and management.** Br. J. Hosp. Med. 2022; 83(2): 1.

[6] S. Kalakenger, S. Y. Arslan, F. Turhan, M. Acar, K. Solak, A. Mavi, Y. Unver. **Heterologous expression of codon-optimized azurin transferred by magnetofection method in MCF-10A cells**. Mol. Biotechnol. 2023; 65: 1.

[7] R. P. Gambhir, S. S. Rohiwal, A. P. Tiwari. **Multifunctional surface functionalized magnetic iron oxide nanoparticles for biomedical applications: a review.** Appl. Surf. Sci. Adv. 2022; 11: 100303.

[8] M. Zuvin, E. Kuruoglu, V. O. Kaya, O. Unal, O. Kutlu, H. Y.Acar, D. Gozuacik, A. Koşar. **Magnetofection of green fluorescent protein encoding DNA-bearing polyethyleneimine-coated superparamagnetic iron oxide nanoparticles to human breast cancer cells.** ACS omega. 2019; 4(7): 12366.

[9] R. Ensenauer, D. Hartl, J. Vockley, A. A. Roscher, U. Fuchs. **Efficient and gentle siRNA delivery by magnetofection.** Biotech. Histochem. 2011; 86(4): 226.

[10] A. Vibhute, T. Patil, R. Gambhir, A. P. Tiwari. **Fluorescent carbon quantum dots: Synthesis methods, functionalization and biomedical applications.** Appl. Surf. Sci. Adv. 2022; 11: 100311.

[11] R. Mehrotra, K. Yadav. **Breast cancer in India: Present scenario and the challenges ahead.** World J. Clin. Oncol. 2022; 13(3): 209.

[12] **Report of the technical group of population projection July 2020 (2011-2036)**. https://main.mohfw.gov.in/reports-0.

[13] G. W. Tseu, K. A. Kamaruzaman. **A review of different types of liposomes and their advancements as a form of gene therapy treatment for breast cancer.** Molecules. 2023; 28(3): 1498.

[14] T. T. Dongsar, T. S. Dongsar, M. A. Abourehab, N. Gupta, P. Kesharwani. **Emerging application of magnetic nanoparticles for breast cancer therapy**. Eur. Polym. J. 2023; 187:111898.

[15] M. V. Tuttolomondo, S. Municoy, M. I. Echazú, L. M. López, G. S. Alvarez. Tuttolomondo MV, Municoy S, Echazú1 MI, López LM, Alvarez GS. **Magnetic Nanoparticles for Nucleic Acid Delivery: Magnetofection, Gene Therapy and Vaccines**. Mag. Nano. Biomed. Appl. 2023; 143: 278.

[16] R. Stein, F. Pfister, B. Friedrich, P. R. Blersch, H. Unterweger, A. Arkhypov, A. Mokhir, M. Kolot, C. Alexiou, R. Tietze. **Plasmid-DNA Delivery by Covalently Functionalized PEI-SPIONs as a Potential Magnetofection Agent.** Molecules. 2022; 27(21): 7416.

[17] T. Wang, H. Zhao, S. Jing, Y. Fan, G. Sheng, Q. Ding, C. Liu, H. Wu, Y. Liu. **Magnetofection of miR-21 promoted by electromagnetic field and iron oxide nanoparticles via the p38 MAPK pathway contributes to osteogenesis and angiogenesis for intervertebral fusion**. J. Nanobiotechnology. 2023; 21(1): 1.

[18] V. Mulens-Arias, Y. Portilla, S. Pérez-Yagüe, R. Ferreras-Martín, M. E. Martín, V. M. González, D. F. Barber. **An electrostatically conjugated-functional MNK1 aptamer reverts the intrinsic antitumor effect of polyethyleneimine-coated iron oxide nanoparticles in vivo in a human triple-negative cancer xenograft**. Cancer Nanotechnol. 2023; 14(1): 1.

[19] L. Prosen, S. Prijic, B. Music, J. Lavrencak, M. Cemazar, G. Sersa. **Magnetofection: a reproducible method for gene delivery to melanoma cells.** BioMed Res. Int. 2013; 2013: 209452.

[20] A. N. Danthanarayana, D. C. Manatunga, R. M. De-Silva, N. V. Chandrasekharan, K. M. De-Silva. **Magnetofection and isolation of DNA using polyethyleneimine functionalized magnetic iron oxide nanoparticles**. R. Soc. Open Sci. 2018; 5(12): 181369.

[21] A. Ito, M. Kamihira, Ito A, Kamihira M**. Tissue engineering using magnetite nanoparticles.** PMBTS. 2011; 104: 355.

[22] M. Filippi, B. Dasen, A. Scherberich, Filippi M, Dasen B, Scherberich A. **Rapid magneto-sonoporation of adipose-derived cells.** Materials. 2021; 14(17): 4877.

[23] C. Plank, O. Zelphati, O. Mykhaylyk. **Magnetically enhanced nucleic acid delivery. Ten years of magnetofection— progress and prospects**. Adv. Drug Deliv. Rev. 2011; 63(14-15): 1300.

[24] A. Sizikov, P. I. Nikitin, M. P. Nikitin, Sizikov AA, Nikitin PI, Nikitin MP. **Magnetofection *in-vivo* by nanomagnetic carriers systemically administered into the bloodstream**. Pharmaceutics. 2021; 13(11): 1927.

[25] J. Singh, I. Mohanty, R. C. Sobti, S. Rattan. **Targeted gene delivery through magnetofection: the new face of medicine**. J. Biomed. Transl. Res. 2022; 447: 303.

[26] Q. Bi, X. Song, A. Hu, T. Luo, R. Jin, H. Ai, Y. Nie. **Magnetofection: magic magnetic nanoparticles for efficient gene delivery**. Chin. Chem. Lett. 2020; 31(12): 3041.

[27] P. Kamble, D. Malavekar, A. P. Tiwari. **Natural biowaste derived fluorescent carbon quantum dots: synthesis, characterization and biocompatibility study**. J. Fluoresc. 2023: 1.

[28] W. E. Omer, M. F. Abdelbar, N. M. El-Kemary, N. Fukata, M. A. El-Kemary, "**Cancer antigen 125 assessment using carbon quantum dots for optical biosensing for the early diagnosis of ovarian cancer**," RSC Adv. 2021; 11 (49): 31047.

Chapter 6

SARS-CoV-2 RNA detection based on glycine-modified iron oxide nanoparticle–RNA conjugate formation

6.1. INTRODUCTION

Corona virus disease 2019 (COVID-19) is an infectious disease which is caused due to SARS-CoV-2 virus [1]. Further, in the late 2019, SARS-CoV-2 was emerged as a novel corona virus in Wuhan, China; causing the COVID-19 pandemic. The "2" specifically distinguishes a different strain of the original SARS corona virus [2].

Figure 6.1 shows number of cumulative total COVID-19 cases reported to World Health Organization (WHO). As per the data, seven hundred seventy four million six hundred thirty one thousand four hundred forty-four (774,631,444) COVID-19 cases have been reported till the date 11th February 2024. United States of America (USA) reports 103.4 million cases whereas China and India report 99.3 and 45 million cases, respectively.

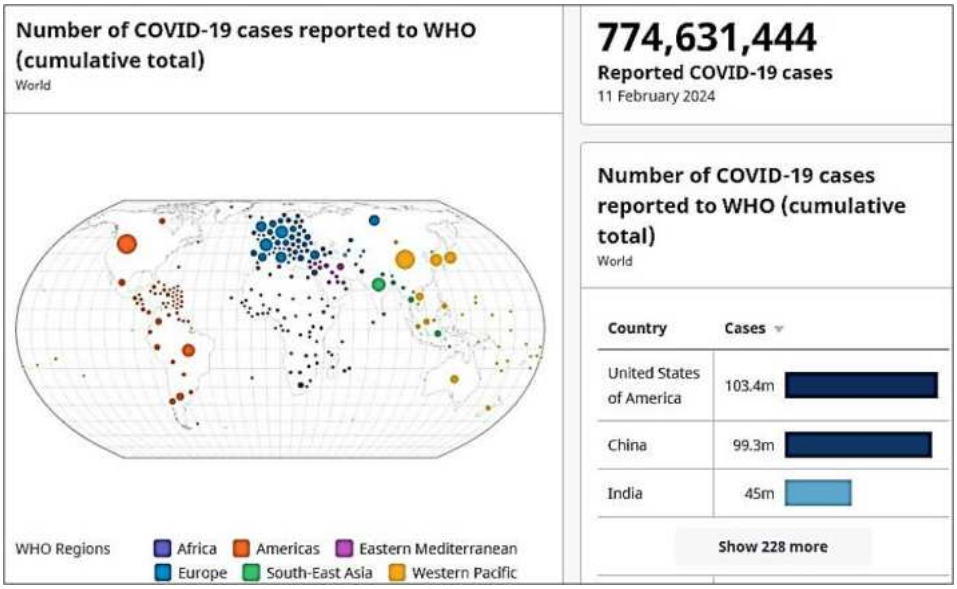

Figure 6.1 Number of COVID-19 cases reported to WHO till the date 11th February 2024 [3].

The virus is highly contagious and primarily spreads through respiratory droplets when an infected person coughs, sneezes, talks, or breaths. It can also spread by touching surfaces contaminated with the virus and then touching the face, although that is not main mode of transmission.

Traditional methods for virus detection, such as culturing viruses in the laboratory, indeed have limitations in terms of sensitivity, specificity,

and detection time. These methods can be labor-intensive and time-consuming, often taking days or even weeks to yield results. Additionally, they may not always detect low levels of viral presence accurately, leading to false negatives or delays in diagnosis.

To address these shortcomings, modern methods for virus detection have been developed. These include molecular methods such as polymerase chain reaction (PCR), nucleic acid amplification tests (NAATs), and other molecular diagnostic assays. These methods are more sensitive, specific, and can provide results much faster than the traditional methods. Furthermore, advances in technology have led to the development of rapid diagnostic tests (RDTs) based on immunological and antigen-antibody interactions. These tests offer quick and easy detection of viral antigens or antibodies, making them valuable tools for screening and early diagnosis, especially in resource-limited settings. Overall, the shift towards molecular and rapid diagnostic methods has significantly improved virus detection capabilities, enabling quicker and more accurate identification of viral infections [4].

Moreover, the ongoing COVID-19 pandemic has highlighted the importance of scaling up virus detection capacity to meet global health challenges.

Rapid development of diagnostic tests, vaccines, and therapies are being implemented to raise high public health measures by identifying and tracking SARS-CoV-2 affected individuals. The advances in molecular biology, genomics, and rapid diagnostic technologies have revolutionized our ability to identify and understand viral pathogens as shown in **Figure 6.2**.

The **Figure 6.2** shows currently used diagnosis methods to detect COVID-19 diseases. Basically, NA-based serological and other tests are already in the market for commercial use. NA amplification tests are – reverse transcriptase polymerase chain reaction (RT-PCR), and clustered regularly interspaced short palindromic repeats (CRISPR) tests. Further, serological tests contain enzyme-linked immunosorbent assay (ELISA) and

lateral flow immunoassay (LIFA). Other tests contain computed topography (CT scan) and point-of-care biosensors [5].

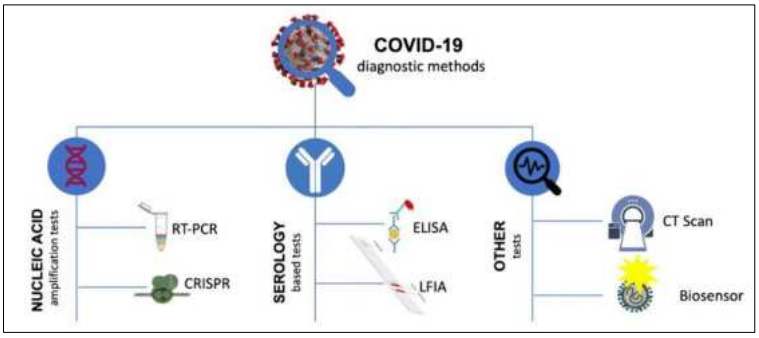

Figure 6.2. Current methods for COVID-19 detection [5].

Despite the remarkable progress made in virus detection, several challenges persist. One of the major hurdles is the constant evolution of viruses, leading to genetic variability and the emergence of new strains. This necessitates continuous surveillance and the development of robust detection methods that can adapt to the ever-changing viral landscape. Additionally, the need for standardized protocols, quality control measures, and harmonization across different laboratories and diagnostic platforms is vital to ensure accurate and reliable results.

Rapid diagnosis of SARS-CoV-2 is crucial for mitigating the impact of the COVID-19 pandemic on public health, healthcare systems, and society as a whole. It plays a pivotal role in early treatment, transmission control, public health surveillance, resource allocation, and research endeavors aimed at combating the virus.

6.2. SIGNIFICANCE OF THE CHAPTER

The commonly used conventional RNA separation methods for separating and purifying RNA not only need to contact with a variety of organic solvents and toxic reagents but are also comprised of complicated steps which can be difficult to control. Conventionally, there are several common methods available for RNA separation; one is organic separation method which involves monophasic solution of phenol and isothiocyanate. RNA separation is achieved through organic separation and RNA

precipitation through several centrifugation steps. Crude lysate approach is another method of RNA separation which consists of two buffer solutions viz. lysis buffer and stop buffer. Lysis buffer contains several enzymes and detergents that lyses the cell and RNA is separated from cell. Followed by, addition of stop buffer which ceases the lysis and thereby further damage to the RNA. However this method is lacking the further separation of RNA from solution.

Most widely used method is silica column method where RNA is isolated with spin column and reagents via selective silica binding. Above methods of RNA separation tend to not only be rather expensive as but are also time-consuming. Thus, the selective adsorption of the RNA to a surface of nanoparticle has become the most common and efficient method in the last decade. Once adsorbed, the soluble contaminants are usually physically removed while the co-adsorbed contaminants are removed by selective washing. The purified RNA is desorbed from the particle with the help of water or a weak buffer. Due to the high density of negative charges on the RNA, it tends to be relatively easy to separate it from a variety of closely related contaminants. These methods, involving selective adsorption, provide an advantage of yielding high purity RNA in a relatively short span of time.

A majority of the laboratories today also use RNA separation kits that are readily available by diagnostic companies. These diagnostic kits are easy to use and handle but tend to be expensive. These conventional separation protocols require the use of sophisticated laboratory equipment and are based on the use of chemicals that may degrade the quality of RNA.

Hence, Fe_3O_4 based adsorption of different nucleic acids has already gained interest with respect to its separation and detection. The advantages of Fe_3O_4-based nucleic acid separation over other methods are easy processing, quick results, reusability of particles and cost effectiveness. However, they require use of centrifuges and other large equipment making

an immediate separation of RNA difficult. Thus, there is a need to develop a simple, cost effective RNA detection methodologies [6].

Fe_3O_4-based detection methods offer a powerful and versatile platform for disease diagnosis, including detection of infectious pathogens like SARS-CoV-2 [7-12]. Continued research and development in this field holds a promise for further improving the performance and accessibility of nanoparticle-based diagnostic methods.

Fe_3O_4-based SARS-CoV-2 RNA detection studies highlight the effectiveness of Fe_3O_4 in capturing and detecting SARS-CoV-2 RNA with high sensitivity and specificity. The methodologies employed, including synthesis, functionalization, RNA adsorption, magnetic separation, RNA desorption, and detection using techniques like RT-PCR and qPCR, demonstrate the versatility and reliability of Fe_3O_4-based assays for COVID-19 diagnosis. The table highlights the significance of Fe_3O_4-based assays in the context of SARS-CoV-2 RNA detection and emphasize their potential for advancing diagnostic capabilities in the fight against COVID-19.

However, there are some potential limitations of Fe_3O_4-based SARS-CoV-2 RNA detection methods. While Fe_3O_4-based assays can offer high sensitivity and specificity, they may still have limitations in detecting low viral loads or distinguishing between closely related viral strains. This can impact the accuracy of diagnosis, especially in cases with low viral shedding or in the presence of other interfering substances like proteins in clinical samples. Fe_3O_4-based assays often require complex sample preparation steps, including RNA extraction, purification, and concentration. These steps can be time-consuming and labor-intensive, increasing the risk of sample contamination and errors in the detection process. The synthesis and functionalization of Fe_3O_4 can be costly and may require specialized equipment and expertise. Additionally, the scalability of nanoparticle-based assays for large-scale diagnostic testing may be limited by production costs and resource constraints. Non-specific binding of nanoparticles to other biomolecules or contaminants in clinical samples can lead to false-positive

results and compromise the accuracy of SARS-CoV-2 RNA detection. Strategies to minimize non-specific interactions and optimize assay specificity are crucial for reducing the risk of false positives. Fe_3O_4-based assays for SARS-CoV-2 RNA detection may require regulatory approval and validation to ensure their safety, efficacy, and reliability for clinical use. The process of obtaining regulatory clearance can be time-consuming and may delay the translation of nanoparticle-based assays from research settings to clinical practice. Access to Fe_3O_4-based assays may be limited in resource-constrained settings or areas with inadequate infrastructure and technical expertise.

Efforts to improve accessibility and promote technology transfer are essential for maximizing the impact of nanoparticle-based diagnostics in global health initiatives [9-12]. Addressing these limitations through continued research, innovation, and collaboration can enhance the utility and effectiveness of Fe_3O_4-based assays for SARS-CoV-2 RNA detection, ultimately contributing to improved disease surveillance, patient care, and public health outcomes. As described in previous chapter, glycine@Fe_3O_4-nucleic acid conjugates establish stable conjugation. Hence, these nanoparticles were incorporated for separating and thereby detecting SARS-CoV-2 RNA.

6.3. EXPERIMENTAL

6.3.1. MATERIALS

Himedia laboratories Pvt. Ltd. provided the following supplies: sodium hydroxide (NaOH), sodium chloride (NaCl), ethylenediaminetetraacetic acid (EDTA), powdered Tris buffer, glycine powder, agarose powder, ethidium bromide (etBr), Triacetate EDTA buffer (TAE), DNA ladder, and loading dye. In addition, Sigma Aldrich Pvt. Ltd. was the supplier of potassium bromide (KBr) and pure ethanol. We bought the RT-PCR kit and the RNA extraction kit from MBPCR243 Himedia Pvt. Ltd. and MB615 Himedia Pvt. Ltd., respectively.

6.3.2. SAMPLE PREPARATION AND SAFETY MANAGEMENT

Viral transport medium (VTM) was used to collect SARS-CoV-2 RNA samples from patient nasal swabs using a conventional RNA extraction kit (MB615 - Hipor A viral RNA extraction kit - Himedia Pvt. Ltd.). The samples were then stored at -20°C for further studies. Throughout the experimentation, COVID19 standard safety protocols have been adhered to. Throughout the study, kits of personal protective equipment (PPE) were used. There was no direct SARS-CoV-2 viral exposure. Clinical samples, extracted RNA, RT-PCR samples, and laboratory garbage were all kept apart in distinct yellow plastic bags labelled with a cytotoxicity symbol. Used materials and samples were disposed of as per the biological waste management policy.

6.3.3. VIRUS DETECTION

The process of pH responsive RNA detection by using glycine@Fe_3O_4 is divided into five stages – adsorption of RNA on glycine@Fe_3O_4, magnetic separation of glycine@Fe_3O_4–RNA complex, washing, desorption of RNA from glycine@Fe_3O_4, and amplification of separated RNA. Samples containing patient's RNA were utilized. Major modifications in protocol set by Zhao et al [12] have been done to perform easy and cost effective SARS-CoV-2 RNA extraction such as chemicals used for synthesis of nanoparticles were reduced in this study.

Adsorption, washing, and desorption buffers were made with the composition which is shown **Table 6.1**. As this adsorption and desorption of RNA using glycine@Fe_3O_4 is pH-responsible, the pH 5 and 7 were maintained for adsorption and desorption processes, respectively.

Table 6.1. Composition of adsorption, washing, and desorption buffers

No.	Buffers		
	Adsorption	Washing	Desorption
1.	EDTA (10 mM)	Ethanol (75%)	Tris-acetate (10 mM)
2.	NaCl (5 M)		pH (7)
3.	pH (5)		

SARS-CoV-2 RNA samples (collected from nasal swab) was directly added in adsorption buffer in 1:2 (v/v) ratio. The mixture was incubated on shaker at room temperature (RT), 500 rotation per minutes (rpm) for 30 minutes. Further, mixture was exposed to an external magnetic field for 60 seconds. Obtained supernatant was discarded and pellet was washed with washing buffer.

Desorption buffer was added into the pellet at RT, 500 rpm for 30 minutes. Again, the mixture was exposed to an external magnetic field for 60 seconds. This time, supernatant was collected in separate sterile tubes. Pellet was washed with washing buffer and stored at 4°C for re-use.

Supernatant was stored at 4°C for further validation. This supernatant contains separated SARS-CoV-2 RNA. Whereas pellet contains glycine@Fe_3O_4 nanoparticles. Hence, separated RNA was directly run for RT-PCR, and agarose gel electrophoresis.

6.3.4. VALIDATION OF SARS-CoV-2 RNA DETECTION

All RT-PCR samples were carried out in 25 µL reaction volume. According to manufacturer's instructions, primers were added into the reaction mixture. RT-PCR was performed on a HiPCR coronavirus (COVID19) multiplex probe PCR kit – MBPCR243 Himedia Pvt. Ltd. 40 thermal cycles were carried out. RT-PCR conditions were 15 minutes cDNA synthesis at 50°C. Followed by, initial denaturation for 3 minutes at 95°C, 40 cycles of 15 seconds at 95°C, 30 seconds at 58°C. Obtained RT-PCR products were analyzed on 1.2% agarose gel containing ethidium bromide and were stored at 4°C and interpreted results.

Absorbance of the separated RNA samples at 260 and 280 nm was measured using spectrophotometer. 260/280 ratio was calculated by dividing absorbance at 260 nm by the absorbance at 280 nm. The ratio close to 2 indicates the good RNA purity.

6.4. RESULTS AND DISCUSSION

6.4.1. GLYCINE MODIFIED IRON OXIDE NANOPARTICLES-RIBONUCLEIC ACID (glycine@Fe_3O_4-RNA) CONJUGATES

The interactions between Fe_3O_4 and RNA in Fe_3O_4-RNA conjugates are governed by a combination of surface chemistry, electrostatic forces, covalent bonding, hybridization, and specific ligand-receptor interactions [12-15].

Here, glycine molecules present on the Fe_3O_4 may be conjugated onto the RNA via amino groups, creating a platform for glycine@Fe_3O_4-RNA conjugates. These conjugates can be formed by amide bonds between the carboxyl group of glycine and the phosphate backbone of RNA. Glycine has a positive charge below isoelectric pH (< pH 6), while RNA molecules are negatively charged due to the phosphate backbone. Electrostatic interactions between positively charged amino groups on glycine and negatively charged phosphate groups on RNA can facilitate their association. Glycine contains a hydrogen atom bound to its amino group, which can participate in hydrogen bonding with functional groups on RNA molecules, such as nitrogenous bases or sugar moieties [15-18]

pH-responsiveness of glycine adsorbs the RNA and further, Fe_3O_4 separates the adsorbed RNA in presence of introduction of external magnetic field. Hence, the glycine@Fe_3O_4 nanoparticles symbiotically captures the SARS-CoV-2 RNA from clinical sample and thereby detection of SARS-CoV-2 is established.

6.4.1. PREPARATION OF BUFFERS

SARS-CoV-2 RNA detection was carried out by using adsorption, washing, and desorption buffers. Following components were used for making of adsorption buffer – EDTA and NaCl. EDTA is used to chelate divalent cations. It helps to inhibit the activity of ribonucleases (RNases) and prevent RNA degradation [19]. The concentration of EDTA used in RNA extraction buffers is usually in the range of 0.1 mM to 10 mM [20]. Hence, the 10 mM EDTA concentration was considered for this study.

Further, NaCl in adsorption buffer promotes RNA binding and adjust the ionic strength and pH of the buffer [21]. Typically, 0.1 M to 1.6 M NaCl concentration range is considered [22]. Hence, 1.6 M NaCl concentration was used in this study.

75% ethanol serves as an effective washing buffer in RNA extraction protocols, helping to decontaminate RNA, remove impurities, and promote RNA precipitation while maintaining the RNA integrity [23].

Further, tris buffer in desorption buffer maintain stability, solubility, and compatibility with downstream applications, making it a popular choice for desorption buffer in RNA extraction protocols [24]. Typically, 10 mM concentration is considered for tris buffer [25].

pH values for adsorption and desorption buffers were maintained at 5 and 7, respectively with the constant room temperature (RT). Determination of these pH values are based upon the surface charges of glycine@Fe_3O_4. As reported earlier, isoelectric pH of glycine is 6 [26]. Thus, glycine@Fe_3O_4 possess positive and negative surface charges in acidic (below pH 6) and basic (above pH 6) environments, respectively.

Basically, adsorption buffer carries out glycine@Fe_3O_4-RNA conjugate formation due to electrostatic interactions between positively charged glycine@Fe_3O_4 nanoparticles and negatively charged RNA at pH 5. Further, desorption buffer breaks the conjugate to separate out RNA from the nanoparticles due to same charge repulsion between negatively charged glycine@Fe_3O_4 nanoparticles and RNA at pH 7. External magnetic field is applied to separate glycine@Fe_3O_4 from RNA.

6.4.2. VALIDATION OF RNA DETECTION

The results (quality and quantity) of separated RNA were analyzed for purity check. The separated RNA was compared with market-based RNA extraction kit (MB615 Himedia Pvt. Ltd.).

Kit-extracted RNA (positive control) and glycine@Fe_3O_4–extracted RNA were checked for A260/280 RNA purity analysis. From the obtained values, it is calculated that positive control-based RNA purity is 1.981 ± 0.004. Whereas, glycine@Fe_3O_4–extracted RNA is 1.963 ± 0.003.

A260/280 RNA purity analysis is used to determine quality and purity of RNA. The ratio refers to the absorbance measurements at wavelengths of 260 nm and 280 nm. An ideal ratio is around 2.0, indicating pure RNA without contamination from other impurities [27]. Hence, pure RNA is present after extraction as the obtained values are close to 2.0. Orderly equivalent data is obtained for glycine@Fe_3O_4-mediated extraction when compared with positive control.

Hence, study was further processed for confirmatory tests. Extracted RNAs were converted into cDNA and amplified by performing RT-PCR analysis and results were compared with RNA extracted by market-based extraction kit. **Figure 6.3** shows RT-PCR graph of glycine@Fe_3O_4-mediated SARS-CoV-2 RNA separation. This process converts SARS-coV-2 RNA into complementary DNA (cDNA) to maintain the stability of RNA and then amplified into million copies to gain abundant sample for the detection of COVID-19. The graph typically represents the amplification curves obtained during RT-PCR reaction. The X-axis of the graph represents cycle number (also known as cycle threshold or Cq value). Each cycle corresponds to the one round of amplification during RT-PCR process. Y-axis of the graph represents fluorescence signals emitted by the RT-PCR reaction as amplification progresses. The fluorescence signal is directly proportional to the amount of RT-PCR product (SARS-CoV-2 cDNA) generated during each cycle.

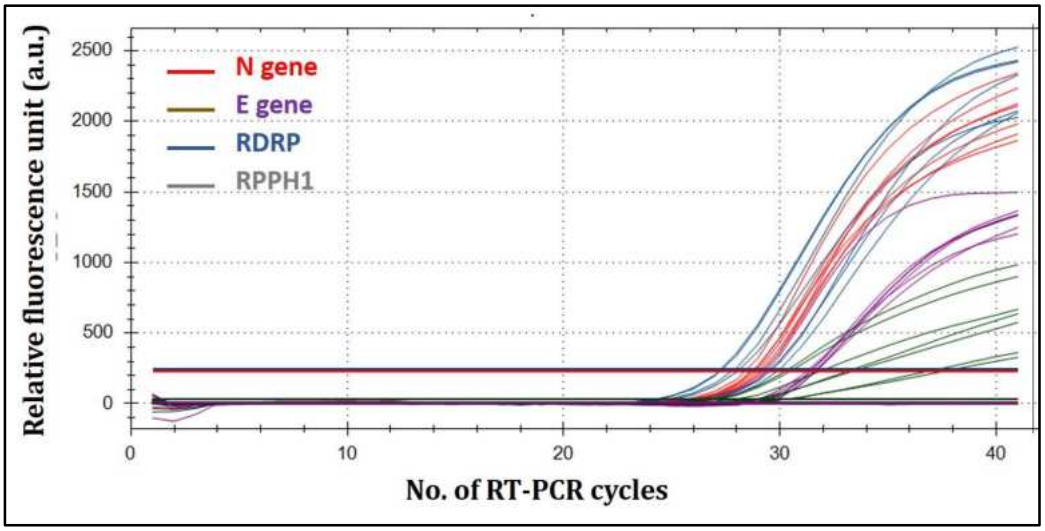

Figure 6.3. RT-PCR of SARS-CoV-2 RNA detection based on glycine@Fe_3O_4-RNA conjugate formation (N=6). Highest peak for each gene shows positive control group. Straight lines indicate negative control group.

Further, the graph shows baseline for each gene of SARS-CoV-2 (N, E, RDRP, and RPPH-1) which is the initial phase of amplification curve where the fluorescence signal is relatively stable and low. It represents the background fluorescence level before the start of amplification. Following the baseline, the amplification curve enters the exponential phase. During this phase, the fluorescence signal increases rapidly with each cycle as the target cDNA is amplified exponentially.

After 25 cycles of RT-PCR, the curve starts exponential phase for all four above mentioned genes of SARS-CoV-2 cDNA. This leads to the conformation of glycine@Fe_3O_4-mediated SARS CoV-2 RNA separation and detection.

Highest peak line for each gene represents the positive control (Market-kit extracted SARS-CoV-2 RNA). Whereas, negative control (Sample without SARS-CoV-2 RNA) shows no exponential phase as there is no occurrence of SARS-CoV-2 cDNA amplification due to absence of RNA.

The graph also shows threshold line which is horizontal to the X-axis set at a predefined fluorescence intensity level above the baseline. The Cq Value is determined by the cycle at which the amplification curve intersects

the threshold line. It indicates the cycle number at which the fluorescence signal becomes detectable above the background noise.

Furthermore, amplification curve represents the fluorescence signal recorded during each cycle of the RT-PCR. It shows (from 25 to 40 cycles) the progress of amplification overtime and provides information about the abundance of the target RNA in the sample.

RT-PCR was carried out for extracted RNA samples (6) and compared with positive (kit extracted RNA) as well as negative control (sample without SARS-CoV-2 RNA). Nucleocapsid (N) gene, Envelope (E) gene, and RNA dependent RNA polymerase (RDRP) genes of SARS-CoV-2 were targeted to obtain SARS-CoV-2 RNA amplification and to check efficiency of extraction from the sample. Quantification of the glycine@Fe_3O_4 mediated RNA extraction is shown in **Table 6.2**.

Interpreting the RT-PCR graph for SARS-CoV-2 RNA detection involves analyzing the Cq Values obtained for the SARS-CoV-2 specific genes (N, E, RDRP, and RPPH-1) of interest as added in **Table 6.2**. A lower Cq Value indicates a higher initial concentration of the extracted SARS-CoV-2 RNA from the sample, while a higher Cq Value suggest lower initial concentration of RNA in the sample.

The nucleocapsid (N) gene codes for the nucleocapsid protein which is essential for viral RNA packaging and replication. The envelope (E) gene encodes the enveloped protein of virus which plays a role in viral assembly and release. RNA dependent RNA polymerase (RDRP) gene is a specific gene of SARS-CoV-2, responsible for production of an essential enzyme which is involved in viral RNA replication and transcription. Ribonuclease P RNA component H1 (RPPH1) encodes the RNA component of the ribonuclease P (RNase P) enzyme complex, which is involved in the processing of transfer RNA (tRNA) molecules. The figure shows RNA detection for all four genes. Targeting multiple genes in RT-PCR assay for SARS-CoV-2 amplification

enhances the sensitivity, specificity, and reliability of diagnostic tests, enabling the accurate detection and diagnosis of Covid-19.

Table 6.2: Quantitative estimation (Cq values) of RT-PCR products (SARS-CoV-2 cDNA) amplified by glycine@Fe_3O_4-mediated SARS-CoV-2 RNA extraction.

Gene	C_q values							
	NC	PC	Sample 1	Sample 2	Sample 3	Sample 4	Sample 5	Sample 6
RDRP	-	25.41	29.01	28.33	27.71	28.89	27.30	28.86
N	-	30.03	27.28	27.34	29.55	29.66	28.16	27.94
E	-	29.08	28.94	28.76	29.20	29.20	28.68	28.39

From the obtained RT-PCR graph and Cq Values, equivalent results are obtained for glycine@Fe_3O_4-mediated SARS-CoV-2 RNA detection when compared with market based kit-mediated RNA detection.

Figure 6.4 shows bar graph of glycine@Fe_3O_4-based RT-PCR product (SARS-CoV-2 cDNA genes: N, E, RDRP, and RPPH1) with respect to the number of RT-PCR cycles. Negative control (NC) represents product without SARS-CoV-2 cDNA. No cDNA is detected in NC as there is no presence of SARS-CoV-2 RNA in patient's sample. Positive control (PC) shows kit-extracted product where all the four genes of SARS-CoV-2 cDNA are amplified till 30 cycles of RT-PCR. Samples 1 to 6 represent glycine@Fe_3O_4-extracted cDNA products. That means, all the four genes of SARS-CoV-2 RNA are amplified and detected by RT-PCR. This confirms the successful detection of SARS-CoV-2 RNA from patient's samples (6) by using glycine@Fe_3O_4.

Orderly equivalent data was obtained for glycine@Fe_3O_4 mediated extraction when compared with RNA extracted by kit, as indicated in **Figure 6.3** and **6.4**.

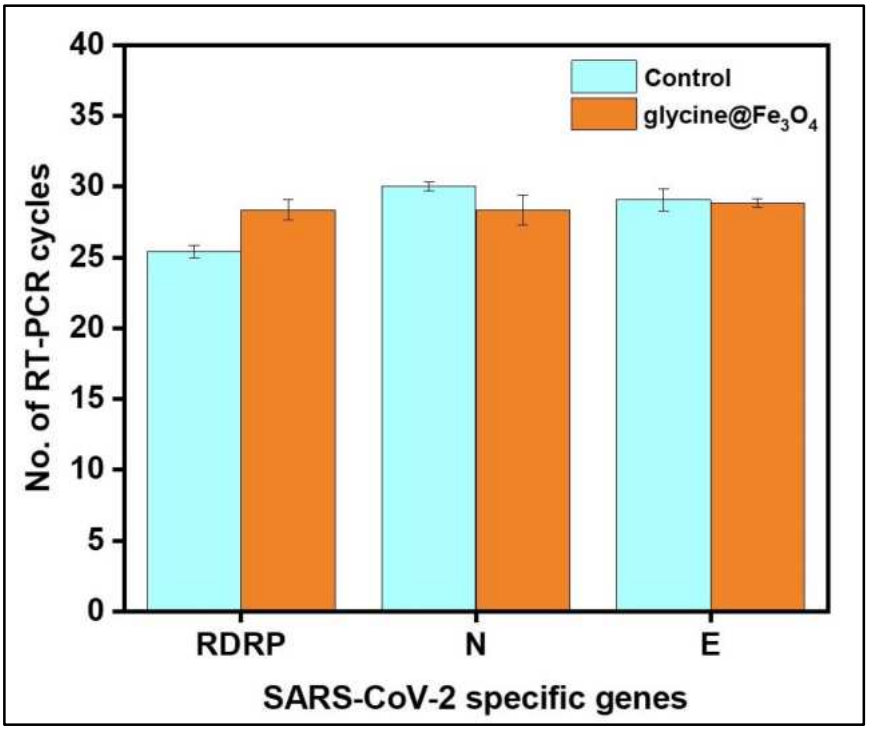

Figure 6.4. Bar graph of glycine@Fe_3O_4-based RT-PCR product (SARS-CoV-2 cDNA genes: N, E, RDRP, and RPPH1) with respect to number of RT-PCR cycles. Negative control represents product without SARS-CoV-2 cDNA. Positive control shows kit-extracted product. Samples 1 to 6 represent glycine@Fe_3O_4-extracted cDNA.

For further confirmation, cDNA of SARS-CoV-2 were analyzed by 1.2% agarose gel electrophoresis. Significant cDNA bands could observe on an agarose gel as illustrated in **Figure 6.5** that shows agarose gel electrophoresis which is a common technique to analyze the product (SARS-CoV-2 cDNA) of RT-PCR for SARS-CoV-2 detection (mediated by glycine@Fe_3O_4). M represents the reference 1Kb DNA ladder (100 to 1000 base pairs) which is a molecular weight marker. The ladder is composed of a mixture of DNA fragments of known lengths, which are derived from various sources such as Bacteriophages or plasmids. These fragments are precisely sized using restriction enzymes [28]. Wells 1 to 6 represent RT-PCR products (cDNA) obtained from glycine@Fe_3O_4-mediated SARS-CoV2 RNA extraction. Whereas, Well 7 is a market based RNA extraction kit–mediated RT-PCR product which is considered as a positive control. The presence of DNA bands corresponds to the size of obtained RT-PCR product. This indicates visual success of SARS-CoV-2 RNA detection by using

glycine@Fe_3O_4. It provides quantitative information about the size of obtained RT-PCR product (~200 base pairs). Visualization of RT-PCR product is achieved by using et-Br staining and UV-transilluminator.

Due to the negatively charged phosphate backbone present in all nucleic acids, their overall surface charge becomes negative. cDNA was extracted using glycine@Fe_3O_4, were put into the wells near the end of a cathode, or negatively charged electrode, and voltage (50V) and current (30A) were provided. On an agarose gel matrix, negative-charged cDNA moves in the direction of the anode, or positively charged electrode, when voltage is applied. Before the agarose gel solidified, an intercalating dye called ethidium bromide (EtBr) was applied. It intercalates cDNA and releases fluorescence. As a result, fluorescence was detected at the location of cDNA onto the gel. To maintain pH levels, the entire electrophoresis assembly was immersed in 1X TAE buffer.

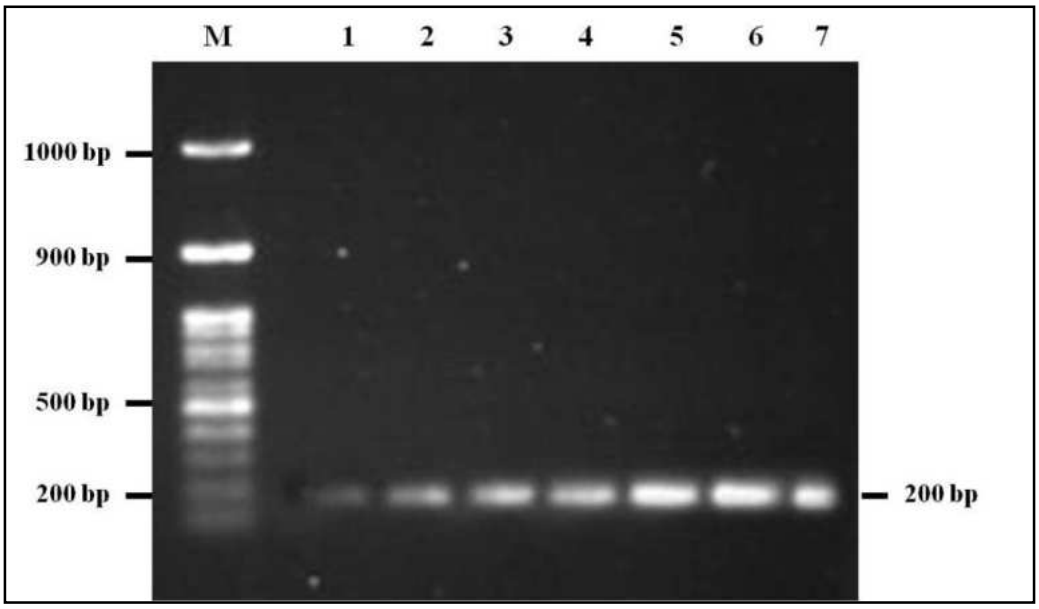

Figure 6.5. Agarose gel electrophoresis of RT-PCR products for SARS-CoV-2 RNA detection. M represents the reference ladder; wells 1-6 are RT-PCR products obtained by glycine@Fe_3O_4-mediated RNA extraction; Well 7 represents the RT-PCR product obtained by market kit-mediated RNA extraction (positive control).

6.5. CONCLUSIONS

Glycine-modified iron oxide nanoparticles (Glycine@Fe_3O_4) demonstrate the effectiveness in the detection of SARS-CoV-2 RNA. Here, Glycine@Fe_3O_4-RNA conjugation is established for the detection of SARS-CoV-2 RNA. Adsorption, washing, and desorption buffers were prepared with the minimal use of chemicals (3 to 5) to cut down the overall diagnosis cost.

These nanoparticles gain positive surface charge at pH 5 and negative surface charge at pH 7 as the isoelectric pH of glycine is 6. Hence, at pH 5, glycine@Fe_3O_4-RNA conjugate was formed due to opposite electrostatic charge attraction and thus the SARS-CoV-2 RNA was captured from the patient's sample. Further, RNA was separated from glycine@Fe_3O_4 at pH 7 due to the repulsion of same charges. In this way, SARS-CoV-2 RNA was separated with the help of glycine@Fe_3O_4 and detected by RT-PCR.

The separated RNA was compared with market-based RNA extraction kit (positive control). This comparison is carried out by using RNA purity check, RT-PCR and agarose gel electrophoresis. From the obtained RNA purity values, it is calculated that positive control-based RNA purity is 1.981 ± 0.004. Whereas, glycine@Fe_3O_4–extracted RNA is 1.963 ± 0.003. This suggested equivalent RNA purity for both the extraction methods.

Further, RT-PCR analysis was performed up to 40 cycles. After 25 cycles, the graph showed successful RNA amplification for 4 specific genes of SARS-CoV-2 viz. N, E, RDRP, and RPPH1. This amplification and obtained Cq values from RT-PCR graph suggested successful SARS-CoV-2 RNA amplification and detection. Furthermore, agarose gel electrophoresis of obtained RT-PCR products provided visual success of glycine@Fe_3O_4–mediated SARS-CoV-2 RNA detection. Also, around 200 base-pairs size of cDNA was obtained for glycine@Fe_3O_4–extracted RNA form electrophoresis. This was equivalent to the market-based RNA detection. These findings contribute to the growing body of knowledge in the field and pave the way

for future advancements in the detection and diagnosis of viral infections like COVID-19.

6.6. REFERENCES

[1] B. S. Chhikara, B. Rathi, J. Singh, F. N. Poonam. **Corona virus SARS-CoV-2 disease COVID-19: Infection, prevention and clinical advances of the prospective chemical drug therapeutics.** Chemical Biology Letters. 2020; 7(1): 63.

[2] M. A. Lauxmann, N. E. Santucci, A. M. Autrán-Gómez. **The SARS-CoV-2 coronavirus and the COVID-19 outbreak.** International braz j urol. 2020; 46: 6.

[3] https://data.who.int/dashboards/covid19/cases?n=

[4] N. Zhang, L. Wang, X. Deng, R. Liang, M. Su, C. He, L. Hu, Y. Su, J. Ren, F. Yu, L. Du. **Recent advances in the detection of respiratory virus infection in humans**. J. Med. Virol. 2020; 92(4): 408.

[5] Giri, Basant, Shishir Pandey, Retina Shrestha, Krisha Pokharel, Frances S. Ligler, and Bhanu B. Neupane. **Review of analytical performance of COVID-19 detection methods**. Anal. Bioanal. Chem. 2021; 413(1): 35.

[6] C. Ambrosi, C. Prezioso, P. Checconi, D. Scribano, M. Sarshar, M. Capannari, C. Tomino, M. Fini, E. Garaci, A. T. Palamara, G. De Chiara. **SARS-CoV-2: Comparative analysis of different RNA extraction methods**. Journal of virological methods. 2021; 287: 114008.

[7] Y. Zhang, P. Li, M Hou, L. Chen, J. Wang, H. Yang, W. Feng. **An electrochemical biosensor based on ARGET ATRP with DSN-assisted target recycling for sensitive detection of tobacco mosaic virus RNA**. Bioelectrochemistry. 2022; 144(1): 108037.

[8] M. A. Islam, M. Z. Ahsan. **Plausible approach for rapid detection of SARS-CoV-2 virus by magnetic nanoparticle based biosensors**. Am. J. Nanosci. 2020; 6(2): 1.

[9] S. Khizar, H. B. Halima, N. M. Ahmad, N. Zine, A. Errachid, A. Elaissari. **Magnetic nanoparticles in microfluidic and sensing: From transport to detection**. Electrophoresis. 2020; 41(13): 1206.

[10] R. P. Gambhir, S. S. Rohiwal, A. P. Tiwari. **Multifunctional surface functionalized magnetic iron oxide nanoparticles for biomedical applications: A review**. Appl. Surf. Sci. Adv. 2022; 11(1): 100303.

[11] S. Yasamineh, H. G. Kalajahi, P. Yasamineh, Y. Yazdani, O. Gholizadeh, R. Tabatabaie, H. Afkhami, F. Davodabadi, A. K. Farkhad, D. Pahlevan, A. Firouzi-Amandi, K. N. Koshki, M. Dadashpour. **An overview on nanoparticle-based strategies to fight viral infections with a focus on COVID-19**. J. Nanobiotechnology. 2022; 20(1): 440.

[12] Z. Zhao, H. Cui, W. Song, X. Ru, W. Zhou, X. Yu. **A simple magnetic nanoparticles-based viral RNA extraction method for efficient detection of SARS-CoV-2**. BioRxiv. 2020; 1(1): 1.

[13] I. Gessner, X. Yu, C. Jüngst, A. Klimpel, L. Wang, T. Fischer, I. Neundorf, A. C. Schauss, M. Odenthal, S. Mathur. **Selective capture and purification of microRNAs and intracellular proteins through antisense-vectorized magnetic nanobeads.** Scientific Reports. 2019; 9(1): 2069.

[14] K. M. Pang, D. Castanotto, H. Li, L. Scherer, J. J. Rossi. I**ncorporation of aptamers in the terminal loop of shRNAs yields an effective and novel combinatorial targeting strategy.** Nucleic acids research. 2018; 46(1): 6.

[15] F. Khan, M. A. Daniëls, G. E. Folkers, R. Boelens, S. M. Saqlan Naqvi, H. Van Ingen. **Structural basis of nucleic acid binding by Nicotiana tabacum glycine-rich RNA-binding protein: implications for its RNA chaperone function.** Nucleic Acids Research. 2014; 42(13): 8705.

[16] B. Lustig, S. Arora, R. L. Jernigan. **RNA base-amino acid interaction strengths derived from structures and sequences**. Nucleic acids research. 1997; 25(13): 2562.

[17] K. Cheng, C. Zhang, Y. Lu, J. Li, H. Tang, L. Ma, H. Zhu. **The Glycine-Rich RNA-Binding Protein Is a Vital Post-Transcriptional Regulator in Crops.** Plants. 2023; 12(19): 3504.

[18] H. X. Zhou, X. Pang. **Electrostatic interactions in protein structure, folding, binding, and condensation**. Chemical reviews. 2018; 118(4): 1691.

[19] S. El-Ashram, I Al-Nasr, X. Suo. **Nucleic acid protocols: Extraction and optimization.** Biotechnology reports. 2016; 12: 33.

[20] O. Nath, S. J. Fletcher, A. Hayward, L. M. Shaw, R. Agarwal, A. Furtado, R. J. Henry, N. Mitter. **A comprehensive high-quality DNA and RNA extraction protocol for a range of cultivars and tissue types of the woody crop avocado. Plants**. 2022; 11(3): 242.

[21] R. F. Garmann, A. M. Goldfain, C. R. Tanimoto, C. E. Beren, F. F. Vasquez, D. A. Villarreal, C. M. Knobler, W. M. Gelbart, V. N. Manoharan. **Single-particle studies of the effects of RNA–protein interactions on the self-assembly of RNA virus particles**. Proceedings of the National Academy of Sciences. 2022; 119(39): 2206292119

[22] S. C. Tan, B. C. Yiap. **DNA, RNA, and protein extraction: the past and the present.** BioMed Research International. 2009; 2009: 574398.

[23] L. S. Toni, A. M. Garcia, D. A. Jeffrey, X. Jiang, B. L. Stauffer, S. D. Miyamoto, C. C. Sucharov. **Optimization of phenol-chloroform RNA extraction**. MethodsX. 2018; 5: 599.

[24] N. Ali, R. D. Rampazzo, A. D. Costa, M. A. Krieger. **Current nucleic acid extraction methods and their implications to point-of-care diagnostics.** BioMed research international. 2017; 2017: 2314.

[25] I. Smyrlaki, M. Ekman, A. Lentini, N. Rufino-de-Sousa, N. Papanicolaou, M. Vondracek, J. Aarum, H. Safari, S. Muradrasoli, A. G. Rothfuchs, J. Albert. **Massive and rapid COVID-19 testing is feasible by extraction-free SARS-CoV-2 RT-PCR**. Nature communications. 2020; 11(1): 1.

[26] H. Borsook, D. A. Macfadyen. **The effect of isoelectric amino acids on the pH+ of a phosphate buffer solution: A contribution in support of the" zwitter ion" hypothesis.** The Journal of General Physiology. 1930; 13(5): 509.

[27] P. Li, M. Li, F. Zhang, M. Wu, X. Jiang, B. Ye, Z. Zhao, D. Yue, Q. Fan, H. Chen. **High-efficient nucleic acid separation from animal tissue samples via surface modified magnetic nanoparticles.** Separation and Purification Technology. 2021; 262: 118348.

[28] V. T. Lan, P. T. Loan, P. A. Duong, L. T. Thanh, N. T. Ha, T. B. Thuan. **Straightforward procedure for laboratory production of DNA ladder**. Journal of Nucleic Acids. 2012; 2012: 254630.

Chapter 7
Summary and conclusions

FLOWCHART OF THE FINDINGS

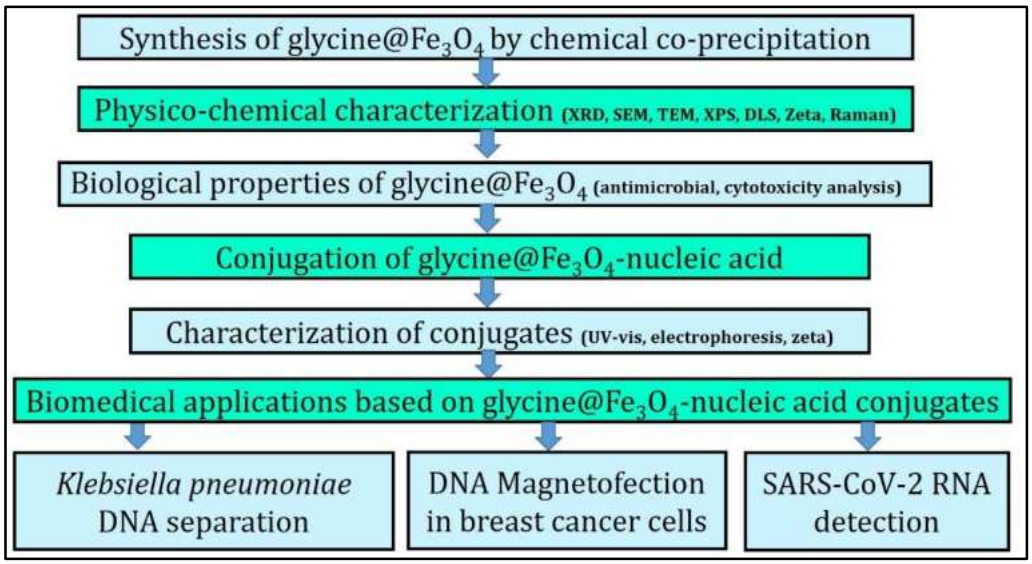

Figure 7.1. Flowchart of findings

Chapter 1 summarizes the **introduction** of the study on biomedical applications based on **iron oxide nanoparticle-nucleic acid conjugates** lays the foundation for exploring the potential of these innovative nanomaterials in the field of medicine. The focus of the study is on combining iron oxide nanoparticles with nucleic acids, such as **DNA or RNA**, to create **multifunctional nanocarriers** with promising **biomedical applications**. The introduction highlights the importance of targeted drug delivery, gene therapy, and diagnostic imaging in modern medicine, and the need for novel and efficient approaches to address these challenges. Iron oxide nanoparticles' unique properties, including **biocompatibility, magnetic responsiveness, and facile surface functionalization**, are emphasized as key factors contributing to their potential for biomedical applications. The introduction also presents the research objectives, outlining the specific biomedical areas that will be investigated using **iron oxide-nucleic acid conjugates**. Furthermore, it underscores the **significance** of this study in advancing the understanding of nanomedicine and its potential impact on personalized and

precision medicine. Overall, the introduction sets the context for the research, underscoring the importance of exploring the applications of iron oxide-nucleic acid conjugates and their potential to revolutionize the landscape of biomedical sciences and healthcare. It summarizes the literature review on iron oxide-nucleic acid conjugate formation in this field. The focus of the chapter is on the synthesis and characterization of conjugates formed by combining iron oxide nanoparticles with nucleic acids, such as DNA or RNA. It highlights the diverse biomedical applications of these conjugates. Targeted drug delivery, gene therapy, and diagnostic imaging are among the key areas of interest. The chapter provides insights into how the **unique properties** of iron oxide nanoparticles, such as their **magnetic responsiveness** and biocompatibility, enhance the potential of nucleic acids for precise and effective biomedical applications. It consolidates the current knowledge on iron oxide-nucleic acid conjugates, identifying gaps and potential directions for future research. It serves as a valuable resource for researchers, seeking to harness the capabilities of these conjugates for advancing personalized and targeted applications in the field of biomedicine.

Chapter 2 summarizes the **synthesis and characterization** of glycine-modified magnetic iron oxide nanoparticles (**glycine@Fe_3O_4**). In the synthesis process, iron oxide nanoparticles were prepared through a **chemical co-precipitation** method. Subsequently, the nanoparticles were modified with glycine through an incubation process. The **characterization** of the nanoparticles was carried out using various **physico-chemical techniques** such as transmission electron microscopy (TEM), X-ray diffraction (XRD), dynamic light scattering (DLS), and X-ray photoelectron spectroscopy (XPS) provided valuable information about particle size, crystal structure, and colloidal stability. Additionally, **biological characterization techniques** (biocompatibility and antimicrobial property) have been studied. Overall, the successful synthesis and characterization of glycine@Fe_3O_4 provided valuable insights into their **potential applications in targeted biomedical fields**.

These nanoparticles held promise as versatile and efficient nanocarriers in biomedical applications, offering opportunities for further exploration in future research endeavors.

Chapter 3 summarizes the study of the **adsorption and desorption of nucleic acid** with glycine@Fe_3O_4. The focus of the chapter is on surface modification with glycine to functionalize the iron oxide nanoparticles for enhanced adsorption affinity with nucleic acids. Moreover, the study delves into desorption process, where the nucleic acids can be released from the nanoparticles under controlled conditions. **Table 7.1** showed the **optimized parameters** for mentioned adsorption and desorption processes. Overall, the research sheds light on the fundamental aspects of adsorption and desorption of nucleic acids with surface-modified iron oxide nanoparticles (glycine@Fe_3O_4), providing insights into potential strategies for developing effective nanocarriers in biomedical applications. The findings from this study held great promise in further biomedical applications.

Table 7.1 – Optimized parameter conditions for DNA and glycine@Fe_3O_4 adsorption and desorption interactions.

No.	Parameters	Adsorption conditions	Desorption conditions
1	DNA	100 µg/mL	100 µg/mL
2	Glycine@Fe_3O_4	50 µg/mL	50 µg/mL
3	pH	5	7
4	Time	30 min	30 min
5	Temperature	25°C	25°C

Chapter 4 summarizes the use of glycine@Fe_3O_4 magnetic nanoparticles for **DNA separation from bacterial (*Klebsiella pneumoniae*) sample**. This presents a promising approach for detecting nosocomial infections caused by *Klebsiella pneumoniae* pathogen with the help of **electrochemical sensing**. Glycine-modified magnetic iron oxide nanoparticles (glycine@Fe_3O_4) offered a versatile platform for **selective separation**, purification, and enrichment of target DNA from complex biological samples.

By utilizing glycine@Fe_3O_4 in the development of an electrochemical DNA separation methodology, the separation of nucleic acid from clinical samples became possible. The **electrode surface** acted as a site of reaction between the glycine@Fe_3O_4 and target DNA, and the proposed methodology demonstrated precise response to DNA **within 10 minutes**. Glycine@Fe_3O_4 exhibited high sensitivity towards DNA, efficiently separating as **low as 20 nM DNA** from interfering biomolecules like whole cells and proteins in clinical samples. The non-enzymatic and **label-free** nature of this method ensured sensitive, labor-free, and **cost-effective DNA separation and detection** for nosocomial infections, contributing to advancements in healthcare, environmental monitoring, and related fields.

Chapter 5 summarizes **magnetofection** (gene delivery) in breast cancer cells (MCF-7) using surface-modified magnetic nanoparticles, glycine@Fe_3O_4 conjugated with **fluorescent carbon quantum dots (QDs)** and standard nucleic acid (DNA). The successful delivery of **glycine@Fe_3O_4@QD@DNA** into the cells was assessed using fluorescence quenching and microscopy analyses. The results demonstrated the potential of glycine@Fe_3O_4@QD-based magnetofection as an effective approach for gene delivery in **breast cancer cells**. Fluorescence intensity measurements indicated a significant decrease in signal, indicating successful **quenching** due to interactions with intracellular components. This decrease in **fluorescence intensity** strongly suggested that glycine@Fe_3O_4@QD@DNA was internalized within the cellular environment. Further, UV-visible spectroscopy provided the increase in DNA absorbance after magnetofection. Combination of magnetic nanoparticles and fluorescence quenching provided a powerful tool for **tracking and monitoring of gene** delivery, facilitating the optimization of magnetofection protocols and enhancing understanding of cellular uptake mechanisms. Importantly, the incorporation of glycine@Fe_3O_4@QD@DNA collectively **reduced cell cytotoxicity**, enabling successful magnetofection efficiency. The study also revealed that glycine@Fe_3O_4@QD@DNA-transfected

cells emitted **blue fluorescence** in the UV range around 350 to 420 nm, confirming the presence of the delivered genetic material. These findings demonstrated the potential of glycine@Fe_3O_4@QD-based magnetofection as a promising strategy for gene delivery in breast cancer cells, providing valuable insights for future biomedical applications and gene therapy research.

Chapter 6 summarizes a novel method for **viral (SARS-CoV-2) RNA detection** by employing amino acid glycine-modified magnetic iron oxide nanoparticles (glycine@Fe_3O_4). These nanoparticles offered a larger surface area and charge, enabling efficient binding of RNA to their surface. The surface charge of glycine@Fe_3O_4 was **pH-dependent**, facilitating achievable **adsorption and desorption** of RNA onto and from the nanoparticle surface, respectively. In **acidic pH**, glycine gained a positive charge, leading to effective binding of negatively charged RNA. Conversely, elution of RNA from glycine@Fe_3O_4 occurred in **basic pH** due to repulsive charges. The extraction process was made cost-efficient and simple by preparing binding and elution buffers with minimal chemicals. RNAs extracted using this method were successfully detected through **RT-PCR**, and the obtained **cDNA of SARS-CoV-2** showed distinct bands on 1.2% agarose gel stained with ethidium bromide (etBr). Comparing the results with **kit-extracted SARS-CoV-2 RNA** revealed equivalent outcomes for glycine@Fe_3O_4-extracted RNA. The pH-responsive glycine@Fe_3O_4-based SARS-CoV-2 RNA extraction process exhibited promise for COVID-19 detection, demonstrating robust and effective diagnostic potential.

80 Recommendations

8.1. RECOMMENDATIONS

The glycine-modified iron oxide nanoparticles (glycine@Fe_3O_4) were synthesized by chemical co-precipitation method. These nanoparticles can be synthesized in an inert environment to achieve uniform particle size distribution.

The study presents conjugation of glycine@Fe_3O_4-DNA due to electrostatic interactions between positively charged glycine@Fe_3O_4 and negatively charged DNA. Similar to positively charged glycine, studies can be explored best positive amine containing biological entity to know the potential for DNA adsorption and desorption studies. Also, other biological components can be studied as alternatives to glycine for better biocompatibility towards biological systems.

The thesis presents electrochemical approach for *Klebsiella pneumoniae* DNA separation by glycine@Fe_3O_4 nanoparticles to detect nosocomial (hospital-acquired) infections. Other infections can be explored with the similar approach. Basic mechanism-based electrochemical DNA separation can be upgraded with the automation of process which will lead to point-of-care devices for hospital-acquired infections.

The thesis also presents quantum dots-labelled glycine@Fe_3O_4 (glycine@Fe_3O_4@QDs) for DNA magnetofection in breast cancer cells. These labelled nanoparticles can be further utilized in CRISPR-Cas technology, gene silencing, and animal studies to establish glycine@Fe_3O_4@QDs-based therapeutics.

The thesis further presents the SARS-CoV-2 RNA detection using glycine@Fe_3O_4 nanoparticles. The market-based SARS-CoV-2 detection kits cost around ₹ 4,500/RNA sample. The present thesis work is cost-effective. However, the actual working cost needs to be calculated prospectively. The method can be used for teaching and training purpose in primary research. This method can be studied for other viruses like Dengue, Zika and can be used as an alternative method for potential pandemics. This methodology is patented by Patent Office, India with the application no. 202221045186.

Publications

J Mater Sci

Materials for life sciences

pH-responsive glycine functionalized magnetic iron oxide nanoparticles for SARS-CoV-2 RNA extraction from clinical sample

Rutuja Prashant Gambhir[1], Arun Kumar Parthasarathy[2], Shimpa Sharma[3], Shital Kale[4], Vikas Vijay Magdum[5], and Arpita Pandey Tiwari[1,*]

[1] *Department of Stem Cell and Regenerative Medicine, Centre for Interdisciplinary Science, D.Y. Patil Education Society, Kolhapur, India*

[2] *Department of Microbiology, D.Y. Patil Medical College and Hospital, Kolhapur, India*

[3] *D.Y. Patil Medical College and Hospital, Kolhapur, India*

[4] *Department of Materials Science and Engineering, Chonnam National University, Gwangju, South Korea*

[5] *Centre for Interdisciplinary Science, D.Y. Patil Education Society, Kolhapur, India*

Received: 21 February 2022
Accepted: 18 June 2022

ABSTRACT

The recent outbreak of the novel corona virus disease 2019 (COVID-19) has been made a serious global impact due to its high infectivity and severe symptoms. The Severe Acute Respiratory Syndrome (SARS-CoV-2) RNA extraction is considered as one of the most important steps in COVID-19 detection. Several commercially available kits and techniques are currently being used for specific extraction of SARS-CoV-2 RNA. However, such methods are time consuming and expensive due to the requirement of trained labors, and several chemical reagents. To overcome the mentioned limitations, magnetic RNA adsorption methodology of glycine functionalized iron oxide nanoparticles (GNPs) was established. It showed an efficient potential in SARS-CoV-2 RNA extraction due to pH responsive nature of GNPs. The highly magnetic pH responsive GNPs were synthesized by one-pot co-precipitation method. Random morphology and average 20 nm size of GNPs were denoted by Transmission Electron Microscopy (TEM). X-ray diffractometer (XRD) showed the crystalline magnetite nature. Fourier transform infrared spectroscopy (FT-IR) and UV–visible spectrometry confirmed the presence of glycine on the surface of magnetic nanoparticles. Furthermore, the magnetic nature and thermal properties of GNPs were examined by vibrating sample magnetometer (VSM) and thermogravimetric analysis (TGA), respectively. In this study, glycine performed the role of RNA adsorbent. The adsorption of RNA onto the surface of GNPs was achieved in acidic medium (pH 6). In contrary, the elution of RNA from the

Handling Editor: Dale Huber.

Address correspondence to E-mail: arpitaptiwari@gmail.com

https://doi.org/10.1007/s10853-022-07464-6

Published online: 13 July 2022

Applied Surface Science Advances 11 (2022) 100303

Contents lists available at ScienceDirect

Applied Surface Science Advances

journal homepage: www.sciencedirect.com/journal/applied-surface-science-advances

Multifunctional surface functionalized magnetic iron oxide nanoparticles for biomedical applications: A review

Rutuja Prashant Gambhir [a], Sonali S Rohiwal [b], Arpita Pandey Tiwari [a,*]

[a] Department of Stem Cell and Regenerative Medicine and Medical Biotechnology, D.Y. Patil Education Society, Institution Deemed to be University, Kolhapur 416006, India

[b] Laboratory of Cell Regeneration and Plasticity, Institute of Animal Physiology and Genetics AS CR, v.v.i. Rumburska 89, Libechov 277 21, Czech Republic

ARTICLE INFO

Keywords:
Magnetic
Nanoparticles
Multifunctional
Surface functionalization
Biomedical applications
COVID19

ABSTRACT

Magnetic iron oxide nanoparticle-based multifunctional platforms have been explored extensively in biomedical applications. Modifications and integrations of IONPs with different entities viz. organic polymer, doping with inorganic materials, loading with drug, fluorescent dye, or antibodies make them appropriate for their application in broad spectrum of biomedical fields. This review presents and summarizes the fabrication strategies of multifunctional magnetic nanoparticles based on the modification and surface functionalization of MNP. Multifunctional IONPs based recent advances covering a wide array of applications like biosensing and pathogen detection, magnetic resonance imaging (MRI) and biomarker tracking, magnetofection and gene therapy, hyperthermia and chemotherapy, drug delivery and targeted cell killing, bioimaging and therapeutics, stem cell detection and therapy, tissue engineering and organ transplant, nano-vaccines and immune system activation, microbe targeting and destruction, and COVID19 management are also covered.

1. Introduction

Magnetic nanoparticles (MNPs) gain central attraction in the area of nano-biomedicine, nano-chemistry, electronics, and nano-therapeutics. Consistent improvements are being made in synthesis methods, physico-chemical characterization, and surface functionalization of MNPs to achieve desirable size, morphology, and structural chemistry. This tunability is achieved according to their physico-chemical nature at the time of their synthesis. Structurally, they are made up with three layers; surface layer which exhibits functionalized small molecules, doped metals, or polymers, antibodies, proteins, etc., shell layer exhibits chemical components different than the prominent component, and core layer consists of the main chemical entity which normally refers to nanoparticle [1]. The incorporation of MNPs for biomedical applications is associated with their inherent physical and chemical properties, size, crystalline or amorphous nature, biocompatibility, etc. Additionally surface functionalization on MNPs diminishes their limitations. MNPs exhibit several advantages over the other mentioned particles due to intrinsic tunable physico-chemical properties, cost-effectiveness, low--cost synthesis, easy availability of precursors, rapid synthesis, *in-vitro* and *in-vivo* take-up, magnetic switchable on-off nature, versatility in surface functionalization, manipulating nature with external magnetic field, etc. [2]. They comprise magnetic elements; iron (Fe), cobalt (Co), manganese (Mn) and nickel (Ni). Specifically, magnetic iron oxide nanoparticles (IONPs) are majorly studied and used in biomedical activities due to their high spin magnetic moments, and less toxicity. Iron refers to the backbone of earth's chemical composition due to its abundant presence in crust. It is economical and plays significant roles in various geological and biological processes. At natural state, iron (Fe) combines with oxygen molecule (O) and forms iron oxide. There are three most common forms of IONPs; magnetite (Fe_3O_4), maghemite (γ-Fe_2O_3), and hematite (α-Fe_2O_3) found in nature. Further oxidation of magnetite results in the formation of hematite. In recent period, magnetite has gained powerful research attention when compared with other forms of IONPs. They possess prominent advantages like superparamagnetism, larger surface area, high surface-to-volume ratio, and rapid and easy methodology of target separation from solution due to external magnetic field movements. Hence, IONPs (magnetite) have excellently been studied and applied in the fields of biomedicine [3]. There are some limitations related to use of MNPs in biomedical activities, such as toxicity issue; but it can be minimized by surface functionalization to them with biocompatible entity (eg, like polymer, antibodies, aptamers,antibodies, fkuorophores etc.) that covers the complete surface of MNP and hence provides biocompatibility.

* Corresponding author.
E-mail address: arpitaptiwari@gmail.com (A.P. Tiwari).

https://doi.org/10.1016/j.apsadv.2022.100303
Received 30 May 2022; Received in revised form 6 September 2022; Accepted 8 September 2022

Surface-Functionalized Iron Oxide (Fe_3O_4) Nanoparticles for Biomedical Applications

Rutuja P. Gambhir, Anuja A. Vibhute, Tejaswini P. Patil, and Arpita P. Tiwari

Abbreviation

ab@IONP	Antibody functionalized IONP
AC	Alternating current
APTES	3-aminopropyltriethyloxysilane
AuNPs	Gold nanoparticles
BBB	Blood-brain barrier
BSA	Bovine serum albumin
CEA	Carcinoembryonic antigen
CMC	Carboxymethylcellulose
CNT	Carbon nanotube
CT	Computed tomography
DNA	Deoxyribonucleic acid
GET	Glycosaminoglycan binding-enhanced transduction
GFP	Green fluorescent protein
HA	Hyaluronic acid
HEK	Human embryonic kidney cell
IgG	Immunoglobulin G
IONP	Iron oxide nanoparticle
LDH	Layered double hydroxide
MNP	Magnetic nanoparticle
MPA	Mercaptopropionic acid
MPTES	Mercaptopropyltriethoxysilane
MR	Magnetic resonance

R. P. Gambhir · A. A. Vibhute · T. P. Patil · A. P. Tiwari (✉)
Department of Medical Biotechnology, D Y Patil Education Society, (Deemed to be University), Kolhapur, Maharashtra, India

F. I. Ezema et al. (eds.), *Chemically Deposited Metal Chalcogenide-based Carbon Composites for Versatile Applications*, https://doi.org/10.1007/978-3-031-23401-9_15

J Nanopart Res (2023) 25:83
https://doi.org/10.1007/s11051-023-05735-0

RESEARCH PAPER

Green synthesized magnetic nanoparticles for selective inhibition of osteosarcoma cancer

Rutuja Prashant Gambhir · Shital Kale · Tukaram Dongale · Snehal Patil · Dhanaji Malavekar · Arpita Pandey Tiwari

Received: 18 August 2022 / Accepted: 3 April 2023

Abstract Here, selective anti-cancer activity of poly-l-lysine-functionalized iron oxide nanoparticles (PLL@IONPs) has been shown against osteosarcoma cancer. The mentioned nanoparticles were synthesized from *Spinacia oleracia* (spinach) leaf extract. In-vitro, osteosarcoma cells incubated with the synthesized nanoparticles showed the selective cytotoxicity. Particles exposed to the normal fibroblast cells displayed significantly less cytotoxic effects. Interestingly, the reactive oxygen species (ROS) generation was inhibited by the synthesized material with their intrinsic free radical scavenging activity. In-vivo, PLL@IONPs significantly inhibited the site-specific angiogenesis in chick embryo. This could lead to the site-specific therapeutic efficiency. In addition, suspected carcinogenic dyes were degraded by the particles and provided a cancer-preventive aspect. The results suggest that PLL@IONPs could be significantly applied as a therapeutic against osteosarcoma cancer as well as carcinogen degradation measure.

Keywords Iron oxide; Anti-cancer; Anti-angiogenesis · Photocatalytic · Green synthesis · Anti-oxidative · Nanomedicine

Rutuja Prashant Gambhir is the first author and Shital Kale is the second author.

Supplementary information The online version contains supplementary material available at https://doi.org/10.1007/s11051-023-05735-0.

R. P. Gambhir · A. P. Tiwari (✉)
Department of Stem Cell and Regenerative Medicine and Medical Biotechnology, D. Y. Patil Education Society (Deemed to be University), Maharashtra, Kolhapur, India
e-mail: arpitaptiwari@gmail.com

S. Kale
Leibniz Institute for Catalysis, Albert-Einstein-Strasse 29a, 18059 Roctock, Germany

T. Dongale · S. Patil
School of Nanoscience and Biotechnology, Shivaji University, Kolhapur, Maharashtra, India

D. Malavekar
Department of Materials Science and Engineering, Optoelectronic Convergence Research Center, Chonnam National University, Gwangju 61186, South Korea

Introduction

Nanobiotechnology facilitated the principal development worldwide in the past few decades. Nanomaterials have attained major importance in several biomedical activities like disease diagnosis, drug delivery, gene transfection, and biosensing, according to their physicochemical nature [1–3]. Among these, magnetic nanomaterials show enormous applicability in the area of disease theranostics [4]. Recently, the iron oxide nanoparticles have been approved by Food and Drug Administration (FDA) for treating iron deficiency and drug delivery for several diseases. Several

INTELLECTUAL PROPERTY INDIA
PATENTS | DESIGNS | TRADE MARKS
GEOGRAPHICAL INDICATIONS

सत्यमेव जयते

क्रम सं/SL No :022125888

पेटेंट कार्यालय,भारत सरकार | The Patent Office, Government Of India

पेटेंट प्रमाण पत्र | Patent Certificate

(पेटेंट नियमावली का नियम 74) | (Rule 74 of The Patents Rules)

पेटेंट सं. / Patent No.	:	440563
आवेदन सं. / Application No.	:	202221045186
फाइल करने की तारीख / Date of Filing	:	08/08/2022
पेटेंटी / Patentee	:	D.Y.PATIL EDUCATION SOCIETY (DEEMED TO BE UNIVERSITY)
आविष्कारकों का नाम /Name of Inventor(s)	:	1.DR.ARPITA PANDEY TIWARI 2.MS.RUTUJA PRASHANT GAMBHIR

प्रमाणित किया जाता है कि पेटेंटी को, उपरोक्त आवेदन में यथाप्रकटित *A METHOD FOR RNA ISOLATION FROM VIRAL/HUMAN SERUM SAMPLES USING FUNCTIONALIZED MAGNETIC NANOPARTICLE* नामक आविष्कार के लिए, पेटेंट अधिनियम, 1970 के उपबंधों के अनुसार आज तारीख अगस्त 2022 के आठवें दिन से बीस वर्ष की अवधि के लिए पेटेंट अनुदत्त किया गया है।

It is hereby certified that a patent has been granted to the patentee for an invention entitled *A METHOD FOR RNA ISOLATION FROM VIRAL/HUMAN SERUM SAMPLES USING FUNCTIONALIZED MAGNETIC NANOPARTICLE* as disclosed in the above mentioned application for the term of 20 years from the 8th day of August 2022 in accordance with the provisions of the Patents Act,1970.

अनुदान की तारीख :
Date of Grant : 26/07/2023

पेटेंट नियंत्रक
Controller of Patents

टिप्पणी - इस पेटेंट के नवीकरण के लिए फीस, यदि इसे बनाए रखा जाना है, अगस्त 2024 के आठवें दिन को और उसके पश्चात प्रत्येक वर्ष मे उसी दिन देय होगी।

Note. - The fees for renewal of this patent, if it is to be maintained, will fall / has fallen due on 8th day of August 2024 and on the same day in every year thereafter.

INTELLECTUAL PROPERTY INDIA
PATENTS | DESIGNS | TRADE MARKS
GEOGRAPHICAL INDICATIONS

सत्यमेव जयते

ORIGINAL
क्रम सं/ Serial No. : 146201

पेटेंट कार्यालय, भारत सरकार The Patent Office, Government Of India

डिजाइन के पंजीकरण का प्रमाण पत्र | Certificate of Registration of Design

डिजाइन सं. / Design No. : 393145-001

तारीख / Date : 21/08/2023

पारस्परिकता तारीख / Reciprocity Date* :

देश / Country :

प्रमाणित किया जाता है कि संलग्न प्रति में वर्णित डिजाइन जो *ELECTROCHEMICAL BIOSENSOR APPARATUS FOR DETECTING STEM CELLS* से संबंधित है, का पंजीकरण, श्रेणी 10-04 में 1.Dr. Arpita Pandey Tiwari 2. Ms. Rutuja Prashant Gambhir 3.D.Y. Patil Education Society के नाम में उपर्युक्त संख्या और तारीख में कर लिया गया है।

Certified that the design of which a copy is annexed hereto has been registered as of the number and date given above in class 10-04 in respect of the application of such design to *ELECTROCHEMICAL BIOSENSOR APPARATUS FOR DETECTING STEM CELLS* in the name of 1.Dr. Arpita Pandey Tiwari 2. Ms. Rutuja Prashant Gambhir 3.D.Y. Patil Education Society.

डिजाइन अधिनियम, 2000 तथा डिजाइन नियम, 2001 के अध्यधीन प्रावधानों के अनुसरण में।

In pursuance of and subject to the provisions of the Designs Act, 2000 and the Designs Rules, 2001.

जारी करने की तिथि :
Date of Issue : 17/10/2023

महानियंत्रक पेटेंट, डिजाइन और व्यापार चिह्न
Controller General of Patents, Designs and Trade Marks

*पारस्परिकता तारीख (यदि कोई हो) जिसकी अनुमति दी गई है तथा देश का नाम। डिजाइन का स्वत्वाधिकार पंजीकरण की तारीख से दस वर्षों के लिए होगा जिसका विस्तार, अधिनियम एवं नियम के निबंधनों के अधीन, पाँच वर्षों की अतिरिक्त अवधि के लिए किया जा सकेगा। इस प्रमाण पत्र का उपयोग विधिक कार्यवाहियों अथवा विदेश में पंजीकरण प्राप्त करने के लिए नहीं हो सकता है।

The reciprocity date (if any) which has been allowed and the name of the country. Copyright in the design will subsist for ten years from the date of Registration, and may under the terms of the Act and Rules, be extended for a further period of five years. This Certificate is not for use in legal proceedings or for obtaining registration abroad.

INTELLECTUAL PROPERTY INDIA
PATENTS | DESIGNS | TRADE MARKS
GEOGRAPHICAL INDICATIONS

सत्यमेव जयते

Extracts from the Register of Copyrights

प्रतिलिप्यधिकार कार्यालय, भारत सरकार | Copyright Office, Government Of India

दिनांक/Dated:26/09/2023

1.	पंजीकरण संख्या/Registration Number	:	**L-133610/2023**
2.	आवेदक का नाम, पता तथा राष्ट्रीयता Name, address and nationality of the applicant	:	THE REGISTRAR , D. Y. PATIL EDUCATION SOCIETY, DEEMED TO BE UNIVERSITY, KASABA BAWADA, KOLHAPUR-416006 INDIAN
3.	कृति के प्रतिलिप्यधिकार में आवेदक के हित की प्रकृति Nature of the applicant's interest in the copyright of the work	:	PUBLISHER
4.	कृति का वर्ग और वर्णन Class and description of the work	:	LITERARY/ DRAMATIC WORK
5.	कृति का शीर्षक Title of the work	:	MULTIFUNCTIONAL NANOPARTICLES FOR BIOMEDICAL APPLICATIONS
6.	कृति की भाषा Language of the work	:	ENGLISH
7.	रचयिता का नाम, पता और राष्ट्रीयता तथा यदि रचयिता की मृत्यु हो गई है, तो मृत्यु की तिथि Name, address and nationality of the author and if the author is deceased, date of his decease	:	DR. ARPITA PANDEY TIWARI, ASSOCIATE PROFESSOR , DEPARTMENT OF STEM CELL AND REGENERATIVE MEDICINE, CENTRE FOR INTERDISCIPLINARY RESEARCH, D. Y. PATIL EDUCATION SOCIETY, DEEMED TO BE UNIVERSITY, KASABA BAWADA, KOLHAPUR-416006 INDIAN MS. RUTUJA PRASHANT GAMBHIR, PH. D. SCHOLAR , DEPARTMENT OF STEM CELL AND REGENERATIVE MEDICINE, CENTRE FOR INTERDISCIPLINARY RESEARCH, D. Y. PATIL EDUCATION SOCIETY, DEEMED TO BE UNIVERSITY, KASABA BAWADA, KOLHAPUR-416006 INDIAN
8.	कृति प्रकाशित है या अप्रकाशित Whether the work is published or unpublished	:	PUBLISHED
9.	प्रथम प्रकाशन का वर्ष और देश तथा प्रकाशक का नाम, पता और राष्ट्रीयता Year and country of first publication and name, address and nationality of the publisher	:	2023 INDIA THE REGISTRAR , D. Y. PATIL EDUCATION SOCIETY, DEEMED TO BE UNIVERSITY, KASABA BAWADA, KOLHAPUR-416006 INDIAN
10.	बाद के प्रकाशनों के वर्ष और देश, यदि कोई हों, और प्रकाशकों के नाम, पते और राष्ट्रीयताएँ Years and countries of subsequent publications, if any, and names, addresses and nationalities of the publishers	:	N.A.
11.	कृति में प्रतिलिप्यधिकार सहित विभिन्न अधिकारों के स्वामियों के नाम, पते और राष्ट्रीयताएं और समनुदेशन और अनुज्ञप्तियों के विवरण के साथ प्रत्येक के अधिकार का विस्तार, यदि कोई हो। Names, addresses and nationalities of the owners of various rights comprising the copyright in the work and the extent of rights held by each, together with particulars of assignments and licences, if any	:	THE REGISTRAR , D. Y. PATIL EDUCATION SOCIETY, DEEMED TO BE UNIVERSITY, KASABA BAWADA, KOLHAPUR-416006 INDIAN
12.	अन्य व्यक्तियों के नाम, पते और राष्ट्रीयताएं, यदि कोई हों, जो प्रतिलिप्यधिकार वाले अधिकारों को समनुदेशित करने या अनुज्ञप्ति देने के लिए अधिकृत हों Names, addresses and nationalities of other persons, if any, authorised to assign or licence of rights comprising the copyright	:	N.A.
13.	यदि कृति एक 'कलात्मक कृति' है, तो कृति पर अधिकार रखने वाले व्यक्ति का नाम, पता और राष्ट्रीयता सहित मूल कृति का स्थान। (एक वास्तुशिल्प कृति के मामले में कृति पूरी होने का वर्ष भी दिखाया जाना चाहिए) If the work is an 'Artistic work', the location of the original work, including name, address and nationality of the person in possession of the work. (In the case of an architectural work, the year of completion of the work should also be shown).	:	N.A.
14.	यदि कृति एक 'कलात्मक कृति' है जो किसी भी माल या सेवाओं के संबंध में उपयोग की जाती है या उपयोग किए जाने में सक्षम है, तो आवेदन में प्रतिलिप्यधिकार अधिनियम, 1957 की धारा 45 की उप–धारा (i) के प्रावधान के अनुसार व्यापार चिह्न रजिस्ट्रार से प्रमाणन शामिल होना चाहिए। If the work is an 'Artistic work' which is used or capable of being used in relation to any goods or services, the application should include a certification from the Registrar of Trade Marks in terms of the provision to Sub-Section (i) of Section 45 of the Copyright Act, 1957.	:	N.A.
15.	यदि कृति एक 'कलात्मक कृति' है, तो क्या यह डिजाइन अधिनियम 2000 के अंतर्गत पंजीकृत है? यदि हां, तो विवरण दें। If the work is an 'Artistic work', whether it is registered under the Designs Act 2000, if yes give details.	:	N.A.
16.	यदि कृति एक 'कलात्मक कृति' है, जो डिजाइन अधिनियम 2000 के तहत एक डिजाइन के रूप में पंजीकृत होने में सक्षम है, तो क्या यह औद्योगिक प्रक्रिया के माध्यम से किसी वस्तु पर प्रयुक्त की गई है और यदि हाँ, तो कितनी बार पुनरुत्पादित किया गया है? If the work is an 'Artistic work', capable of being registered as a design under the Designs Act 2000.whether it has been applied to an article though an industrial process and ,if yes ,the number of times it is reproduced.	:	N.A.
17.	टिप्पणी, यदि कोई हो/Remarks, if any	:	

Registrar of Copyrights

डायरी संख्या/Diary Number: 21013/2023-CO/L

आवेदन की तिथि/Date of Application: 09/08/2023

प्राप्ति की तिथि/Date of Receipt: 09/08/2023

Registrar of Copyrights

INTELLECTUAL PROPERTY INDIA
PATENTS | DESIGNS | TRADE MARKS
GEOGRAPHICAL INDICATIONS

सत्यमेव जयते

Extracts from the Register of Copyrights

प्रतिलिप्यधिकार कार्यालय, भारत सरकार | Copyright Office, Government Of India

दिनांक/Dated:26/09/2023

1.	पंजीकरण संख्या/Registration Number	:	**L-133651/2023**
2.	आवेदक का नाम, पता तथा राष्ट्रीयता Name, address and nationality of the applicant	:	THE REGISTRAR , D. Y. PATIL EDUCATION SOCIETY, DEEMED TO BE UNIVERSITY, KASABA BAWADA, KOLHAPUR-416006 INDIAN
3.	कृति के प्रतिलिप्यधिकार में आवेदक के हित की प्रकृति Nature of the applicant's interest in the copyright of the work	:	PUBLISHER
4.	कृति का वर्ग और वर्णन Class and description of the work	:	LITERARY/ DRAMATIC WORK
5.	कृति का शीर्षक Title of the work	:	DETECTION OF BACTERIAL DNA BY SURFACE FUNCTIONALIZED MAGNETIC NANOPARTICLES
6.	कृति की भाषा Language of the work	:	ENGLISH
7.	रचयिता का नाम, पता और राष्ट्रीयता तथा यदि रचयिता की मृत्यु हो गई है, तो मृत्यु की तिथि Name, address and nationality of the author and if the author is deceased, date of his decease	:	DR. ARPITA PANDEY TIWARI, ASSOCIATE PROFESSOR , DEPARTMENT OF STEM CELL AND REGENERATIVE MEDICINE, CENTRE FOR INTERDISCIPLINARY RESEARCH, D. Y. PATIL EDUCATION SOCIETY, DEEMED TO BE UNIVERSITY, KASABA BAWADA, KOLHAPUR-416006 INDIAN MS. RUTUJA PRASHANT GAMBHIR, PH. D. SCHOLAR , DEPARTMENT OF STEM CELL AND REGENERATIVE MEDICINE, CENTRE FOR INTERDISCIPLINARY RESEARCH, D. Y. PATIL EDUCATION SOCIETY, DEEMED TO BE UNIVERSITY, KASABA BAWADA, KOLHAPUR-416006 INDIAN
8.	कृति प्रकाशित है या अप्रकाशित Whether the work is published or unpublished	:	PUBLISHED
9.	प्रथम प्रकाशन का वर्ष और देश तथा प्रकाशक का नाम, पता और राष्ट्रीयता Year and country of first publication and name, address and nationality of the publisher	:	2023 INDIA THE REGISTRAR , D. Y. PATIL EDUCATION SOCIETY, DEEMED TO BE UNIVERSITY, KASABA BAWADA, KOLHAPUR-416006 INDIAN
10.	बाद के प्रकाशनों के वर्ष और देश, यदि कोई हों, और प्रकाशकों के नाम, पते और राष्ट्रीयताएँ Years and countries of subsequent publications, if any, and names, addresses and nationalities of the publishers	:	N.A.
11.	कृति में प्रतिलिप्यधिकार सहित विभिन्न अधिकारों के स्वामियों के नाम, पते और राष्ट्रीयताएं और समनुदेशन और अनुज्ञप्तियों के विवरण के साथ प्रत्येक के अधिकार का विस्तार, यदि कोई हो। Names, addresses and nationalities of the owners of various rights comprising the copyright in the work and the extent of rights held by each, together with particulars of assignments and licences, if any	:	THE REGISTRAR , D. Y. PATIL EDUCATION SOCIETY, DEEMED TO BE UNIVERSITY, KASABA BAWADA, KOLHAPUR-416006 INDIAN
12.	अन्य व्यक्तियों के नाम, पते और राष्ट्रीयताएं, यदि कोई हों, जो प्रतिलिप्यधिकार वाले अधिकारों को समनुदेशित करने या अनुज्ञप्ति देने के लिए अधिकृत हों Names, addresses and nationalities of other persons, if any, authorised to assign or licence of rights comprising the copyright	:	N.A.
13.	यदि कृति एक 'कलात्मक कृति' है, तो कृति पर अधिकार रखने वाले व्यक्ति का नाम, पता और राष्ट्रीयता सहित मूल कृति का स्थान। (एक वास्तुशिल्प कृति के मामले में कृति पूरी होने का वर्ष भी दिखाया जाना चाहिए) If the work is an 'Artistic work', the location of the original work, including name, address and nationality of the person in possession of the work. (In the case of an architectural work, the year of completion of the work should also be shown).	:	N.A.
14.	यदि कृति एक 'कलात्मक कृति' है जो किसी भी माल या सेवाओं के संबंध में उपयोग की जाती है या उपयोग किए जाने में सक्षम है, तो आवेदन में प्रतिलिप्यधिकार अधिनियम, 1957 की धारा 45 की उप–धारा (i) के प्रावधान के अनुसार व्यापार चिह्न रजिस्ट्रार से प्रमाणन शामिल होना चाहिए। If the work is an 'Artistic work' which is used or capable of being used in relation to any goods or services, the application should include a certification from the Registrar of Trade Marks in terms of the provision to Sub-Section (i) of Section 45 of the Copyright Act, 1957.	:	N.A.
15.	यदि कृति एक 'कलात्मक कृति' है, तो क्या यह डिजाइन अधिनियम 2000 के अंतर्गत पंजीकृत है? यदि हां, तो विवरण दें। If the work is an 'Artistic work', whether it is registered under the Designs Act 2000, if yes give details.	:	N.A.
16.	यदि कृति एक 'कलात्मक कृति' है, जो डिजाइन अधिनियम 2000 के तहत एक डिजाइन के रूप में पंजीकृत होने में सक्षम है, तो क्या यह औद्योगिक प्रक्रिया के माध्यम से किसी वस्तु पर प्रयुक्त की गई है और यदि हाँ, तो कितनी बार पुनरुत्पादित किया गया है? If the work is an 'Artistic work', capable of being registered as a design under the Designs Act 2000.whether it has been applied to an article though an industrial process and ,if yes ,the number of times it is reproduced.	:	N.A.
17.	टिप्पणी, यदि कोई हो/Remarks, if any	:	

Registrar of Copyrights

डायरी संख्या/Diary Number: 21031/2023-CO/L

आवेदन की तिथि/Date of Application: 09/08/2023

प्राप्ति की तिथि/Date of Receipt: 09/08/2023

Registrar of Copyrights